# THE NANOFORMULATION OF BRAIN DERIVED NEUROTROPHIC FACTOR AND REFORMULATION WITH PEG-FREE POLYMERS

James M. Fay

A dissertation submitted to the faculty at the University of North Carolina at Chapel Hill in partial fulfillment of the requirements for the degree of Doctor of Philosophy in the Department of Biochemistry and Biophysics in the School of Medicine

Chapel Hill
2022

Approved by:

Brian Kuhlman

Alexander V. Kabanov

Wolfgang Bergmeier

Patricia Maness

Rihe Liu

Samuel Lai

**ABSTRACT**

James M. Fay: The Nanoformulation of Brain Derived Neurotrophic Factor and Reformulation with PEG-free Polymers
(Under the direction of Alexander V. Kabanov)

Therapeutic proteins and other biologics are becoming increasingly common across wide swathes of the healthcare system. However, biological macromolecules are particularly susceptible to immune recognition, systemic clearance, and degradation. Various methods of evading the immune system and prolonging the bioavailability of a given therapeutic have been devised and implemented. Polyion complexation, whereby a block ionomer is complexed with a polyelectrolyte to form a core-shell structure, has become an increasingly popular method of encapsulation. Notably, the most common shell forming block is poly(ethylene glycol) (PEG). Understanding the complexity of polyion complex systems requires background knowledge of how complexation is driven. Chapter 1 of this dissertation reviews polymer complexation, encapsulation of proteins, PEG characteristics and alternative options, and the biology around brain derived neurotrophic factor (BDNF).

Chapter 2 of this dissertation addresses the nanoformulation of BDNF and PEG-*b*-poly(glutamic acid) to yield a polyion complex nanoparticle, termed Nano-BDNF. Extensive characterization indicates a spherical, core-shell particle with size and dispersity appropriate for administration. Association is driven by electrostatic attraction between the polymer and protein, then stabilized via a hydrogen bonding network. The particle is stable in high ionic strength solutions, protects from common mucosal opsonins, and selectively releases to specific binding partners. Encapsulation preserves activity in the brain and mediates delivery via the intranasal to brain pathway. Also, treatment in a Parkinson's disease model is efficacious.

However, the particle was formulated with a polymer containing PEG. There are several issues with PEG, (reviewed in Chapter 1), primarily immunogenicity. Chapter 3 deals with the reformulation of Nano-BDNF with two novel polymers. Reformulation yielded relatively small and narrowly dispersed particles which have similar morphology and behavior to the original Nano-BDNF formulation. Additionally, we confirm cooperative binding and investigate the effects of pH change on formation. Indeed, we observe behavior consistent with the polyelectrolyte complexes which inspired the development of polyion complexes. This reformulation can offer a way to diversify and supplement the therapeutic arsenal in order to avoid disruptions by immunogenic PEG.

This dissertation is dedicated to my father, Michael Fay. Your dedication to your family, professional accomplishments, and determination have served as inspiration in my own life and work.

**ACKNOWLEDGEMENTS**

I owe gratitude to many people who have offered me guidance, aid, and support during my graduate work. First and foremost, I owe many thanks to Dr. Alexander Kabanov. It is through his support and guidance that the below works were made possible. I would also like to express my deep appreciation for all of the members of my committee, Dr. Brian Kuhlman, Dr. Wolfgang Bergmeier, Dr. Patricia Maness, Dr. Rihe Liu, and Dr. Sam Lai. Additionally, two emeritus members who pursued positions at other universities deserve thanks for their contributions and guidance as well, Dr. Leslie Parise and Dr. Nikolay Dokholyan. In particular, Dr. Dokholyan and I worked together for several years before I began graduate school. He introduced me to the world of science and I would not be here if it was not for the opportunity he gave me as well as the community of Dokholyan Lab.

I would also like to thank the members of the Kabanov Lab, past and present. In particular, Dr. Elena Batrakova provided much necessary guidance and help in moving forward in this work. I hope her lab continues in its remarkable success. I also need to express my deepest gratitude to Dr. Yuhang Jiang who was a graduate student when I joined the lab and was my first mentor in the lab. His instruction and discussion have made the following works possible. Thank you also to Dr. Dongfen Yuan, who's friendship made the early years in the lab fly by. I also want to thank Matthew Haney for his help and friendship, I appreciate his willingness to listen to me grouse. Dr. Chaemin Lim deserves many thanks for his contributions to the work described in Chapter 3 of this dissertation as well as his scientific conversations. I also want to thank Dr. Dina Yamalaeva and Dr. Natasha Vinod for their friendship and support while we pursued our PhD studies, I wish them the best as they pursue their next endeavors. Additionally, I want to thank the other members of the lab by names as well, their myriad

contributions too extensive to list; Ms. Jubina Bregu, Ms. Yuling Zhao, Dr. Duhyeong Hwang, Dr. Youngee Seo, Dr. Elizabeth Wayne, Dr. Marina Sokolsky, Dr. Yusuf Kemal Demir, Dr. Lida Ghazanfari, Dr. Olesia Gololobova, Dr. Mingzhen Zhang, and Ms. Bridget Newman. From the bottom of my heart, Thank you.

Man, of course, does not survive on science alone. I want to thank a few of my friends, without whom I would be lost. Eric Arnell and Alexander Winkle have stood by me since high school. They are two of my staunchest friends and I appreciate all of the good times, the late night conversations, and enduring friendships. I want to thank Mr. Ryan Hamm-Kelly, Dr. Colleen Hamm-Kelly, Mr. Nicholas Wilson, Dr. William Andrew Clark III, Mr. Steven "Scuba Steve" Hawkes, and Mr. Austin Conklin, the core group of friends from our undergraduate studies at UNC-Chapel Hill and after. Their enduring friendship has sustained me through the years. I also want to thank Dr. Kevin Knight and Dr. Logan Howard who started graduate school in my cohort. They have been like brothers to me in times good times and bad. Finally, I have had the good fortune of finding a local community here in Chapel Hill and would like to specifically thank a few people for their friendship and support; Dr. Lance Thurlow, Dr. Cindy Gode, Dr. Brian Reisenberg, Mr. Wayne Faust, Mrs. Susan Halverson Madayag, Dr. Aric Madayag, Mr. Patrick Kiernan, Mr. Christopher Neal, Mr. Phillip Ivy, Mr. Jackson Cox, Mr. Ralph French, Ms. Jessica Bridgers, Mr. Micah Kaiser, Ms. Meirra Birath, Ms. Natalie Gillespie, Ms. Imalai Negron Martinez, Mr. Nick Heerschap, Mr. Tony Burnett, Mr. Joseph Herrin, Mr. Tim Garret, Ms. Lori Lewis, Mr. Patrick McCallum, Ms. Jennifer Zappa-Higgins, Ms. Bethany Boring, Ms. Jenna White, Ms. Kayla Hensley, Ms. Sara Head, Ms. Shana Mobley, Mr. Mark Anderson, Dr. Jonathan Rowell, Ms. Jenna Brophy, Dr. Shane Elliot, Mr. Neil Resler, Mr. Aaron Brown, Ms. Allie Park, Mr. Talal Asad, Mr. Joe Kousouros, Mr. Thomas MacPherson, and others, too numerous to name. Thank you all for your many acts of kindness, both large and small.

I especially want to thank Ms. Emma Crenshaw who has seen through all of the ups and downs of graduate school. I cannot wait to join you in Boston and begin building a life up there. I also want to thank her parents, Dr. Donna Crenshaw and Dr. Hugh Crenshaw, and her sister, Ms. Kaitlyn Crenshaw, who have all made me feel as part of their family. Their kindness and generosity cannot be overstated.

Lastly, I want to thank my own family. Much of my own motivation is to make them proud through my actions. I want to start by thanking my mother and father, Mr. Michael Fay and Mrs. Sandra Fay. Despite my many and myriad rebellions, their influence, love, and direction have been some of the largest influences on my life. I would not be here without them, both literally and metaphorically. I also want to specifically thank my grandmother, Ms. Connie Valdez. While she was known to spoil me as a child, her love and encouragement have brought me here today. I love you Grandma. I also want to thank my Aunts and Uncles who encouraged my progress through the current day; Uncle Robert, Auntie Barbara, Auntie Yolie, Auntie Belia, and Uncle Mac. I also want to thank my two Godmothers, Belen and Diana. Their encouragement and interest in my work is greatly appreciated. I also want to thank my Cousin Jonathan who was my first friend and remained so since we were children. Lastly I want to thank my remaining cousins and brother, Ryan, Lisa, Andy, and Sally. Thanks for everything guys.

Lastly, I want to thank a few people in memoriam. My grandparents James Fay, Catherine Fay, and Ramiro Valdez. This last year was particularly difficult with an overabundance of loss. I owe many thanks to the following people; My Uncle Darrel, Ron Mayse, Dave Ryan, and Chip Bowman who all passed in the last year.

## PREFACE

This dissertation reports the work completed during my time as a member of the Kabanov Lab under the direction of Dr. Alexander Kabanov. His guidance, resources, and insightful contributions made all of the following work possible. The primary focus of this work was to redesign the polyion complex, Nano-BDNF, that was developed by my colleague and mentor Dr. Yuhang Jiang. Secondarily, I worked to elucidate the mechanism and characteristics of the associations between our polymers and the protein, brain derived neurotrophic factor (BDNF). This dissertation exists in four chapters which are described with notable attributions to significant contributors.

Chapter 1, the introduction, reviews significant phenomena and relevant literature which informs the reader of the necessary context to fully understand the work presented in Chapters 2 and 3. This work is expected to form the base of a review to be submitted for peer review.

Chapter 2 needs to be specifically addressed. The work described in this chapter was primarily conceived of and driven by Dr. Yuhang Jiang in concert with Dr. Alexander Kabanov, his graduate mentor at the time. As such, it should be recognized that the majority of the work presented here, in chapter 2, is properly attributed to Dr. Jiang who is the first author in Jiang, et al. However, due to substantial and significant contributions by myself, the committee and Dr. Kabanov have deemed it worthwhile for inclusion in this dissertation. Here I will detail my exact contributions.

1. During the submission and review process, Dr. Jiang and I collaborated extensively in interpreting all of the data and writing the manuscript. From introduction to discussion, my thoughts and ideas influenced the final drafts submitted for publication.

2. The microfluidic mixer was developed by Natasha Vinod and introduced after Dr. Jiang had graduated from the laboratory. I proposed and executed the experiments utilizing the mixer, the results of which are found in **Figure 2.2**
3. Molecular dynamics simulations were performed by Dr. C. D. Poon though it was our responsibility to analyze and interpret the data. I contributed significantly to all results presented concerning simulations. I performed the charge analysis on the surface of BDNF as well. Most notably, I wrote and executed a program which assessed the frequency of interaction of each amino acid of BDNF with PEG-PLE. I used the data from this analysis to construct the images and interpretations for **Figure 2.7** and **Table 2.1.** I contributed significantly to **Figures 2.5, 2.6, 2.7, and 2.8** and the accompanying text.
4. I conducted the first experiments analyzing the migration of TrkB and BDNF via HAGE and observed that TrkB could abstract BDNF from the Nano-BDNF complex. Dr. Jiang proceeded with the experiments which are shown in **Figure 2.9** and is responsible for the conceptualization of the experiments. My contribution is significant though in demonstrating an unexpected result which led to an impactful finding.

All other experiments were performed by Dr. Jiang or collaborators. I would also note that Dr. Jiang is a dear friend and was a fantastic mentor during the start of my graduate career. None of this is to take away from his accomplishments. Instead I would thank him for his kind instruction and inclusion in this project. This paper has been published in the literature and may be properly attributed with the following citation.

*Jiang, Y.; Fay, J.M.; Poon, C.D.; Vinod, N.; Zhao, Y.; Bullock, K.; Qin, S.; Manickam, D.S.; Yi, X.; Banks, W.A.; et al. Nanoformulation of Brain-Derived Neurotrophic Factor with Target Receptor-Triggered-Release in the Central Nervous System. Adv. Funct. Mater.* ***2018****, 28, 1–11, doi:10.1002/adfm.201703982.*

Chapter 3 details the reformulation of Nano-BDNF with PEG-free alternative polymers. Dr. Chaemin Lim designed, synthesized, and characterized a series of poly(oxazoline) polymers

which were complexed with BDNF. This work has recently been published and may be properly attributed with the following citation.

*Fay, J.M.; Lim, C.; Finkelstein, A.; Batrakova, E. V; Kabanov, A. V PEG-Free Polyion Complex Nanocarriers for Brain-Derived Neurotrophic Factor. Pharmaceutics 2022, 14, 1391, doi:10.3390/pharmaceutics14071391.*

**TABLE OF CONTENTS**

## LIST OF FIGURES

## LIST OF TABLES

## LIST OF ABBREVIATIONS

| | |
|---|---|
| ACN | Acetonitrile |
| AFM | Atomic force microscopy |
| AUC | Area under the curve |
| BBB | Blood brain barrier |
| BDNF | Brain derived neurotrophic factor |
| BIC | Block ionomer complex |
| BSA | Bovine serum albumin |
| CNS | Central nervous system |
| CSF | Cerebrospinal fluid |
| $D_{eff}$ | Effective diameter |
| DLS | Dynamic Light Scattering |
| ERK | Extracellular signal regulated kinase |
| HAGE | Horizontal agarose gel electrophoresis |
| HC | Hippocampus |
| HRP | Horseradish peroxidase |
| HSA | Human serum albumin |
| HT | Hypothalamus |
| IACUC | Institutional Animal Care and Use Committees |
| ICV | Injected to cerebral ventricle |
| IDP | Intrinsically disordered Proteins |
| IgG | Immunoglobulin G |
| INB | Intranasal to brain |

| | |
|---|---|
| IV | Intravenous |
| $K_d$ | Dissociation constant |
| LCROP | Living cationic ring opening polymerization |
| LPS | Lipopolysaccharides |
| LR | Lactated Ringer's Solution |
| LR | Lactate buffered Ringer's solution |
| MB | Midbrain |
| MeOD | Deuterated methanol |
| MeOTf | Methyl triflate |
| MestOx | Methoxycarboxyethyl-2-oxazoline |
| MW | Molecular weight |
| NIH | National Institute of Health |
| NMR | Nuclear magnetic resonance |
| NSPEC | Nonstoichiometric polyelectrolyte complex |
| NTA | Nanoparticle tracking analysis |
| OB | Olfactory Bulb |
| PBS | Phosphate buffered saline |
| PDI | Polydispersity index |
| PEC | Polyelectrolyte complex |
| PEG | Poly(ethylene glycol) |
| PEG-DET | PEG-*b*-poly(N-(N-(2-aminoethyl)-2-aminoethyl)aspartamide) |
| PEG-PLE | Poly(ethylene glycol)-*b*-poly(L-glutamic acid) |
| Peptoids | Poly(N-substituted glycines) |
| PIC | Polyion complex |

| | |
|---|---|
| PICsome | Polyion complex membrane vesicles |
| PLE | Poly(L-glutamic acid) |
| PLK | Poly(L-lysine) |
| PMeOx | Poly(2-methyl-oxazoline) |
| PMeOx-PPaOx-PMeOx, B5 | Poly(methyl-2-oxazolines)$_{38}$-*b*-poly(oxazolepropanoic acid)$_{27}$-*b*-(poly(methyl-2-oxazoline)$_{38}$ |
| PMeOx$_x$-PPaOx$_y$-PMeOx$_z$ or B1-5 depending on block length | Poly(methyl-2-oxazolines)$_x$-*b*-poly(oxazolepropanoic acid)$_y$-*b*-(poly(methyl-2-oxazoline)$_z$ |
| PON | Pons |
| POX | Poly(oxazoline) |
| PPaOx | Oxazolepropanoic acid |
| PSR | Poly(sarcosine) |
| PSR-PLE | Poly(sarcosine)$_{127}$-b-poly(glutamic acid)$_{50}$ |
| PTS | Protein thermal shift |
| RB | Rest of the brain |
| RT | Room Temperature |
| r.u. | Repeating units |
| sIgA | Secretory immunoglobulin A |
| SN | Substantia nigra |
| SSIS | Simple single set of identical sites |
| TBS | Tris buffered saline |
| TCA | Trichloroacetic acid |
| TEM | Transmission electron microscopy |
| TH | Tyrosine hydroxylase |
| $T_m$ | Melting temperatures |
| TrkB | Tropomyosin receptor kinase B |

| | |
|---|---|
| $Z_{-/+}$, Z-/+ | Charge Ratio |

# CHAPTER 1: INTRODUCTION[1]

## 1.1 Introduction

This chapter consists of several sections which give critical background which is necessary to understand the fullness of the work described in this dissertation. It is common in science to refer to only the most recent works with naught but a cursory mention of the seminal developments in a given field. Through a quirk of scientific lineage, my mentor, Dr. Alexander Kabanov, learned from and collaborated with his father, Dr. Viktor Kabanov. The elder Kabanov was a leader of Russian science in the field of polyelectrolyte complexes (PECs) as well as other related fields. Dr. Alexander Kabanov built off of this work and has mentored many students who continue to do so in the field of polyion complexes (PICs), alternatively called block ionomer complexes (BICs) in the literature. The first section of this introduction will review the subject of polyelectrolyte complexes with a special focus on the contributions of Dr. Viktor Kabanov. Second, we will present the challenges facing effective delivery of protein therapeutics and the application of PIC technology. Third, we will consider one of the pillars of modern nanoparticle technology, poly(ethylene glycol) (PEG); both its utility and its deficiencies. Finally, we will conclude with a brief review of the literature surrounding brain derived neurotrophic factor (BDNF) and its nanoformulation which is the focus of chapter two and the model for chapter three.

Through the review of these subjects we intend to leave the reader with the needed background to fully understand the scope and importance of our work. The subsequent chapters

[1]This work is expected to appear in part as a peer reviewed manuscript

discuss a protein-polyelectrolyte complex initially designed for delivery past the blood brain barrier (BBB) that was then reformulated to exclude PEG.

### 1.1.1 Historic polyelectrolyte complexes

PECs, roughly defined, might be considered the complexes such as particles, gels, or structures formed when two oppositely charged polymers are mixed. The first observations were made in the 1920's and 1930's by scientists studying colloid systems. In particular, the work of H.G. Bungenberg de Jong and colleagues in describing the coacervation of gum arabic and gelatins [1], ribonucleic salts [2] and pectins [3] are landmark examples of the phenomena. These and further works are described in great depth in *Colloid Sciences* [4]. It is worth noting that these were some of the earliest observations of spontaneous organization of biological macromolecules which influenced early speculation on precellular organization of life [5] and now informs the study of non-organelle structures in cells [6].

The early examples of complex coacervation were accomplished with relatively low charge density, and irregular polyelectrolytes. With improved ability to synthesized high charge density and consistent polyelectrolytes of repeating units came a widespread investigation into the physical properties of these new substances. During the 1950's, active catalase was precipitated using poly(methacrylic acid) and bovine serum albumin (BSA) was also isolated in its native form using several polyelectrolytes [7,8]. Later, in 1956, Peterson and Sober developed cellulose ion exchange resins which laid the foundation for modern ion exchange chromatography [9]. Then in the 1960's, a study of how poly-4-vinylpyridine with different degrees of quaternization with ethyl bromide affected the binding between metal ions and DNA definitively showed that polybases could bind DNA and could even precipitate as a unified complex [10]. In the words of the paper's authors, a "spectacular" result. While the realization of bioactive polyelectrolyte complexes was still many years away, the promise of these new materials was immediately clear.

In the ensuing discussions of PECs, especially in the Russian context, we would be remiss if we did not direct the reader to Viktor Kabanov's review article which discusses the nearly forty years he was an active researcher in the field [11]. Several of these topics are discussed in great depth and the review greatly informed the work here. The reader is again directed to Kabanov [11] for extensive descriptions of relevant phenomenon including how to determine the degree of conversion of a PEC and a discussion of free energy in relation to pH and Gibbs free energy.

During the 1970's, the principles by which polymeric bases and acids interact were explored and formalized. Zezin et al. [12] described an expansive study considering the permutations of both weak and strong polyacids and polybases. Primarily, polyacids and polybases were mixed together then potentiometric titrations were performed. While strong polyelectrolytes bound and precipitated, weak polyelectrolytes exhibited more complicated interactions. Notably, they observed that the complexes exhibited cooperative binding between the partner polyelectrolytes. Furthermore, while weak pairs can be dissociated in high or low pH, if one partner is a strong polyelectrolyte the weak polyelectrolyte partner determines whether the complex breaks down in high or low pH. Lastly, this study also demonstrated that the secondary structure of poly(L lysine) (PLK) or poly(L glutamic acid) (PLE), i.e. the coil/helix transition, can be controlled via polyelectrolyte complexation [12].

This work [12] also observed precipitation of higher molecular weight structures which were later explained through the formation of hydrophobic regions where oppositely charged polyelectrolytes bound electrostatically and were stabilized by secondary bonding, postulated as hydrogen bonding stabilization [13]. This study also visualized the resultant fibrils, via electron micrograph, and noted the possible similarities to the coil/helix transitions of polypeptides which impart structure to biological systems. The cooperativity of the polyelectrolyte complexation was later confirmed using polyelectrolyte oligomers of varying lengths and measuring the propensity of association [14].

The early works discussed above laid out some of the critical properties of PECs though their application outside of specific precipitation [15] remained limited. In 1979, Kharenko et al. published a pair of papers describing nonstoichiometric, water soluble PECs (NSPECs) [16,17] where an equilibrium exists, dependent on conditions, such that a longer polyelectrolyte binds to a shorter one, creating regions of hydrophobicity. These hydrophobic regions associate and form a core-shell structure where the shell is comprised of the free stretches of the longer polyelectrolyte. Later formalization described these reagents as the host polyelectrolyte (HPE) and the guest polyelectrolyte (GPE) [11].

Early studies identified the susceptibility of PECs to increasing ionic strength [18]. NSPECs demonstrated similar behavior in three regimes such that at low ionic strength $I<I_2$ the NSPEC is unaltered and the solution is homogenous, in the second regime, $I_2<I<I_3$, the system is heterogeneous and there is phase separation of the solution, and in the third regime of high ionic strength, the polyelectrolytes have separated and are in solution. Notably, in regime one, the rise in ionic strength is accompanied by a decrease in radius of gyration and the second virial coefficient as the quality of solvent deteriorates [19]. These effects are heavily influenced by the identity of the polyelectrolytes, the low molecular weight electrolytes used, and the length of the HPE [19–21]. Concurrent with these studies, polyelectrolyte complexation with model proteins was also being investigated which will be discussed further in part 2 of this review [22].

With the basic principles of PECs established, deeper investigations into the mechanisms of association, polyelectrolyte switching, and the importance of non-electrostatic interactions were performed. While cooperativity had been established as an important aspect of how PECs associated, the minimum length was not determined. As it turns out, polymers as short as 6 units could instigate similar reactions as their longer chain counterparts. This was demonstrated when polybases of various molecular weight were complexed with heparin or poly(acrylic acid) [23]. Furthermore, it was confirmed that GPEs could switch over from one HPE to a second, though the mechanism was unclear. With the advent of fluorescence quenching experiments,

the formation of PECs could be confirmed as fluorescent units of a HPE were quenched via interaction with a second GPE. The importance of simple salt was reconfirmed and it was shown that the primary mechanism by which a GPE switched over was via contact in a three component complex [24]. Further investigation confirmed the above and observed disproportionation whereby the GPE distributed unequally [25]. Also, the kinetics of the PEC complexation or substitution reactions are drastically affected by chain length, polymer identity, and ionic strength of solution [25]. Additionally, addition of a stronger HPE to an already formed NPEC will completely convert to the complex to the new HPE [26]. These results were again confirmed and a later study showed that the rate limiting step was the transfer of the GPE to the second HPE when all three polymers combine [27].

The discovery of the above phenomena brought about the question of what, energetically, drives the observed substitution reactions. The total energy of the system ($\Delta G_T$) can be represented as:

$$\Delta G_T = \Delta G_P + \Delta G_C$$

Where $\Delta G_P$ represents the change in energy arising from the interaction of GPE-$HPE_1$ changing to GPE-$HPE_2$, $\Delta G_C$ describes the difference in energy between the counterions in solution interacting with the exposed or occluded regions of $HPE_1$ as opposed to $HPE_2$. While $\Delta G_C$ is entirely dictated by the identity of the HPEs, $\Delta G_P$ is influenced heavily by length of the polymer. Izumrudov, et al. [28] described how chain length affects the propensity for the substitution reaction based on the entropy of the system.

After the thorough exploration of PEC complexation, the next generation of polymers, comprised of two or more distinct blocks, were developed. Block copolymers in the context of PECs generally have one polymer block which is an ionizable polyelectrolyte and a second which can be a non-ionizable, water-soluble polymer. When complexed with an oppositely charged polyelectrolyte, even in stoichiometric amounts, the resulting complex is soluble due to the formation of a macromolecular superstructure where a hydrophobic core forms but is

solubilized by the exterior water soluble block. These complexes have been termed a number of names in the literature; BICs [29,30], polyion complexes (PIC) [31], and complex core coacervate micelles (C3M) [32,33]. Several groups discovered these complexes near the same time and contributed much to the early work.

When considering these systems comprised of block copolymers, we can separate the discussion into distinct parts before reconvening to consider the polymers as a whole. This review will first explore what might be considered the associative blocks, those which drive formation of the complex whether complexation with a second reagent or via self-assembly. Generally, in the context of nanoparticle formulation for drug delivery, these form the core where a drug cargo may be located. Then, later in this review we will consider the exterior block which, in the context of drug delivery, may comprise the corona of a nanoparticle and protect or promote clearance.

Early instances of complexation of block copolymers for pharmaceutical applications were demonstrated using well defined systems [34]. Early on, Kabanov et al. demonstrated the utility of triblock copolymers PEG-poly(oxypropylene)-PEG whereby a micelle with a hydrophobic core was used to load and deliver low molecular weight drugs [35]. This early work demonstrated an interesting principle whereby hydrophobic cores could segregate hydrophobic drugs for delivery or slow release [36]. Generally, the delivery of low molecular weight drugs, especially using hydrophobic blocks, will be considered outside the scope of discussion though there may be occasional reference.

Later though, the same group described the complexation of PEG-*b*-spermine (a cationic polymer) with oligonucleotides [37]. Concurrently, Kataoka and colleagues described similar nanoparticles comprised of PEG-PLK and PEG-*b*-poly(α/β aspartic acid) which formed spherical particles with narrow distributions [31]. A nanoparticle comprised of PEG-PLK and short oligonucleotides soon followed with similar morphology, size, and distribution [38]. Subsequently, a nanoparticle comprised of poly(N-ethyl-4-vinylpyridinium) and PEG-*b*-

poly(methacrylate) was described similarly though it was noted that the stability maintained across a wider range of pH and temperature than the correlating PECs [30]. Later, PEG-*b*-poly(ethyleneimine) and PEG-*b*-poly(spermine) were complexed with DNA to form narrowly disperse, spherical, and stable nanoparticles [39]. Finally, Stuart et al. described a system of poly(dimethylamino)ethyl methacrylate)-*b*-poly-(glyceryl methacrylate) and poly(acrylic acid) which exhibited similar properties as the PIC's described above [32]. While we will not explore every PIC complex described in the literature, these selections were chosen to identity the seminal papers which inaugurated the field and realize, from the earliest examples, the therapeutic potential and opportunities were clear [29].

### 1.1.2 Polyion complexes: polypeptides

The utility of uniform polypeptide polyelectrolytes, which were easily manufactured to exacting specifications, was realized with the advent of PICs [31]. However, it was quickly realized that there were certain limitations which must be taken into account when designing a novel PIC. Harada et. al. demonstrated that complementary block copolymers of PEG-PLK and PEG-*b*-poly(α/β aspartic acid) needed the associative blocks to be of similar length [40]. Furthermore, if one complementary block copolymer was added to a milieu of both high molecular weight (MW) and low MW binding partners, it would selectively associate with the block copolymer of similar length. While this system required similarly sized binding partners, association with a homopolymer generally did not, though mixing ratio and method clearly mattered [41]. With these realizations, much effort was put into improving and diversifying the polypeptide polyelectrolyte toolbox.

Despite early success, stability issues remained as sensitivity to salt and pH was still present with polypeptide PICs. One solution was to chemically cross-link the core of the micelle once associated. The PEG-PLK and PEG-*b*-poly(α/β aspartic acid) system was modified to include thiol groups on PEG-PLK which would cross-link and stabilize the core. The resulting particles were resistant to dissolution with sodium chloride but dissociated in reducing

conditions [42]. This strategy would be used to great effect in the context of protein-block copolymer formulation [43] and we will revisit applications later in this review.

Polypeptide PICs were of immediate interest in gene transfer though association with DNA remained somewhat capricious [29,37,38]. Realizing the diversity of amino acids available to use for association, poly(L-histidine) was used to formulate a particle with DNA. Association was easy, DNA was condensed, and the resultant PIC was comparable to PEG-PLK/DNA PICs. Notably, because histidine is pH sensitive, the particle integrity was also susceptible to changes in pH [44]. Other groups decided to modify already proven biocompatible poly(amino acids). In particular, PEG-*b*-poly(β-benzyl l-aspartate) was modified with diethylamine to yield PEG-*b*-poly(N-(N-(2-aminoethyl)-2-aminoethyl)aspartamide) (PEG-DET) which was less toxic and effected gene transfer [45]. Critically, PEG-DET minimally interacted with cell or organelle membranes at pH 7.4 but was disruptive at pH 5.0, the pH present in endosomal compartments [46]. PEG-DET has been used to encapsulate a variety of macromolecules including DNA [45,46], RNA [47,48], antibodies [49,50], and enzymes [51].

The above examples were all PIC micelles, where a coacervate core forms a phase separated region. However, through careful selection of PEG inclusive block copolymers, it is possible to create a polymer vesicle. Kataoka and colleagues pioneered the technology of semipermeable polyion complex membrane vesicles (PICsomes) [52]. The first PICsomes were large though alteration of its component polymers with alkyl spacers lowered the size to more useful dimensions. Quickly, the technology was used to encapsulate the enzyme myoglobin which remained active even when the complex was exposed to trypsin, a common protease [53]. As interest and utility of PICsomes increased, inclusion of homopolymers, selection of chiral polypeptides, alteration of PEG fraction, and cross-linking enabled control over the morphology and stability of the PICsomes [54–56]. As it stand now, robust PICsomes have been developed as circulating nanoreactors for therapeutic applications [57,58] and may soon be in the clinic [59].

PIC micelles and PICsomes are two of the leading technologies and the later chapters of this work focus on a PIC micelle system. In the discussion of protein-PICs we will reference numerous examples. However, we will diverge to focus on the physics of complexation and new developments in PIC complexes before returning to discussion of the applications and pitfalls of these technologies.

### 1.1.3 General physics of complexation

Similarities between PICs and PECs comprised of homopolymers were clear from the start [11]. However, understanding of the physics determining complexation was needed in order to understand the improved stability and utility to further develop the technology. Much like canonical PECs, an early PIC, PEG-*b*-poly(methacrylate) complexed with hexadecyltrimethylammonium bromide, was sensitive to disruption by altering ionic strength and pH [60]. However, most physiologically relevant conditions were accommodating to PIC formation [61]. The particles were disrupted by high temperature via desolvation of the PEG blocks indicating the importance of the exterior block to particle formation. Later studies showed that the interior was hydrated and reconfirmed temperature sensitivity [62,63], characteristics shared with PECs. Additionally, PICs associate cooperatively, consistent with PECs [64].

Another hallmark of PECs, especially NSPECs, is the ability to mediate interpolyelectrolyte complex reactions where the GPE transfers from one HPE to another. These reactions were also observed in PICs though the rate of the reaction was much lower, likely due to the high charge density in the PIC core and the high aggregation numbers of the complexes [65]. However, when a free GPE was introduced, the substitution reaction proceeds with rates such that NSPEC < PIC < core cross-linked PIC which indicates that the PEG shell does not inhibit penetration and substitution [66]. These two studies indicate the dynamicism of the PIC systems which can be tuned by altering different parameters including ionic strength, pH, and component parts.

As mentioned above, in the case of polypeptide PICs, the associative blocks of PEG-PLK and PEG-*b*-poly(α/β aspartic acid) needed to be similar lengths [40]. A more thorough study by Harada and Kataoka revealed some important properties and explored the underlying mechanisms of association. The specificity of the associative block lengths was reconfirmed and attributed to a balancing of the conformation entropy of the core block stretching and the interfacial energy. Furthermore they also showed that the size of a PLK homopolymer and PEG-*b*-poly(α/β aspartic acid) complex was dependent on PEG length, but not on complementary sizes of the associative, core blocks [67].

The complicated nature of the PEG-PLK and PEG-*b*-poly(α/β aspartic acid) hints at the complexity of the thermodynamics driving the complexation of PICs. Generally, the complexation of PECs can be attributed to electrostatic interactions being stabilized by a hydrogen bond network and hydrophobic regions [11]. PICs are a more complicated case where electrostatic interactions still mediate the initial association and complexation drives water out of the core [68]. Later work recognized the most important contributions come from entropy including counterion release and hydrophobic effects [69]. The system environment was also recognized as important, especially ionic strength or pH changes which minimize the effect of counterion release. Finally, work looking at the entropic contributions found that they outweighed the enthalpic contribution over physiologically relevant salt concentrations [70]. While these results recognize the importance of entropy, confounding results still arise from isothermal titration calorimetry (ITC) studies with proteins and polymers which are even more complicated systems [71,72].

Understanding the critical components and phenomena which dictate PIC formation has enabled the development of technologies which control association, morphology, and architecture of PICs. PICs have been developed which release cargo or dissociate based on polymer architecture [73], temperature [54,63], pH [74], sugar [74], type of ion [75,76], and

hydration [77]. Additionally, the introduction of metals have yielded magnetic nanoparticles which are effective drug carriers [78].

With this basic overview of some of the important concepts needed to understand the formation of PICs we will focus on several areas of research in developing new and novel ways to formulate PECs and PICs.

### 1.1.4 Intrinsically disordered proteins, polyampholytes, and zwitterions

Coacervation is a natural phenomenon observed in nature such that simple systems were described over 70 years ago [4]. These systems were suggested as an early, pre-membrane, method of organizing the molecules necessary for life [5]. In a more modern context, coacervation is recognized as an important biological process which mediates many specific interactions [79]. Notably, one of the critical components to forming many intracellular coacervate structures is intrinsically disordered protein (IDP) [80]. These proteins have one or more domains which are disordered, that is, they do not contain recognizable secondary structure and are generally flexible. However, a hallmark of these domains is strong and specific binding, often with a specific partner. Furthermore, the observation of phase separation mediated by IDPs has led to purposeful design of IDP polyelectrolyte systems [69,79,80].

Two recent reports demonstrate the ability of an IDP, based on the hepatitis C core protein, to associate with RNA and form a nucleocapsid-like particle which looks remarkably like a PEC and may be one depending on the definition used. Another, more classical system of polyampholyte polymers (polymers with both positive and negative sections) was used to model IDPs which self-associate. Specifically, they considered how “blocky” the polymers needed to be in order to mediate self-association and found that blocks of 8-12 charged subunits were necessary to observe cooperative binding and salt resistance [81]. Notably, similar findings were reported for PECs using homopolymers [23]. While the field of controllable IDPs for polyelectrolyte complexation is in a nascent state, there is much promise in using these materials for PECs and PICs for drug delivery in the future.

Zwitterionic polymers are similar to polyampholytic polymers in having both positive and negative charges in a single polymer. However zwitterionic polymers have a positive and negative charge on each subunit, first described by Ladenheim and Morawetz in 1957 [82]. More recently, these molecules have found utility as both the associative core block of block copolymers in PICs or as non-fouling blocks, that is, they can act as either functional block of a block copolymer [83,84]. Self-associative, zwitterionic, tri-block copolymers have even been designed to form PECs [85]. Looking forward, these polymers will continue to be used for non-fouling surfaces, formation of PECs, and designing thermoresponsive complexes [84].

### 1.1.5 Rational design of polymers

From the above discussions, it is clear that our understanding of the physics and phenomena of PICs and PECs has advanced such that more rational design principles can be explored and utilized for developing stable and responsive PIC nanoparticles. One of the earliest examples of formulation requiring careful consideration of components was PEG-PLK and PEG-b-poly(α/β aspartic acid) PIC [40] and the subsequent development of PICsomes [52,53]. Taking inspiration from the plasma membrane ubiquitous in living systems, hydrophobic alkyl spacers were introduced to stabilize the vesicle wall of the PICsome leading to stable particles which did not require cross-linking [86]. Later, inclusion of guanidinium groups stabilized the PICsome even further by increasing the hydrogen bonding network [58].

Chemical modification is not the only method of improving stability of PICs. Recent advances in polypeptide production has enabled fine control of the sequences and chirality present on the associative blocks of block copolymers [87,88]. Additionally development of facile polypeptide synthesis has further expanded the repertoire of available sequences and structures [89]. Notably, for polypeptide coacervate PECs, inclusion of a racemic mixture for one of the binding partners destabilizes the hydrogen bonding network and control the phase of the coacervate [90]. Furthermore, design of the sequence and thus the copolymer architecture, whether by blockiness of charged units [91] or inclusion of hydrophobic residues [92],

drastically affects the electrostatic and entropic contributions to stability [93,94]. It is also worth noting that with advances in computing, rational design of polymers has begun to greater understanding of how to design more stable or responsive PECs and PICs [95].

### 1.1.6 Bio-inspired cationic polymers

The last section of this part of the review chapter will take us away from rational design to focus on bio-inspired polymers. In particular, we will consider bioadhesives inspired by marine animals. These PEC networks function in particularly harsh conditions which often overwhelm chemical adhesives. Since time immemorial, people who lived on the water were familiar with animals which adhere to surfaces extremely strongly or create structures which are remarkably resilient. With modern analysis, our understanding has evolved to know this adhesion is mediated by secreted proteins with specific sequences. During exploratory studies, one of the most notable features was that most of the binding partners were both cationic. Also, they contained high proportions of 3,4-Dihydroxyphenylalanine (Dopa), a catecholic amino acid derivative of tyrosine. These unique amino acids mediate π-π binding and cation-π interactions which form strong bonds in water. The above is a summary of details found in Kord Forooshani, et al., which is a detailed review of mussel foot proteins and bio-inspired bioadhesives [96]. Bioadhesives are of particular interest in wound healing so as to limit the need for mechanical sutures. Similarly, the “cement” made by sandcastle worms is a mixture of sand and a polyelectrolyte complex comprised of a polycationic peptide and a Dopa prevalent anionic peptide [97].

Initially, bioinspired adhesives were developed based on mussel foot proteins which could stably and strongly bind underwater [98]. Later, complex coacervates were formed using two like-charged (cationic) mussel inspired proteins to form a PEC which was spherical [99]. This type of adhesion has been of interest in non-fouling coating for underwater or medical device purposes [100].

### 1.1.7 Conclusions

PECs are present in a wide variety of applications in nature in both well and poorly defined systems. Our own understanding, despite over 50 years or work, is still increasing. Not only that, our ability to design PECs continues to grow in a variety of application. For our purposes, we will focus on PICs from here on out as drug delivery vehicles, particularly for protein therapeutics. As our understanding of PECs continues to grow, we will hopefully see novel applications in material science, drug delivery, and other yet unknown functions.

## 1.2 Protein therapeutic delivery in context of PIC

### 1.2.1 Protein Drugs

Proteins are polypeptide electrolytes which often fold to globular shapes with complicated surface chemistry to effect function and mediate interactions in the biological milieu. Most proteins considered for drug delivery have well defined structure or are short peptides which may or may not have complicated secondary structure [43,101–103]. Per the scope of this review, protein-PECs and the role of proteins in coacervation has be realized since the advent of the field where gliadins were involved in the earliest recognition of coacervate phenomena [3]. As mentioned above, polyelectrolyte resins, and ion exchange columns preceded the development of purposefully designed protein PECs [7–9,11].

Many proteins may be utilized for therapeutic purposes [103], however, delivering a protein drug or mediating its survival in serum may require modification or encapsulation [104,105]. Exogenous proteins are particularly susceptible to immunological clearance and even endogenous proteins can be efficiently cleared [71,103,106]. One of the most successful strategies to reduce opsonization and preserve protein therapeutic efficacy is to modify with hydrophilic and flexible polymers, most notably PEG. Protein-PEC hydrogels, PIC micelles, and PICsomes are also viable strategies [43,105,107]. We will review examples of each below.

While certain principles can be applied across proteins, it is important to remember that proteins are extremely complex and even apparently similar proteins can behave differently in

the context of the same polyelectrolyte homopolymers [108]. Still though, we can make some broad assertions. Electrostatic complexation creates hydrophobic patches such that hydrophobicity in the polymer can stabilize protein PECs or PICs [108]. The complexes are sensitive to salts and environmental manipulation can tune nanoparticle formation [109]. At low ionic strength, association can be entropically driven via counterion release [110]. Notably, these physical principles correlate to many of the principles set down in the early PEC work [11]. However, modern techniques and computation have enabled a deeper understanding and modeling of these complex systems [111].

As a final note on protein drug delivery, we must discuss the complexity of delivering a specific therapeutic to a specific target via a specific route of administration. For instance, oral delivery has many considerations that are not present in intravenous (IV) or intranasal to brain (INB) administration [71,106,112,113]. We will not be discussing routes of administration in depth but it is useful to keep in mind with the below applications. Additionally, we will discuss some methods by which administration is mediated or triggered using targeting moieties [114] or environmental sensitivity [71,115].

### 1.2.2 Polyelectrolyte complexes and PIC micelles

Development of PECs inspired the early development of incorporating proteins into PICs. In 1977, BSA, a protein with multiple charged patches as well as hydrophobic patches, was complexed with quaternized poly-4-vinylpyridines [116]. Later, amphoteric polymers as well as cationic polymers were also complexed with BSA [117,118]. BSA though, is not a particularly useful therapeutic protein. Thus, penicillin amidase, an enzyme, was covalently attached to a cationic polymer where it was active. However, activity was curtailed with addition of the anionic polymer which could impart a level of control over the enzyme, even in the presence of its substrate [119]. Later complexation of enzymes or other proteins with hydrogels was based on these early works [11].

Protein-polymer nanoparticles were immediately recognized as a useful vehicle to protect and preserve therapeutic proteins and peptides. One of the earliest examples was comprised of PEG-poly(lactic acid) and the tetanus toxoid. Spherical particles formed with reasonable size and distribution. Most notably, when a gelatin stabilizer was included, particles continued to release cargo for a full month indicating a stealth effect whereby the particles were ignored by the immune system [120].

Kataoka's group pioneered protein PIC complexes where they worked primarily with lysozyme which deserves some discussion as a model system. Lysozyme has long been a popular model system for protein scientists due to its thorough characterization, stability, easily measured activity, and availability. In the PIC context, the relatively dense and uniform cationic charges on its surface made it somewhat simple to associate with anionic block copolymers. A PIC formulation whereby PEG-*b*-poly(α/β aspartic acid) and lysozyme were complexed demonstrated formation of spherical nanoparticles that were salt sensitive [121]. Also, the PIC occluded access to large substrates so that the protein was inactive until the complex was dissociated with salt [121]. Further characterization showed that for small substrates, the PEG corona could actually act as a reservoir and increase the catalysis rate for the encapsulated protein [122]. A similar PIC micelle was formulated with trypsin, a common protease, which improved its stability and demonstrated the utility of cross-linking using glutaraldehyde in the context of PIC micelles [123,124]. Cross-linking and inclusion of hydrophobic elements were used to improve PIC formulation with lysozyme as well which improved salt and pH resistance [125,126].

Stabilization was useful to a point but control over the size and morphology was another focus as well as where and how to release protein cargo. PICs are complex systems which exist over a range of conformations which can take days to relax into a preferred conformation [127]. Similarly, changes in the solution via ionic strength can alter complex behavior [128]. In one notable example, lipase was ejected from the core and thus became active [129]. Other

experiments using homopolymers to displace lysozyme echoed the interpolyelectrolyte exchange reactions observed by V. Kabanov and colleagues with PEC [130].

While these model systems allowed fruitful exploration of protein PIC formulation, most were not therapeutically useful. Unfortunately, useful proteins tend to be less amenable to nanoformulation which can be overcome in various ways. The ensuing sections will explore ways in which proteins and PIC systems have been manipulated to produce therapeutically interesting formulations. The sections will be organized by application followed by an overview of some cutting edge solutions

### 1.2.3 Charge conversion

One of the most notable features of lysozyme, the premier model protein, is its cationic exterior charge which facilitates formulation with anionic polymers. Most proteins are not so strongly and singly charged, often having a mix of patchy surfaces with cationic, anionic, neutral, and hydrophobic areas. One solution is to convert positive patches to negative so that the surface is only positive or neutral. Citraconic anhydride can be used to convert positive residues on the exterior of the protein to negative moieties [131]. Moreover, these moieties are unstable at pH 5.5 and break down to the original cationic amine. Endosomal pH can be as low as pH 5, thus enabling release of the nanoparticle cargo which was demonstrated using small, fluorescent molecules [50,131]. These technologies have been applied to antibodies aimed at intracellular targets [115]. In the future, other proteins with patchy surfaces may be used.

### 1.2.4 Enzyme encapsulation

Many proteins of therapeutic interest are enzymes, a class of proteins which catalyze chemical reactions, usually of a specific substrate or class of substrates. Exogenous enzymes often cause an immunogenic response or can generally be unstable. Endogenous proteins may be cleared more quickly than desired or may be unstable. In short, there are many reasons to encapsulate or formulate enzymes for delivery. In section 2.3, we discussed a number of papers

which utilized model proteins to elucidate the guiding principles of protein formulation. Below we will review several examples which informed the later chapters of this dissertation.

The nanoformulation of enzymes addresses some major issues in protein drug administration [101]. Most notably, formulation can enable long circulation, improve stability, enable targeting, and even improve enzyme kinetics. However, care must be taken to avoid inactivation [119,132]. These issues are generally easy to avoid with careful formulation [133].

Cu, Zn superoxide dismutase 1 (SOD1) is an extremely well characterized protein involved in reducing reactive oxygen species throughout the body. Reactive oxygen species levels are raised in inflamed tissues, neurodegenerative disease affected brain tissue, and cancerous lesions. SOD1 has been stabilized via genetic manipulation [134] but nanoformulation was still preferred for later administration. An initial nanoformulation of SOD1 cross-linked with PEG-PLK produced small (<20 nm) and narrowly dispersed particles. A later reformulation with two poly(oxazoline) (POX) polymers yielded similarly promising results with reduced cellular toxicity and intracellular delivery [135]. A final nanoformulation using PEG-DET yielded a particles with low toxicity and low mononuclear phagocyte system accumulation [51]. Notably, this formulation demonstrated notably improved outcomes in a mouse model of ischemic stroke [136]. Here, we see how several rounds of reformulation may lead to a much improved final product.

The diversity of enzymes encapsulated by nanoformulations continues to grow and expand with the further development of novel forms and methods of encapsulation. Recently, organophosphate hydrolase, a protein of interest in preventing organophosphate intoxication, was modified with a 6-histidine tail and complexed with PEG-PLE, improving the bioavailability of the enzyme and protecting against lethal doses of organophosphate pesticides and even a chemical weapon [137]. A competing effort grew a zwitterionic polymer on the surface of the protein and yielded similarly successful results [138]. In another unrelated effort, a PICsome was developed to carry glucose oxidase for release in targeted cells where it would induce cell

death by pyroptosis [139]. Yet another study demonstrated encapsulation of the therapeutic protein uricase and nonspecific uptake by macrophages [140].

As we consider novel technology using nanoparticles, the targeting and utility of macrophages becomes more topical. In a series of works, A. Kabanov and Batrakova have led an effort that began with enzyme encapsulation and evolved to macrophage mediated delivery. In the first phase, catalase was packaged with PEG-poly(ethylene imine) and taken up by macrophages, these macrophages released active nanozymes over 24 hours and were able to deliver some of the dose to the brain in a mouse model [141]. A later study confirmed and quantified the results in a mouse model of Parkinson's disease [142]. Most importantly, the strategy improved the bioavailability of catalase at areas of inflammation of the disease model mouse brain [143]. Ultimately, it was found that macrophages mediated protein delivery via release of exosomes [144,145]. Work within these systems has continued in the Batrakova laboratory but the developments leave the scope of this review.

### 1.2.5 Signaling proteins

As with advancements in nanoparticles containing enzymes, the technologies for preservation of signaling macromolecules has benefited from PICs and other polymer based technology. Signaling macromolecules present several distinct challenges in contrast to enzymes. Primarily, the signaling protein must access its receptor or binding partner [101]. Other therapeutic macromolecules face similar challenges such as nucleic acids, antibody therapies, and proteins which must act at specific sites. These alternative macromolecules fall outside the scope of discussion here but the accompanying technologies have informed and improved developments for delivery of signaling molecules.

Careful PEGylation has been one of the leading technologies for signaling molecules. Leptin is a signaling molecule of particular interest in the treatment of obesity and has been called the "satiation signal". Covalent modification of leptin with PEG-*b*-poly(propylene oxide)-*b*-PEG, a polymer know to promote crossing of the BBB, as a single polymer and multiple

polymers, was studied. A single polymer improved the bioavailability in the brain via the leptin transferase and lasted longer in the periphery. Modification with multiple polymers mediated transporter independent accumulation [146]. In order to make a more homogenous protein drug, specific modification to the N-terminus of the leptin protein by the same polymer was tested via delivery using an intranasal to brain (INB) route. The N-terminal modified leptin showed improved brain delivery and stimulation [147]. Finally, in an effort to avoid covalent modification, delivery via macrophage exosome was demonstrated as effective as well [148]. While this example is not a PIC, it does demonstrate the applicability of nanoformulation for signaling proteins.

As is noted before, covalent modification is undesirous when considering formulation of most signaling proteins [133]. Towards that end PIC formulation has been primarily attempted with highly charged proteins. BDNF is a small, dimeric protein which promotes brain health in a variety of ways described in section four of this review [149]. The high charge density of positive charges on the surface of BDNF enabled complexation with PEG-PLE to yield a particle termed Nano-BDNF. Formulation was achieved via simple mixing and demonstrated promising results in the treatment of stroke and Parkinson's disease models [71,106]. The initial formulation led by Dr. Yuhang Jiang is described in chapter two and the reformulation of Nano-BDNF with PEG-free polymers is described in chapter three.

### 1.2.6 Conclusion

The complexation and encapsulation of protein drugs is a promising field with much overlap with the encapsulation of other macromolecules. However, due to complexities of these systems and the regulatory process, the promise of PIC and protein-PECs has not yet been achieved. However, the field is active and it is the general expectation that with increasing technological sophistication and manufacturing ability, more protein polymeric nanoparticles will soon reach the human trial stage.

### 1.3 PEG applications, drawbacks, and alternative technologies

The human immune system is a true marvel of biology which every biomedical scientist should occasionally remember to appreciate, or, for drug delivery specialists, reel in horror at its complexity and efficacy. The body is naturally adept at clearing even endogenous macromolecules, the challenges for molecules or structures are even greater if they are not native to the body. While some therapies, most notably vaccines, take advantage of the natural immune system, much of the work described above has focused on avoiding clearance. The most potent tool in the field of "stealth nanoparticles" and non-fouling surfaces has been PEG. A more thorough review on PEG for the interested reader might be found in the recent publication by Shi, et al. [105].

#### 1.3.1 PEG Function and Application

An early, if not the earliest, report of the immunological properties of PEG was presented by Abuchowski, et al. in 1977 [150]. Covalent attachment of PEG to BSA yielded a nearly complete evasion of the immune system and stymied any immune response [150]. A later study demonstrated that PEG was particularly anti-fouling due to its hydrophilic and flexible properties [151]. Densely PEGylated surfaces or particles exclude opsonins and other immune proteins via entropic exclusion which is mediated by those characteristics [105,151]. This "stealth" effect is commonly utilized in covalently modified biotherapeutics and nanoparticle systems [101,105,133]. Indeed, further study has demonstrated that dense PEGylation can effect mucus and brain penetration, two environments which often stymy unprotected pharmaceutical candidates [152,153]. Furthermore, protein PEGylation has been particularly effective in developing protein drugs present in the clinic [102]. The utility of PEG is demonstrated by its inclusion in numerous pharmaceutics in the clinic and it will continue to be used for the foreseeable purpose.

### 1.3.2 PEG Drawbacks

While the utility of PEG is not in question, there are some clear drawbacks and concerns which have been raised in recent years. Summarily, PEG is immunogenic and due to that property, repeat administration of PEGylated therapeutics can lower efficacy, immune reactions are possible, and anaphylactic allergic reactions can be triggered [105]. Complicating these effects is the ubiquity of PEG in modern society. It is present in common consumer products, cosmetics, food, and many medicines. It is generally regarded as safe and its use is not regulated beyond the general safety assessment consumer products undergo. It is also worth mention that PEG was present in the Moderna and Pfizer vaccines against the SARS-COVID-2 virus which was widely distributed.

The repeat administration of PEGylated therapeutics leads to the rapid clearance of the therapeutic agents, identified as the accelerated blood clearance effect [154]. The cause of this effect has been identified as the presence of anti-PEG antibodies in the sera [155]. Anti-PEG antibodies have been identified as a cause of reduced mobility in mucus as well [156]. Recognition of these phenomena led to investigations of the prevalence of anti-PEG antibodies in the general population and over time [156,157]. Notably, incidence of antibodies in the general population was as high as 72 % in contemporary populations [157]. Even more worrying, anti-PEG antibodies were found in blood samples from several decades before though at lower incidence level [157] indicating that increased use of PEG in pharmaceutical agents and consumer products may be the cause of increased anti-PEG antibody prevalence.

Anti-PEG antibodies may be part of the normal milieu of antibodies in the body and should not be identified as a negative trait, rather formulation scientists and medical doctors must be careful to identify individuals who may have negative allergic reactions [158]. Recent incidents have brought this issue to the public consciousness due to the government sponsored and distributed SARS-COVID-2 virus vaccines and their unfortunate politicization. Despite their nearly miraculous efficacy and minimal toxic effects, incidents of allergic reactions were

identified and attributed to PEG sensitization in some cases [159]. Anaphylaxis was found to be correlated to presence of anti-PEG antibodies and the mechanism was identified through several routes including contact system activation by nucleic acids, complement activation of immune system, direct mast cell activation, and most relevant to us, the presence of anti-PEG antibodies [160]. As an interesting aside, incidents were higher in women and it was hypothesized this may be to higher exposure to PEG in consumer products [161].

Despite these possible drawbacks and the worrying prevalence of PEG in everyday life, these works should not be taken to insinuate that PEG is not a useful molecule. The utility of PEG is self-evident in the many approved drugs which contain PEG for the purposes described above. It is an incredibly useful molecule which will continue to be the gold standard noun-fouling molecule for the foreseeable future. The following sections will describe alternatives in development. It should be noted that, in most cases, the purpose is not to replace PEG, but rather to expand the repertoire of molecules which can achieve similar results.

### 1.3.3 Poly(sarcosine) polymers

Poly(N-substituted glycines) (Peptoids) are a class of molecules very similar to amino acids and polypeptoids are analogous to amino acid polypeptides. The simplest of these peptidomimetic molecules is poly(sarcosine) (PSR) which is analogous to the amino acid alanine [162]. Like PEG, it is flexible and hydrophilic, allowing entropic exclusion of opsonins and has been recognized as a prime candidate for PEG substitution [163,164]. PSR has been identified as anti-fouling and appropriate for inclusion in nanoparticles as a “stealth” component [165,166]. A recent study also shows that it can protect conjugated proteins from proteolysis [167]. In another study, an unexpected result was observed that PSR coated liposomes avoided the accelerated blood clearance effect [168]. These findings and others inspired part of the work described in chapter 3 of this dissertation and in our recent publication describing reformulation of Nano-BDNF [72].

### 1.3.4 Poly(oxazoline) Polymers

POX polymers are a versatile set of polymers composed of oxazoline monomers which can be modified in a number of ways to include hydrophobic moieties, charged groups, and flexible, hydrophilic monomers. Facile synthesis, via living cationic ring opening polymerization (LCROP), has made them a useful and diverse set of polymers for formulation science. In particular poly(2-methyl-oxazoline) (PMeOx) has been identified as a strong candidate to replace PEG [36,169–171]. In 1994, liposomes coated with PMeOx demonstrated an immune evasion effect similar to PEG, this was later confirmed again by the same group [172,173]. Conjugates with proteins have also shown immune evasion by shielding against opsonins [170]. POX polymers have been demonstrated as appropriate for non-fouling surfaces [174]. Indeed, numerous POX micelles have been developed with hydrophobic cores for delivery of small molecules demonstrating the diversity of possible polymers as well as the protective ability of hydrophilic and flexible POX polymers [72,135,175–181].

### 1.3.4 Zwitterionic Polymers

Finally, we will describe the utility of zwitterionic polymers as alternatives to PEG. Zwitterionic polymers contain both a positive and negative charge on each monomer. These polymers have been of particular interest in non-fouling surfaces where several recent works have reported successful synthesis of non-adsorptive surface coatings [84,182–184]. Another application reported is the protection of organophosphate hydrolase with polymers grown on the surface of the protein which successfully protected the immunogenic protein from clearance and preserved activity [138]. Notably, the application of zwitterionic polymers is a relatively new field where rapid advances have been made recently. Novel applications and inclusion in particles is an exciting area of research with many novel complexes being designed.

### 1.3.5 Conclusions

PEG has been the gold standard, non-fouling polymer and is successfully used in many therapeutic applications currently. There are clear concerns with its overuse though. Allergic reactions and accelerated clearance have been reported, most likely due to specific recognition by the immune systems. Many alternatives have been proposed and shown some level of efficacy. However, their novelty has precluded extensive use in the clinic. It is worth noting though that more PEG-free formulations are expected in the future. The main purpose of the work described in chapter 3 is to design PEG-free alternatives of know formulations indicating that complete reformulation may not be necessary if acceptable substitutions can be made.

## 1.4 Brain derived neurotrophic factor and Nano-BDNF

Chapters 2 and 3 deal with the initial formulation of BDNF with PEG-PLE to yield Nano-BDNF and the reformulation with PEG-free polymers respectively. In this section of the review we will more thoroughly describe BDNF, its structure and function, its role in the body, prospective therapeutic effects, and existing formulation work.

### 1.4.1 Endogenous BDNF

BDNF is a homodimeric protein of approximately 28 kilodaltons which is involved in various brain signaling pathways [149,185]. The protein is found in the central nervous system as well as peripherally from where it can be transported across the blood brain barrier by a designated transporter [186]. The primary receptor is the tropomyosin receptor kinase B which stimulates the Ras-mitogen-activated protein kinase pathway, the phosphatidylinositol-3-kinase pathway, and the phospholipase Cγ pathway [185,187–189]. A second, low affinity receptor also exists, the p75 receptor though the effects are less well defined [190]. These stimulatory pathways function in proper brain development, synaptic plasticity, neuropotentiation, axonal pathfinding, and neuron survival [185,189]. While BDNF function is complicated, the effects of BDNF deprivation is clear in improper brain development and it is notably downregulated in a

number of disease states [185]. Hence, BDNF has been suggested as a potential therapeutic option in a myriad of brain and neuronal diseases and disorders.

### 1.4.2 The Therapeutic Potential of BDNF

BDNF is notably downregulated in a number of psychiatric and neurodegenerative disorders. Additionally, application of BDNF to many of these disorders or diseases has yielded promising results. Giacobbo et al., has provided an expansive account of publications reviewing these disorders and BDNF's role, of which we will review several notable applications [185].

From a review of the literature, BDNF seems to have a possible therapeutic application across many diseases and has demonstrated utility in many animal models. In Mecp2 null mice, the gold-standard animal model for Rett syndrome, administration of BDNF to the brain rescued synaptic function [191,192]. BDNF has also shown great promise in the treatment of various peripheral neuropathies [193,194]. Application to amyotrophic lateral sclerosis patients yielded promising results though ultimately the therapy failed in clinical trials [195]. In Alzheimer's disease, application of BDNF to rodent and primate models yielded improved outcomes and reduced amyloid plaques [196]. However, the exact effect and role of BDNF in Alzheimer's disease is still not completely understood and the efficacy is variable [185]. BDNF has also shown great promise in the treatment of major depressive disorder and schizophrenia [185,197,198]. Finally, one of the most promising applications is in the treatment of stroke where rapid deployment may significantly alter the course of recovery [113,199]. The above references may serve as a starting place for the interested reader though multiple reviews exist for the application of BDNF to almost any neurodegenerative, neurodevelopmental, or psychiatric disease. BDNF's wide array of functions and effects make it an attractive candidate for system and brain administration.

### 1.4.3 Our previous work

Our interest in BDNF stems from the rapid clearance of administered BDNF from the serum as well as the rapid efflux from the brain [186]. PIC encapsulation is particularly attractive for two reasons, 1) BDNF is densely and positively charged [149], and 2) PICs offer a way in which to noncovalently preserve BDNF in the brain. BDNF is already known to associate with the lightly negatively charged branches of polysialic acid which comprise a major part of the brain's extracellular matrix [200,201]. Chapter 2 describes the simple self-assembly of BDNF with PEG-PLE to yield Nano-BDNF PEG-PLE which mediates transport via the INB brain pathway and preserves BDNF in the brain parenchyma [71]. This nanoparticle has demonstrated potential efficacy in the treatment of a common Parkinson's disease model and an ischemic stroke model [71,106]. Chapter 3 describes the reformulation without PEG for the reasons described above.

## 1.5 Summary

This review chapter describes several phenomena which inform the following chapters. The promise of PECs identified in during the 1970's is slowly being realized with the development of PICs, modern PECs, hydrogels, and other similar technologies. Part of our effort here is to emphasize the historical nature of science where one work builds on the generations before and attempts to clarify part of the historical timeline. Furthermore, we can see how various interconnected efforts inform and support each other. Briefly, we will discuss each section and the final conclusion which should be drawn.

The early work, especially by V. Kabanov and colleagues, established many of the defining principles which continue to inform later works. Understanding the mechanisms of association and cooperative nature of complexation continues to inform more recent developments. PEC technology led directly into the application of block copolymers and PIC micelles. The studies exploring the mechanisms of association were dependent on the description of PEC complexation. Understanding these principles has led to the development of

new nanoparticles including PICsomes. The recent development and application of rationally designed polymers and bioinspired polymers are understood through the lens of PECs and often contrast these novel chemistries to the earlier studies using uniform, charged polymers. Furthermore, the packaging of therapeutic cargos is best understood as polyelectrolyte complexation in many cases.

Many nanoparticles described are dependent on PEG which can help drive complexation in addition to providing a protective effect. Despite the success of PEG, the drawbacks are well documented. Additionally, ubiquitous use can eventually lead to population level problems with PEG resistance or anaphylactic reactions. Alternative polymers which can provide similar effects are needed to diversify and supplement the therapeutic arsenal. We have described several leading candidates for PEG-free alternatives.

Finally, we have introduced BDNF which is central to chapters 2 and 3. BDNF is a clearly promising therapeutic candidate with which numerous groups have developed promising drug candidates. While the promise of BDNF has not yet been realized, the application in many diseases may soon be implemented in the clinic. It is likely that nanotechnology will play an important role.

## CHAPTER 2: NANOFORMULATION OF BRAIN-DERIVED NEUROTROPHIC FACTOR WITH TARGET RECEPTOR-TRIGGERED-RELEASE IN THE CENTRAL NERVOUS SYSTEM[2]

### 2.1 Summary

Brain-derived neurotrophic factor (BDNF) is identified as a potent neuroprotective and neuroregenerative agent for many neurological diseases. Regrettably, its delivery to the brain is hampered by poor serum stability and rapid brain clearance. Here, a novel nanoformulation is reported composed of a biocompatible polymer, poly(ethylene glycol)-b-poly(l-glutamic acid) (PEG-PLE), that hosts the BDNF molecule in a nanoscale complex, termed here Nano-BDNF. Upon simple mixture, Nano-BDNF spontaneously forms uniform spherical particles with a core–shell structure. Molecular dynamics simulations suggest that binding between BDNF and PEG-PLE is mediated through electrostatic coupling as well as transient hydrogen bonding. The formation of Nano-BDNF complex stabilizes BDNF and protects it from nonspecific binding with common proteins in the body fluid, while allowing it to associate with its receptors. Following intranasal administration, the nanoformulation improves BDNF delivery throughout the brain and displays a more preferable regional distribution pattern than the native protein. Furthermore, intranasally delivered Nano-BDNF results in superior neuroprotective effects in the mouse brain with lipopolysaccharides-induced inflammation, indicating promise for further evaluation of this agent for the therapy of neurologic diseases.

[2]Part of this chapter has previously been published as an article in *Advance Functional Materials*, proper attribution is as follows: *Jiang, Y.; Fay, J.M.; Poon, C.D.; Vinod, N.; Zhao, Y.; Bullock, K.; Qin, S.; Manickam, D.S.; Yi, X.; Banks, W.A.; et al. Nanoformulation of Brain-Derived Neurotrophic Factor with Target Receptor-Triggered-Release in the Central Nervous System. Adv. Funct. Mater. 2018, 28, 1–11, doi:10.1002/adfm.201703982.* Editorial decisions were made for formatting coherence, though the best efforts were made to keep the original text

## 2.2 Introduction

Nanoformulations of therapeutic protein should enable efficient loading and retention of the protein in a nanocarrier, be stable in biological milieu, and ensure rapid release of a functionally active protein to interact with its receptor at the site of action. No current nanoparticle formulation has simultaneously achieved these goals because strong entrapment of the protein in a nanoparticle simultaneously restricts its availability to receptors. Current formulations solve this dilemma by releasing the protein over a period of time, after which the released protein immediately loses protection, often resulting in aggregation, activity loss or immunogenicity. Here we demonstrate that the brain-derived neurotrophic factor (BDNF) self-assembles with an anionic block copolymer into nanosized complexes, stabilized by cooperative electrostatic interactions and H-bonds. While the complexes remain stable in the presence of salt and serum proteins, active BDNF is readily abstracted from them upon interaction with its specific receptors. As a result, nanoformulated BDNF (Nano-BDNF) is as active as the free neurotrophin in activating its receptor and downstream signaling. The seamless transition between the “preservation” and “action” states of BDNF minimizes the potential side effects caused by nonspecific release. Nano-BDNF shows profoundly improved delivery to the brain and neuroprotective effects in vivo.

BDNF promotes neuronal survival and modulates long term potentiation of synaptic transmission, which implicates this neurotrophin as a prime therapeutic candidate for a host of neurological disorders [202]. However, despite the ability of BDNF to cross the blood-brain barrier (BBB), it has a short serum half-life and is rapidly cleared from the brain, which severely limits the brain bioavailability of this neurotrophin after peripheral administration [186]. To bypass the BBB and minimize exposure to peripheral tissues, some proteins can be delivered more directly to the central nervous system (CNS) using the intranasal to brain (INB) route [203]. In this approach, the drug is administered into the nasal cavity to the level of the olfactory nerve/cribriform plate where it can travel up along the olfactory and/or trigeminal nerves to

reach the CNS [204]. However, BDNF delivered via INB route is primarily found in the olfactory bulb and trigeminal nerve and shows little penetration to the therapeutically targeted brain regions, such as cortex or hippocampus [205]. The poor intranasal-to-brain bioavailability of BDNF can be attributed to its cationic surface charges and extensive binding to a variety of polysaccharides, resulting in its entrapment and degradation within the negatively charged and sialic-acid-rich nasal mucosa [113]. Although nasal adsorption of proteins can be ameliorated by PEGylation [206], this approach requires covalent modification of BDNF with poly(ethylene-glycol) (PEG) chains, which can potentially hinder interaction of the neurotrophin with its receptor and therefore entails tedious separation of the more active populations [207]. In this study, we propose a new approach for noncovalent, spontaneous, and agile nanoformulation of BDNF by simply mixing it with PEG-poly(l-glutamic acid) (PEG-PLE) in an aqueous solution. Driven by electrostatic interactions and hydrogen bonding, BDNF and PEG-PLE form stable nanoparticles that are negatively charged and coated by noncovalently attached PEG chains. We present compelling data on the stability of these nanoparticles in physiological conditions, the unaffected activity of encapsulated BDNF, the improved nasal to brain delivery and the decreased brain clearance of BDNF in the Nano-BDNF formulation, which is novel and practically significant.

## 2.3 Material and methods

### 2.3.1 Materials

Methoxy-poly(ethylene glycol)-block-poly(L-glutamic acid sodium salt) (PEG-PLE) was purchased from Alamanda Polymers™ (Huntsville, AL). Its molecular mass determined by gel permeation chromatography was 13 KDa, and polydispersity index was 1.00-1.20; the PEG molecular mass was 4.5 - 5.5 KDa and the degree of polymerization of the PLE block was 45-55. Recombinant human BDNF was purchased from PeproTech (Rocky Hill, NJ). Human Serum Albumin (HSA), Bovine Serum Albumin (BSA) powder, and SuperSignal™ West Pico Chemiluminescent Substrate was from Thermo Fisher (Waltham, MA). Lactate buffered

Ringer's solution (LR), uranyl acetate, Protease&phosphatase Inhibitor Cocktail, and agarose tablet were purchased from Fisher Scientific. Chloramine T, RIPA Buffer, urethane, and IgG from human serum were purchased from Sigma-Aldrich (St. Louis, MO); Mini-PROTEAN® TGX™ Precast Protein Gels, bio-safe Commassie stain solution, sample loading and running buffers for electrophoresis were purchased from Bio-rad (Hercules, CA). Recombinant human TrkB Fc chimera protein (TrkB-Fc) was purchased from R&D systems (Minneapolis, MN). $Na^{125}I$ was purchased from PerkinElmer Life Sciences (Boston, MA); GlutaMAX™ high glucose Dulbecco's Modified Eagle Medium (DMEM) was purchased from Invitrogen (Carlsbad, CA); Anti-Phospho-TrkA (Tyr490)/TrkB (Tyr516) rabbit monoclonal antibody (used in 1:1000 dilutions in 5% BSA), Anti-Phospho-p44/42 MAPK (ERK1/2) (Thr202/Tyr204) rabbit polyclonal antibody (used in 1:1000 dilutions in 5% BSA), Anti-p44/42 MAPK (ERK1/2) Rabbit monoclonal Antibody (used in 1:1000 dilutions in 5% non-fat dry milk), and HRP-conjugated secondary antibodies was purchased Cell Signaling Technologies (Beverly, MA); Anti-TrkB rabbit polyclonal antibody (used in 1:2000 dilutions in 5% non-fat dry milk) was purchased from Millipore (Bedford, MA); Tris-buffered saline (TBS) and Tris-buffered saline with 0.1% Tween 20 (TBST) 10X stock solutions were purchased from Boston Bioproducts (Ashland, MA).

### 2.3.2 Preparation and characterization of Nano-BDNF

Nano-BDNF was prepared by mixing BDNF and PEG-PLE in an aqueous solution. Briefly, a concentrated PEG-PLE solution was added drop-by-drop to a concentrated BDNF solution with gentle vortex at room temperature (RT). The mixture was then diluted with either $10 \times 10^{-3}$ M phosphate buffer (pH = 7.4, PB) or LR to desired concentrations, and gently vortexed for another 30 seconds. Complexes were allowed to incubate at RT for 30 min before use in experiments. The charge ratio (Z−/+) was calculated as the ratio of the total number of carboxylate groups in PEG-PLE (50) to that of arginine and lysine residues in BDNF (44, based on the sequence data provided by the manufacturer). To measure hydrodynamic size with dynamic light scattering (DLS), Nano-BDNF was prepared at various Z−/+ in LR and analyzed

at 25 °C using a Zetasizer Nano ZS (Malvern Instruments Ltd., UK) with a scattering angle of 173°. Transmission electron microscopy (TEM) samples were deposited on thin layers of carbon films coated on copper grids and dried for 5 min. Positive staining was performed for 10 seconds with 2% uranyl acetate, which was then removed using filter paper. All samples were observed under a JEOL 100CX II transmission electron microscope set at 100 kV. Images were acquired with a digital imaging system. Atomic Force Microscopy (AFM) samples were prepared by depositing 5 μL of aqueous dispersion of 0.01 mg $mL^{-1}$ native BDNF or Nano-BDNF (Z−/+ = 10) on the surface of a glass slide followed by air drying for 15 min. A MFP3D system (Asylum Research, Santa Barbara, CA) operated in tapping mode was utilized to image the particles.

### 2.3.3 Horizontal agarose gel electrophoresis (HAGE)

Samples containing 2 μg of BDNF were electrophoresed through a 0.5% agarose gel at 80 V for 1 hour in Tris/Glycine running buffer and then stained using Bio-Safe Coomassie Stain solution (Bio-Rad, Hercules, CA). Images were obtained using the FluorChem E series imager (ProteinSimple, San Jose, CA) with a 100 ms exposure time. The center of mass as determined by optical density was obtained using ImageJ (NIH) and defined as the migration distance of the sample loaded in that lane.

### 2.3.4 Radioactive labelling of BDNF

$^{125}$I-BDNF and $^{125}$I-Nano-BDNF were produced using a previously described Chloramine T method [51,136]. Briefly, 5 μg of BDNF was mixed with 0.5 mCi $Na^{125}I$ in a final volume of 45 μL sodium PB (0.25 m, pH 7.5). Five μL of freshly prepared 2 μg $\mu L^{-1}$ chloramine-T solution in PB was then added to the mixture and incubated for 1 min at RT. $^{125}$I-BDNF was purified from the mixture with Illustra NAP™-5 columns (GE Healthcare, Piscataway, NJ), and fractions were collected in Eppendorf tubes pretreated with either 1% (BSA) in lactated Ringer's solution (1% BSA-LR, for collecting $^{125}$I-BDNF) or 0.1% PEG-PLE solution in LR (for collecting $^{125}$I-Nano-BDNF) to prevent adsorption and the radioactivity of each fraction was counted in a

PerkinElmer γ-counter. The integrity of $^{125}$I-BDNF was determined by trichloroacetic acid (TCA) precipitation. Briefly, 1 μL of each fraction was added to 0.5 mL of 1% BSA-LR and then precipitated in 0.5 mL of 30% TCA followed by centrifugation at 5400 g for 10 min at 4 °C. The radioactivity in the supernatant and pellet were counted with γ-counter and the values used to calculate the integrity of $^{125}$I-BDNF. Samples containing more than 100 000 count per minute (cpm) $\mu L^{-1}$ of radioactivity and precipitate more than 95% in TCA were used for animal studies.

### 2.3.5 Cell culture and western blot

NIH 3T3 cells expressing TrkB were cultured in GlutaMAX DMEM supplemented with calf serum (10%), G418 (100 μg $mL^{-1}$), and penicillin-streptomycin (100–100 μg $mL^{-1}$) and were maintained at 37 °C in a humidified CO2 (5%) incubator. Half a million cells were seeded 24 h before treatment. DMEM, 500 ng $mL^{-1}$ of BDNF, Nano-BDNF (Z–/+ = 946), or equivalent amount of PEG-PLE polymer in the Nano-BDNF formulation were incubated with the cells for 5 minutes at 37 °C in serum-free DMEM then moved to ice for 20 minutes and lysed using radioimmunoprecipitation assay buffer with proteinase and phosphatase inhibitors. Western blot analysis was conducted as reported previously [207–209] with modifications. Briefly, 10 μg total protein from the cell lysates was loaded in each well of 7.5% Mini-PROTEAN® TGX™ precast gels and run at 150 V for 1 h. Proteins were then transferred to 0.45 μm polyvinylidene difluoride membranes at 500 mA current for 1 h. The membranes were then blocked in either 5% BSA (for detection of phosphorylated TrkB and ERK) or 5% nonfat dry milk (for detection of total TrkB and ERK) for 30 min at RT followed by an overnight incubation at 4 °C with primary antibody. Bands were visualized using horseradish peroxidase (HRP)-conjugated secondary antibodies after incubation with SuperSignal West Pic Chemiluminescent Substrate for 1 min. Chemiluminescent signal was recorded by a FluorChem E series imager and quantified by Image J software (National Institute of Health (NIH), Bethesda, MD) using densitometry analysis.

### 2.3.6 Animals

Charles River Laboratories supplied 8-week-old male CD-1 mice (24–28 g) and 11–12-week-old male C57/B6 mice (20–22 g). Animals were housed and humanely handled in accordance with the Principles of Animal Care outlined by National Institutes of Health. They were allowed free access to food and water and were maintained under temperature, humidity, and light-controlled conditions. Institutional Animal Care and Use Committees (IACUC) of the University of North Carolina at Chapel Hill approved all experiments involving animal subjects.

### 2.3.7 INB administration and pharmacokinetic study

INB administration of $^{125}$I-BDNF or $^{125}$I-Nano-BDNF was performed by pipetting 10 μL of sample solution (total radioactivity is 1 000 000 cpm, Z−/+ = 1100, PEG-PLE concentration is 0.91 mg mL$^{-1}$) with a thin tip advanced 5 mm into the left nare of the mice preanesthetized with an intraperitoneal injection of 0.2 mL of 40% urethane. The abdomen and rib cage of the mice were opened and venous blood was collected by cardiac puncture at each time point (5, 10, and 30 minutes) after INB administration. Next, 20 mL of phosphate-buffered saline (PBS) was perfused through the left ventricle of the heart. Mice were quickly decapitated and different brain regions were immediately dissected on ice and weighed. Serum samples were obtained by centrifugation of whole blood at 5000 g for 10 min. Peripheral organs were also collected and weighed. Levels of radioactivity in mice serum, brain regions, and peripheral organs were measured with a γ-counter.

### 2.3.8 BDNF efflux measurement

To measure the rate of BDNF efflux from the brain, the mouse scalp was removed and a hole was made into the skull and 1 μL LR containing 500 000 cpm of $^{125}$I-BDNF or $^{125}$I-Nano-BDNF was slowly injected into the lateral ventricle of the brain. Mice were decapitated at 2, 5, 10, and 20 minutes and the whole brain was removed and weighed. The level of $^{125}$I-BDNF available for transport at t = 0 was estimated in mice that had been overdosed with urethane for

20 minutes and had received an injection of $^{125}$I-BDNF 10 min earlier. To determine the residual levels of radioactivity in the brain, samples were counted with a γ-counter.

### 2.3.9 Neuroinflammation model and treatment regimen

Striatal neuroinflammation was induced in mice as previously reported with slight modifications [210]. Mice were anesthetized with isoflurane (5% for induction and 1%–2% for maintenance) and immobilized using a stereotaxic frame (Stoelting Co., Wood Dale, IL). The skull was exposed and two burr holes were drilled above the striatum of the same hemisphere. The Dura mater was delicately pierced to introduce the injection needle. The coordinates for the injection sites from Bregma in mm were: anterior/posterior (AP) +1.2, medial/lateral (ML) −1.5, dorsal/ ventral (DV) −3.5, and AP −0.3, ML −2.5, and DV −3.2. At each injection sites, 1 μL of LPS at 10 μg $\mu L^{-1}$ was slowly injected at a rate of about 0.5 μL $min^{-1}$ using a 10 μL Hamilton syringe. After injection, the needles were left in place for an additional 5 min to minimize LPS backflow.

Multiple intranasal doses of BDNF (5 μg per animal), Nano-BDNF (5 μg BDNF/animal, Z+/− = 100), or vehicle (0.9% saline) were administered to randomly grouped mice (n = 3) with striatal neuroinflammation. The doses were given 20 minutes prior, 4–8 hours after, and 23 hours after stereotaxic LPS injection. The mice were euthanized 24 hours after LPS injection, perfused intracardially with 20 mL ice-cold PBS followed by 20 mL of 4% paraformaldehyde.

### 2.3.10 Immunohistochemistry

The mice brain was immediately collected after perfusion and postfixed for 24 hours in 4% paraformaldehyde at 4 °C and transferred to 30% sucrose in PBS until the brain tissues sank to the bottom of the solution (a proximately 72 h process). The brain tissue was snap frozen with isopentane/dry ice and cut into 30 μm thick coronal sections containing the substantia nigra (SN) on a cryostat. The sections were then transferred to and stored in Tris Buffered Saline (TBS) with 0.1% sodium azide.

In order to investigate the neuroprotective effect of the nanoformulation, dopaminergic neurons in SN were stained with tyrosine hydroxylase (TH) antibody (MilliporeSigma, Billerica, MA) as previously described [211]. Briefly, the free-floating brain sections were incubated with anti-TH antibody diluted 1:2000 in TBS containing 2% goat serum for 48 hours at 4 °C. The sections were then rinsed in TBS and incubated with secondary antibody, biotinylated goat-antirabbit immunoglobulin G (IgG) (Vector Laboratories, Burlingame, CA), diluted 1:400 in TBS containing 2% goat serum followed by another rinse in TBS. Immunoreactive cells were visualized using the ABC HRP Kit (Vector Laboratories). The sections were finally mounted on glass slides and cover-slipped with Permount (Fisher Scientific) for examination under a Nikon microscope. The outlines of the SN area were determined in the TH stained sections by the distribution of the dopaminergic neurons and by referencing well-established landmarks [212]. Within the SN area of each brain hemisphere, an investigator who was blind to treatment groups quantified the numbers of TH-positive cells with clearly visualized cell bodies.

### 2.3.11 Isothermal titration calorimetry

ITC measurements were performed at 25.0 °C by using an auto-ITC200 titration calorimeter (Malvern Instruments, MA). The sample cell was loaded with 360 µl of BDNF solution (12.5 µM) in 10mM phosphate buffer, pH 7.4 and titrated with 1 mM PEG-PLE solution in 2 µL aliquots with 3 minute intervals. The first injection was 0.2 µL. We used MicroCAl ORIGIN software to determine the site binding model, which provided the best fit (lowest $\chi^2$ value) in order to obtain $\Delta H^o$, $K_d$, and the stoichiometry of association. $\Delta G^o$ and $\Delta S^o$ were obtained using the following equations.

$$\Delta G = \Delta H - T\Delta S$$

$$\Delta G = -RT \ln k$$

### 2.3.12 Molecular dynamics simulation

MD simulations were performed in GROMACS 4.6.3 using OPLS-AA force field with slightly modified parameters to suit for PEG-PLE simulation as previously reported for PEGylated proteins [213]. We extracted the monomer structure (PDB ID 1BND) and constructed a dimer by placing to copies in close vicinity and performing a molecular dynamics simulation until steady state was achieved. We generated a simulation box around the protein and polymers using the *editconf* module of the *GROMACS* package. The dimensions were selected so that the minimum distance between the protein molecule and the edge of the box was 9 Å. Protein models were solvated with the TIP4P water model and, wherever necessary, the system was neutralized with $Na^+$ and $Cl^-$ ions using the program genbox. All MD simulations were performed at constant temperature of 300K and pressure of 1bar for a time period of 100 ns. The electrostatic surface potential of BDNF dimer was calculated using APBS tool 2.1. The numbers of hydrogen bonds and non-bonding contacts in the trajectory were calculated using HBplus program at each step of the trajectory [214] with parameters set the same as described by Baker and Hubbard [215] for maximum comparability. The amino acid sequences forming the β-sheets and β-turns on BDNF were identified by PDBsum: https://www.ebi.ac.uk/thornton-srv/databases/cgi-bin/pdbsum/GetPage.pl?pdbcode=1bnd.

### 2.3.13 Protein thermal shift (PTS) assay

Samples were prepared by mixing 2 μg of BDNF or equivalent amount of Nano-BDNF ($Z_{-/+}$ = 1, 5, and 10) with the environmentally sensitive dye provided in the Protein Thermal Shift™ Dye Kit (Thermo Fisher). We performed the PTS assay using an Applied Biosystems® StepOnePlus™ 7500 Real-Time PCR system, and increased the temperature at a rate of 0.395°C/min. Melting temperature ($T_m$) was visualized by plotting the negative first-order derivative of fluorescence over temperature (-dF/dT) versus temperature (T), and determined as the local minimum of the curve in the range of 70°C to 95°C.

### 2.3.14 Statistical analysis

Statistical analysis was done using Prism 6.01 software (GraphPad, CA). Statistical differences between treatment groups were determined using unpaired Student's t-test for groups of two and one-way ANOVA followed by Tukey's multiple comparison test for groups of three and above. A P-value less than 0.05 was considered significant. Results of all experiments are presented as mean ± SEM unless otherwise specified.

## 2.4 Results

### 2.4.1 Simple and straightforward nanoformulation

Consistent with prior reports [216], native BDNF forms large and highly heterogeneous aggregates with an effective diameter ($D_{eff}$) of about 600 nm and a polydispersity index (PDI) greater than 0.4 (**Figure 2.1 a, b**). Therefore, it cannot be used as an injectable pharmaceutical agent without proper formulation. Our approach addresses this problem by simply mixing BDNF and PEG-PLE in aqueous solutions without sonication or other extensive agitation. This resulted in spontaneous self-assembly of BDNF/PEG-PLE complexes that we will further refer to as “Nano-BDNF”. The properties of such complexes depend on the composition index of the mixture Z−/+, defined here as the molar ratio of the total number of glutamic acid residues of PEG-PLE to the combined number of lysine and arginine residues of BDNF. The Nano-BDNF particles were nearly monodispersed (PDI = 0.026–0.115) at the charge ratios (Z−/+) from 0.5 to 5 (**Figure 2.1 a, b).** The particle size increased from 191 to 246 nm as Z−/+ changed from 0.5 to 3 and then remained essentially constant. At Z−/+ = 10, the polydispersity increased (PDI = 0.214), but it was diminished when we used a microfluidics mixer to mix the components (**Figures 2.2, 2.3**). Transmission electron microscopy (TEM) (**Figure 2.1**) and atomic force microscopy (AFM) (**Figure 2.1 d**) suggested that Nano-BDNF consists primarily of smaller roundish shaped particles, while BDNF formed irregularly shaped aggregates.

### 2.4.2 Formation of overcharged Nano-BDNF species

Polyion complexes form as a result of electrostatic interactions between the reacting polyions [217]. In this regard, one can monitor formation of such complexes by the changes of the electrophoretic mobility of the reacting species in horizontal agarose gel electrophoresis (HAGE). Although naked BDNF is highly positively charged, it does not migrate in agarose gels due to strong binding with the agarose matrix (**Figure 2.1 e**) [200]. In contrast, Nano-BDNF migrates much further toward the anode suggesting that PEG-PLE prevented BDNF from binding with agarose. It also suggests that the positive charges of BDNF are neutralized by PEG-PLE and the complex particles acquired a net negative charge (**Figure 2.1 e**). Notably, albeit the same amount of BDNF was loaded in every well in HAGE experiments, the Nano-BDNF bands always appeared fainter than the native BDNF bands after Coomassie Blue staining. This can be explained by the binding of Coomassie Blue dye to basic/ aromatic amino acids on the protein [218], both of which can be attenuated by encapsulation of the protein in a negatively charged polyion complex with a hydrophilic corona.

As the ratio of PEG-PLE to BDNF increases, we observed progressive incorporation of BDNF in the complex (**Figure 2.1 f**). Several bands corresponding to different complex species emerged as the proportion of PEG-PLE increases, which suggested disproportionation, but eventually only one type of the complex species is observed. Surprisingly, the “saturation” and complete incorporation of BDNF in the complex is achieved at a high excess of PEG-PLE. By plotting the weighted distance of the complex migration in the gel against the charge ratio, the saturation Z−/+ in this experiment was determined to be 6.4 (**Figure 2.1 g**). This value is further supported by an isothermal titration calorimetry (ITC) experiment where the exothermic reaction between BDNF and PEG-PLE was recorded until Z−/+ reached 6.8 (**Figure 2.4**). Therefore, a considerable excess of PEG-PLE appears to have been incorporated in the complex. Hence, the complex becomes strongly negatively charged due to the excess of bound polyanion as was evident from the HAGE experiment.

### 2.4.3 Molecular dynamics (MD) simulation of the complex formation

Overcharging (incorporation of an excess of polyion) is common for polyion complexes like Nano-BDNF when interacting species can aggregate due to hydrophobic or other molecular interactions [27,29,219,220]. However, the charge excess of PEG-PLE (six to seven-fold) incorporated in Nano-BDNF seems to be unusually high compared to similar complexes of other proteins and nucleic acids. If one takes into account the length of the PLE—50 repeating units (r.u.), then each PLE chain in the block copolymer on average would interact with only seven to eight amino groups of the BDNF. Such a small number of ion pairs would be comparable with the minimum number needed for polyion coupling [15]. Consequently, such complexes would not be very stable (especially in the presence of low-molecular-mass salt). To better understand possible molecular interactions between the reacting species, we carried out MD simulations. In this approach, we simulated single PEG-PLE chains and a BDNF dimer for 100 ns using four starting seed positions (**Figure 2.5**). We observe association and binding in every simulation experiment, although the binding at any given residue is transient (**Figure 2.5**). The interaction interface consists of many residues in BDNF and PEG-PLE that come into close contact and is indicative of hydrogen bonding. We used HBplus, a program designed to identify and analyze hydrogen bonds [214], to determine if hydrogen bonds were formed. Thus, we located residues with high frequency of interaction and H-bond formation with the glutamic acid residues of PEG-PLE (**Figure 2.6 a, b** and **Table 2.1**). BDNF is a compact globular protein consisting of ≈70% ß-strands and 20% ß-turns [149]. Our simulations suggest that the binding sites are located primarily in the highly positively charged regions of the BDNF molecule, which are also characterized by high β-turn/ random coil contents (**Figure 2.7** and **Figure 2.6 b,c**). Furthermore, due to the distance between the cationic patches (**Figure 2.7**), a single PEG-PLE chain is unable to saturate both sites present in the BDNF dimer. Hence, we simulated higher molar ratios of PEG-PLE to BDNF (**Figure 2.8**) and found that the maximum number of PEG-PLE chains to form Nano-BDNF with a single BDNF dimer is 3, which is equivalent to Z–/+ of

3.4 and lower than the saturation Z–/+ value we determined earlier. We note that while the MD simulation serves well to locate the binding sites on BDNF, it does not capture the full complexity of the polyion complexes where more than one BDNF molecule participates in the interaction simultaneously as is evident from their size. Therefore, it appears that the combined effect of the crowding behavior of self-assembly and H-bond formation resulted in significant further overcharging of Nano-BDNF complexes.

### 2.4.4 Nano-BDNF complexes are stable in the presence of salt and proteins

Polyion complexes dissociate upon an increase in ionic strength, which usually proceeds in a narrow range of concentration with a low-molecular-mass electrolyte[11,221]. This range depends on the structure of the reacting species as well as the type of electrolyte, and normally does not exceed 0.3–0.7 M NaCl for most biologically relevant systems. Quite surprisingly, depending on the charge ratio, Nano-BDNF displayed two distinct types of behavior. The complexes prepared at low charge ratios (Z–/+ ≤ 3) appeared to disintegrate at 0.15 M NaCl (**Figure 2.9 a, b**). In contrast, complexes prepared at Z–/+ ≥ 5 remain at least partially stable as observed by the presence of the fraction of Nano-BDNF migrating in the gel even in 1.05 M NaCl (**Figure 2.9 c–e**). This fraction features lower migration velocity at high ionic strength, possibly due to partial detachment of BDNF from the complex and subsequent osmotic swelling of the remaining species, which is typical for this type of systems [220]. Remarkably, at a very large excess of PEG-PLE (Z–/+ = 100), the amount of free BDNF that was stripped from the complex greatly diminished, suggesting an easy approach to prepare stable Nano-BDNF (**Figure 2.9 e**). Altogether, the behavior involving differential stability of polyion complexes to ionic strength depending on the PEG-PLE excess is unusual. It could, however, be explained by the transition from a regular polyion complex formed at a lower Z–/+ ratio to the formation of a cooperative H-bond complex along with aggregation and structural rearrangement at high Z–/+ ratios where the complex saturates.

Aside from stability at physiological ionic strengths, polyion complexes for biomedical use need to be stable in the presence of natural polyelectrolytes present in biological fluids that can disintegrate the complex via a polyion interchange reaction [11]. Therefore, we evaluated the integrity of Nano-BDNF using HAGE after incubation with proteins commonly found in body fluids, including human serum albumin (HSA), serum immunoglobulin G (IgG), and secretory immunoglobulin A (sIgA). Surprisingly, the negatively charged HSA showed no competency to disintegrate Nano-BDNF (**Figure 2.9 f**). Similarly, serum IgG and sIgA do not compromise the integrity of Nano-BDNF as evidenced in **Figure 2.9 g, h**. Stability in the presence of proteins may be explained by stabilization of the Nano-BDNF by a cooperative system of H-bonds as well as steric hindrance of the PEG corona, both of which can facilitate intravenous and intranasal delivery of our formulation.

### 2.4.5 Nano-BDNF releases active BDNF without compromising its intrinsic stability

The challenge of the use of nanoparticulate carriers is to maintain integrity of BDNF and release it uncompromised to the relevant receptor, tropomyosin receptor kinase B (TrkB) in the brain. In this context, we characterized the interaction of TrkB and Nano-BDNF by incubating the soluble, recombinant extracellular domain of TrkB with BDNF and Nano-BDNF, and then performing HAGE experiments. Incubation of native BDNF and TrkB yields a single species that migrates as a distinct band (Figure 3i). When mixed with Nano-BDNF, TrkB associates in a 1:1 stoichiometry with the BDNF dimer, thus causing the band containing Nano-BDNF to proportionally decrease in intensity. Formation of a TrkB-BDNF complex was further evidenced by impeded migration of the TrkB band in the agarose gel, which suggests charge neutralization (**Figure 2.9 i**). Similar effects were observed upon mixing Nano-BDNF with a low-affinity BDNF receptor, $p75^{NTR}$ (**Figure 2.9 j**). Therefore, both the high- and low- affinity receptors displace PEG-PLE and abstract BDNF from the Nano-BDNF complex, while HSA, serum IgG, and sIgA at the same molar ratios are not able to do so.

Some previous reports indicated that interaction with polyelectrolytes could destabilize protein cargos [222–224]. Hence, we analyzed the protein stability in two distinct assays to determine how the stability and functionality of BDNF were affected. We assayed the melting temperatures ($T_m$) of BDNF and Nano-BDNF using a fluorometric dye (which responds to environmental changes, namely, hydrophobicity). Here we show that native BDNF has a $T_m$ value of ≈83 °C (**Figure 2.10**), consistent with previous reports [225]. We demonstrate that encapsulation in Nano-BDNF yields a slightly higher stability compared to naked BDNF (≈0.5°C) at Z–/+ of 5 and 10 (**Figure 2.10 B**).

In order to determine if functionality was maintained as well, we incubated BDNF and Nano-BDNF with a genetically engineered NIH 3T3 cell line [226] which stably expresses TrkB without producing BDNF. Activation of TrkB was tested using a phosphospecific antibody to detect phosphorylation in the TrkB kinase domain. TrkB phosphorylation is observed at the same level when stimulated with BDNF and Nano-BDNF, indicating that the vehicle does not inhibit activity or association (**Figure 2.9 k**). We also observed phosphorylated extracellular signal regulated kinase (ERK), a downstream target kinase [227], at similar levels after TrkB stimulation with BDNF and Nano-BDNF (**Figure 2.9 k**).

### 2.4.6 Nano-BDNF enhanced the delivery of BDNF to different brain regions and was neuroprotective against lipopolysaccharides (LPS)-induced neuroinflammation after INB administration

We next performed an in vivo pharmacokinetic study to evaluate the ability of this formulation to deliver BDNF to the brain after INB administration, which is known to bypass the BBB and can potentially deliver therapeutic proteins to a wide range of brain regions [204]. Indeed, in most of the brain regions, both native and nanoformulated $^{125}$I-BDNF was readily detected as soon as 5 min after INB administration (**Figure 2.11 a**). Within 30 min after INB administration, the level of Nano-BDNF accumulation in the brain was significantly higher than that of the native BDNF in all brain regions we examined, except for midbrain where there was a trend for the increase. The areas under the curve (AUC) from 0 to 30 min suggest that Nano-

BDNF increases the delivery of the neurotrophin in all brain regions, most notably in the olfactory bulb (≈6.7 times), hippocampus (≈9.9 times), and brainstem (≈4.0 times) (Figure 4b and Table S2, Supporting Information). The overall increase for the whole brain was also significant albeit less dramatic (≈3.5 times) (**Table 2.2**). By dividing the AUC for different brain regions we further concluded that, compared with native BDNF, the relative brain regional distribution pattern of BDNF after treatment with Nano-BDNF was very different. Specifically, Nano-BDNF was more preferable for distribution to the hippocampus, as compared with olfactory bulb, hypothalamus and the rest of the brain (**Figure 2.12**).

Based on these observations, we further tested in vivo neuroprotective effects of Nano-BDNF using a model of acute neuroinflammation induced via intrastriatal LPS injection (**Figure 2.11 c**) [228]. In animals treated with saline, we observed a clear loss of dopaminergic neurons in the ipsilateral substantia nigra (SN) at 2.7 ± 0.1 mm posterior Bregma. Animals treated with intranasal administration of BDNF showed little or no attenuation of dopaminergic neuronal loss. In contrast, animals treated with Nano-BDNF suffered significantly less dopaminergic neuronal loss induced by LPS injection. Hence, Nano-BDNF demonstrated a neuroprotective effect against LPS induced acute neuroinflammation.

We note that the amount of Nano-BDNF detected in the serum after intranasal administration was lower than native BDNF (**Table 2.2**). Analysis of the peripheral distribution of Nano-BDNF suggests that within 30 min following INB delivery, Nano-BDNF was detected in liver, spleen, kidney, lung, and heart—albeit at levels less than 0.5% inj $g^{-1}$. Marginally higher amounts of the INB delivered Nano-BDNF were found in the esophagus, trachea, and stomach but these amounts still were in the range of 1%–2% inj $g^{-1}$ tissue (**Figure 2.13**) and were likely due to limitations of our INB procedure in a mouse ("post nasal drip"). In addition, literature as well as our own studies suggest the existence of a brain-clearance process for native BDNF [186]. Impressively, we observed a much slower brain-clearance rate of Nano-BDNF ($t_{1/2}$ = 167 min) from brain to blood when it was directly injected to cerebral ventricle (ICV) relative to

native BDNF ($t_{1/2}$ = 25 min, **Figure 2.14**). This observation may help explain why, despite the increased accumulation of Nano-BDNF in the brain, its release into the serum was reduced.

The serum clearance and brain uptake of Nano-BDNF after intravenous (IV) administration is shown in **Figure 2.15**. Consistent with ICV data, IV administered Nano-BDNF displays decreased brain efflux and greater overall brain uptake than the native BDNF. Comparing the Brain/Serum ratios for IV (≈30–40 μL $g^{-1}$) and INB (≈1000– 3000 L $g^{-1}$) of Nano-BDNF, we conclude that the blood to brain route could explain only ≈1%–4% of total brain uptake of Nano-BDNF after nasal administration. Therefore, the increases in BDNF concentration in the brain after intranasal administration of Nano-BDNF are due to the improved delivery of the nanoformulated neurotrophin along the nose-to-brain pathway.

## 2.5 Discussion

We present a novel nanoformulation of BDNF that has immediate translational potential. As a protein delivery system, Nano-BDNF remains stable at high salt concentrations, protects BDNF from nonspecific binding with serum proteins, and is as active as the native neurotrophin in activating its receptor, TrkB and the downstream signaling in the cells. Most current nanoparticulate formulations of BDNF (poly(d,l-lactide-co-glycolide) microspheres [229], nanoporous PLE particles [230], and agarose scaffolds [231]) control the release of the peptide temporally, i.e., release it over a period of time. In contrast, Nano-BDNF releases BDNF in a "spatially controlled" manner. That is, the release of BDNF is triggered by the presence of its target receptors that can abstract BDNF from the complex. Computational molecular modeling suggests that both the PLE chain of the PEG-PLE block copolymer and the receptor interact with approximately the same sites in the BDNF molecule (**Figure 2.6 c**), with the receptor apparently having higher affinity and thereby displacing the copolymer from the complex. Indeed, the apparent dissociation constant ($K_d$) of Nano-BDNF is around 1.8 × 10–6 M as measured in the ITC experiment (**Figure 2.4**). This number is ≈1000 times higher than the reported $K_d$ value of BDNF binding to cell surface-bond TrkB [188], which not only is consistent

with our HAGE result but also explains the demonstrated Nano-BDNF activity in vitro and in vivo. While cooperative polyion displacement has been well known for complexes of synthetic polyelectrolytes and those of DNA [29], this is to the best of our knowledge the first example of such a process in which a polyion is competitively displaced from a complex with a compact globular protein ligand by a receptor that becomes activated during the process. This is a novel and in our view very useful concept in nanomedicine.

Many prior studies attempted to deliver native proteins and peptides to the brain through the INB route in their native form, but the outcomes varied from protein to protein. For example, intranasal delivery of insulin has shown promise in Alzheimer's disease patients [232], yet the same approach did not appear to work for BDNF which was primarily restricted to the olfactory bulb and the trigeminal nerve after INB administration [113].

Surprisingly, very little work has been done to improve BDNF delivery to the brain via this pathway. To the best of our knowledge, there are currently only two such reports. Vaka et al. [233] utilize 0.25% w/v chitosan as a permeability enhancer to disrupt the nasal mucosa barrier, and Chen et al. [234] applied focused ultrasound to induce contractions in the perivascular space of localized brain regions. To this end, our work is the first in this field to improve BDNF delivery with a nanoformulation.

Our data also indicate low accumulation level and restricted regional distribution pattern of native BDNF that are consistent with previous reports [113,233]. The nanoformulation not only increased the amount of BDNF delivered but also significantly altered its distribution pattern. Specifically, Nano-BDNF increased the proportion of BDNF in the brainstem and hippocampus, both being important brain regions widely involved in different CNS disease pathologies. Although neither PEG nor PLE are known nasal absorption enhancers, there is a possibility that the presence of PEG-PLE itself could enhance BDNF delivery to the brain by modulating the composition, viscosity, and permeability of nasal mucosa. However, disruption of the mucosal barrier alone would not explain the altered brain-regional distribution of BDNF.

The passage of therapeutic proteins from nose to brain is known to associate with two pathways: the peripheral olfactory system pathway (transporting to the olfactory bulb and rostral brain regions) and the trigeminal nerve pathway (transporting to the brain stem and caudal brain regions) [204]. The distribution pattern of native BDNF in the brain suggests insufficient entry along either pathway, whereas Nano-BDNF appears to have penetrated into much deeper brain regions (**Figure 2.11 b**). This can be a result from the combined effect of several factors. First, Nano-BDNF is able to stabilize the neurotrophin and minimize its interaction with nasal proteins during its transportation in the nasal tissue, as evidenced in **Figure 2.9 a–j**. Notably, HSA, sIgA, and serum IgG constitute 15%, 15%, and 1%–5% of total proteins in the human nasal lavage fluid, respectively [235]. Second, 5 KDa-PEG-coated and negatively charged nanoformulation of BDNF is expected to reduce its binding to the brain extracellular matrix and substantially increase its diffusion rates in the brain parenchyma [153]. Additionally, higher brain accumulation of Nano-BDNF could also be related to the observed decreased brain clearance of the neurotrophin, as compared with native BDNF, which appears to be cleared from the brain in conjunction with the reabsorption of the cerebrospinal fluid (CSF) [186]. It is known that INB administered proteins are subject to bulk flow within the perivascular space of cerebral blood vessels where CSF plays an important role in their clearance [205,236]. A decreased clearance of the nanoformulated and PEG-coated neurotrophin may be due to its higher diffusion rates in the brain compared to native BDNF [153]. This accelerates their diffusion out of the paravascular space and distribution into the brain parenchyma to a rate that is faster than the turnover rate of CSF clearance and may reflect a general phenomenon resulting in improved brain accumulation of other INB administered proteins delivered by brain-penetrating nanoformulations.

One interesting point that remains unclear in this study is whether BDNF is transported to its final destination in the brain in the form of Nano-BDNF complexes, or is it released somewhere along the way and then transported in a free form. Based on the altered brain

regional distribution observed with Nano-BDNF, if the BDNF was released, it would occur only after the complex distribution from the paravascular space into the brain parenchyma. Besides, the data on the complex stability in vitro argue against premature release of the BDNF from the complex. Nevertheless, this point warrants further investigation of the integrity of Nano-BDNF along the nose-to-brain pathway as well as how exactly the INB delivery outcomes are dependent on the size, charge, and surface properties of these complexes.

The block copolymer chemistry employed in the Nano-BDNF formulation contains two biocompatible materials, PEG and PLE, both of which have been approved by the U.S. Food & Drug Administration (PEG as an inactive ingredient in pharmaceutical preparations, and PLE as a Generally Recognized as Safe food additive) [137]. Relatively low distribution of Nano-BDNF to the blood and peripheral organs should also decrease the risk of side effects associated with systemic exposure to Nano-BDNF. In the present study, the indication of the neuroprotective effect of Nano-BDNF in the brain has been provided using an LPS-induced acute neuroinflammation model. Taken together, our data represent a compelling rationale for advancing the evaluation of Nano-BDNF for treatment for CNS disorders such as stroke [106], Rett syndrome [191], and Alzheimer's disease [196].

The major limitation of this study is using the mice model to evaluate delivery efficiency. Although a similar nose-to-brain pathway exists in both human and rodents [211], the relative surface area of the nasal cavity (surface area/volume) in mice is substantially higher than that in humans [237]. Therefore, a direct translation of data obtained in mice would overestimate the INB delivery efficiency of the same formulation in humans.

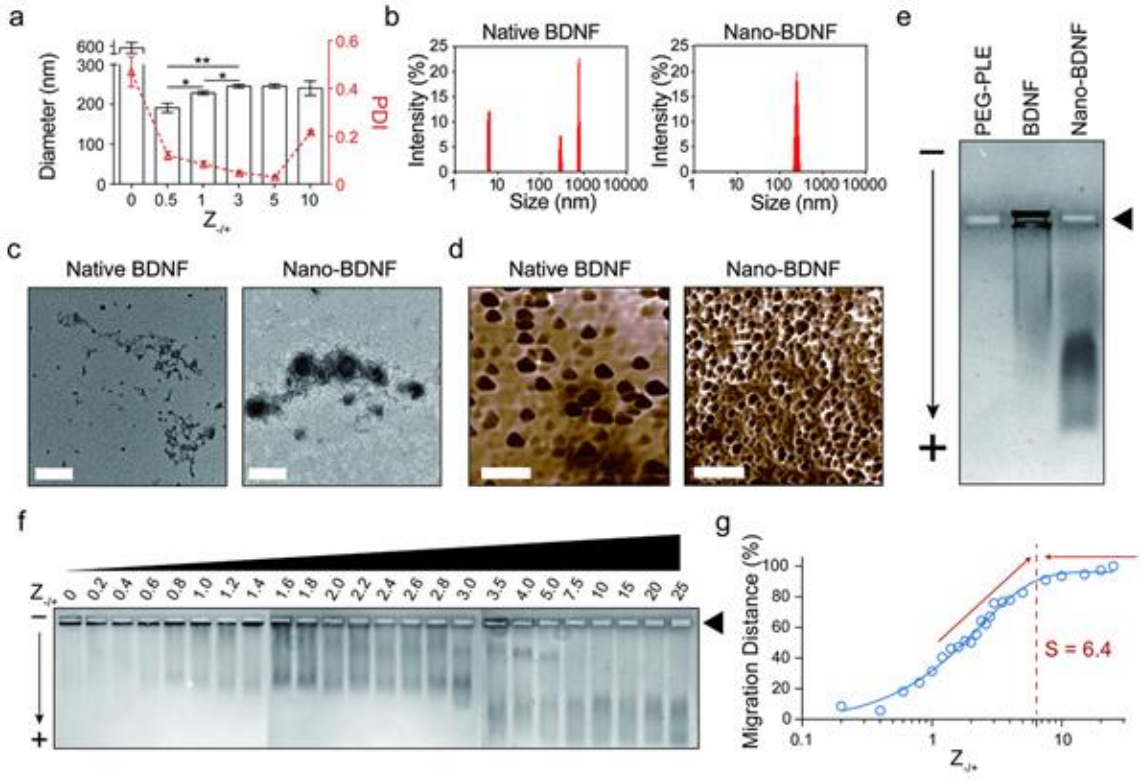


**Figure 2.1 Characterization of Nano-BDNF's physicochemical features and determination of its minimum saturation Z−/+ value.**

(**a**) Effective hydrodynamic diameters of native BDNF and Nano-BDNF samples prepared at different Z−/+ values were measured with DLS. The Z-averaged diameter was plotted to the left Y-axis, and the PDI was plotted to the right Y-axis (n = 5). Statistical significance is defined as P < 0.05 and indicated by *, p < 0.05; **, p < 0.01. (**b**) Representative intensity-size graphs of native BDNF and Nano-BDNF (Z−/+ = 5). (**c**) Representative TEM images of native BDNF and Nano-BDNF (Z−/+ = 10) prepared in 10 × 10−3 M phosphate buffer, pH = 7.4 (scale bar = 200 nm). (**d**) Representative AFM phase diagrams of native BDNF and Nano-BDNF (Z−/+ = 10) in 10 × 10−3 M phosphate buffer, pH = 7.4 (scale bar = 500 nm). (**e**) The electrophoretic mobility of PEG-PLE, native BDNF, and Nano-BDNF (Z−/+ = 100) was determined in 0.5% agarose gel (pore size ≈ 500 nm) at 80 V for 1 h. Samples were loaded in the rectangular wells indicated by the black triangle. The "−" and "+" signs denote cathode and anode, respectively. The black arrow indicates direction of electron flow. Coomassie Blue staining was performed to visualize

BDNF, since it has minimal staining of free PEG-PLE copolymer. Despite the positive charge on BDNF at the pH of the running buffer, a small fraction of BDNF was always observed to migrate toward the anode, possibly due to binding and subsequent charge-conversion by free agarose oligomers and/or polymers that are not completely immobilized in the gel. (**f**) The electrophoretic mobility of Nano-BDNF prepared at different Z–/+ values were evaluated and presented in the same way as described in (**e**). Lanes 1–24 represent samples with different Z–/+ values from 0 to 25. (**g**) To quantify the migration distance of BDNF, we located the center of mass of the BDNF smear in each lane of (**f**) and measured its distance from the loading well of that lane. The distances were then quantified and normalized with the value obtained at Z–/+ = 25 being 100% and plotted against their Z–/+ values on a logarithmic scale. A sigmoidal curve was fitted to the plot, and the minimum saturation Z–/+ value "S" was determined to be about 6.4 by elongating and intersecting the two linear portions of the curve on the graph.

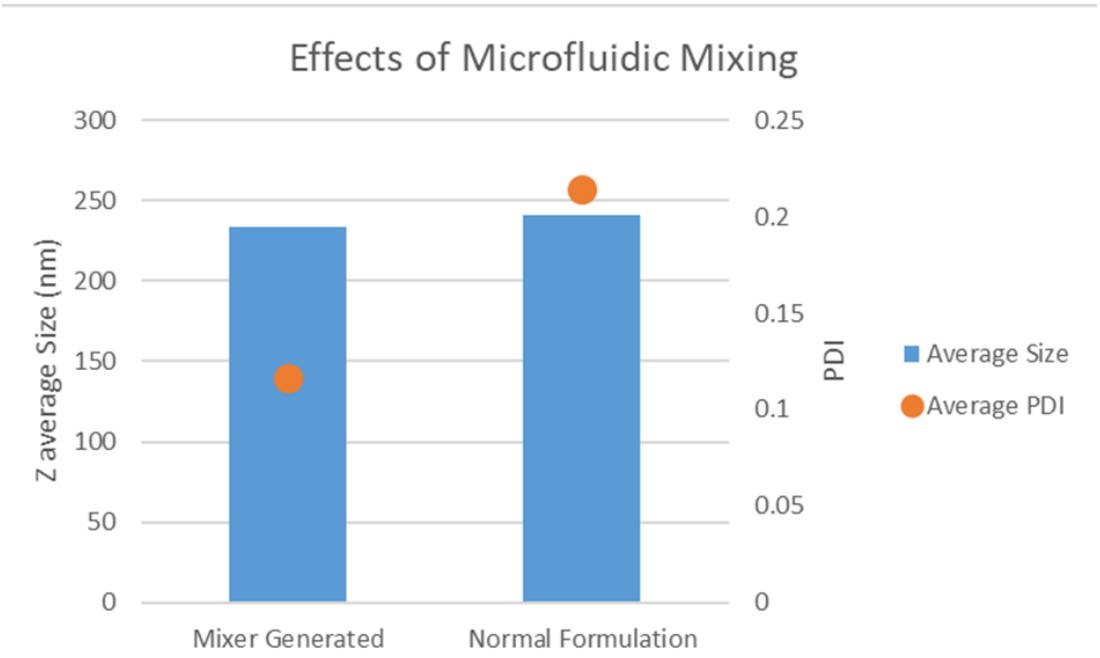


**Figure 2.2 Microfluidic rapid mixing lowers the PDI of Nano-BDNF.**

Microfluidic rapid mixing lowers the PDI of Nano-BDNF at Z-/+ of 10. Nano-BDNF was prepared using a microfluidic mixer (see **Figure 2.3**) and through manual mixing using a pipet and vortex. While sizes of the mixer-generated and manually prepared nanoparticles are similar (234 nm and 241 nm respectively) the PDI of the mixer-generated nanoparticle is 0.12 whereas the PDI of the ordinarily formulated Nano-BDNF is 0.21.

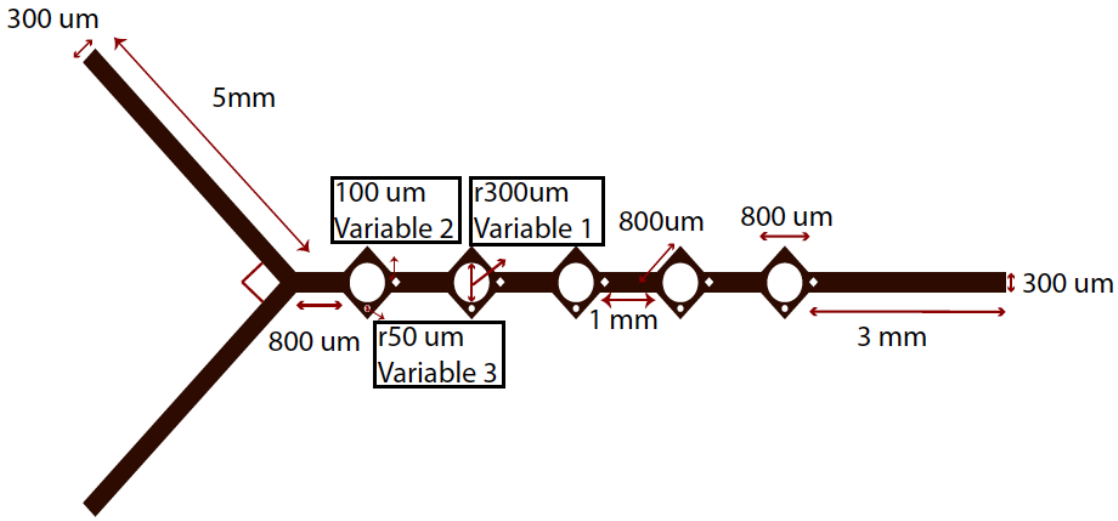


**Figure 2.3 The schematic of the custom-made microfluidic mixer.**

We used COMSOL multi-physics finite element modeling software to design a microfluidic mixer, which uses lamination to achieve lateral mixing. The design model utilizes incompressible flow with convection and diffusion. Water density was set to 1 g/mL. We simulated mixing of a FITC dye with diffusivity of 0.5*10-9 $m^2/s$ with water to determine mixing efficiency. The master device was fabricated using soft photolithography of a silicon wafer with Epoxy SU-8 photoresist. The final device was cast using polydimethylsiloxane. We tested the device using FITC at 10 mM mixed with pure DI water at a flow rate of 10 µL/min. The mixer has a mixing efficiency of approximately 48.61 % at a Reynolds number of 1, which corresponds to a flow rate of 10 µL/min.

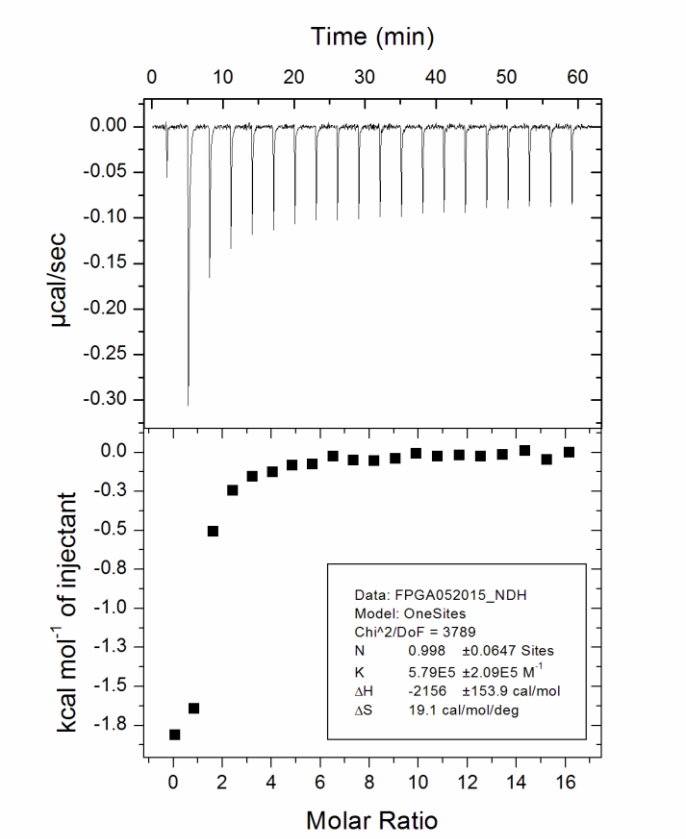


**Figure 2.4 ITC measurement of complexation process between BDNF and PEG-PLE.**

Both PEG-PLE and BDNF were dissolved in 10mM phosphate buffer, pH = 7.4. ITC data was obtained by slowly titrating PEG-PLE solutions into an isothermal chamber containing BDNF and corroborates the saturation Z-/+ of Nano-BDNF to be between 6 and 7. The apparent Kd between mBDNF and PEG-PLE is around 1.8µM, assuming a one-site binding model which is consistent with the BDNF/TrkB binding mode.

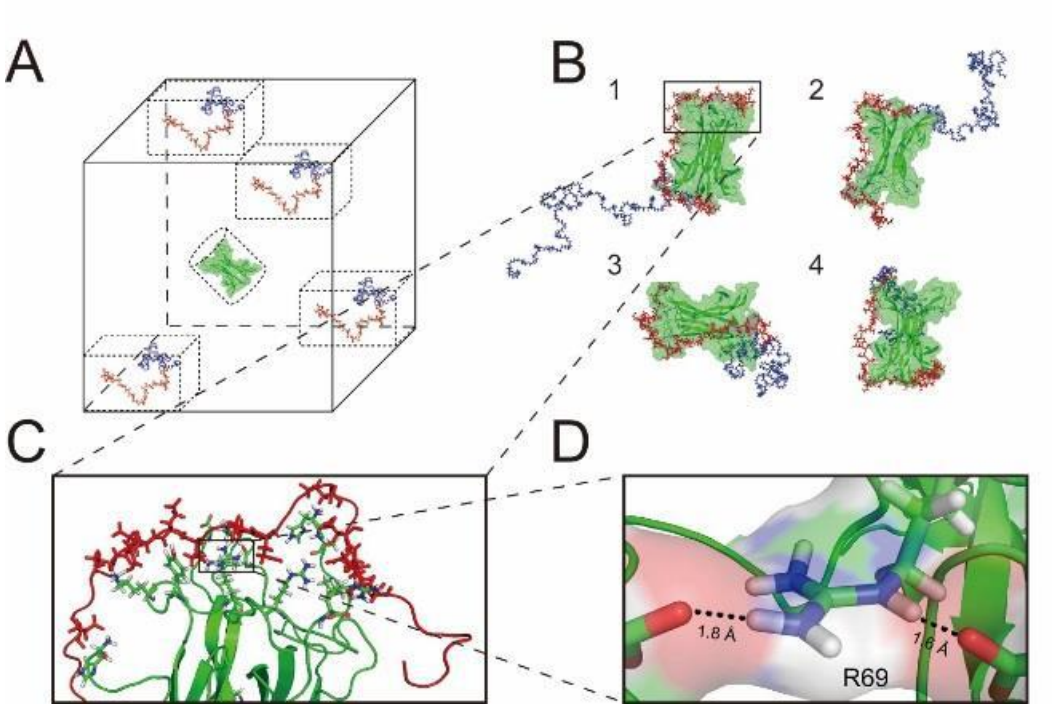


**Figure 2.5 Molecular dynamics simulation.**

(**A**) Simulations were prepared with PEG-PLE in various starting positions (Boxed Polymers). (**B**) Final frames of all the trajectories indicated tight binding between BDNF (visualized in cartoon mode) and PEG-PLE (visualized in stick mode) resulted from the simulations. (**C**) Magnified picture of the squared area shown in (**B**). The amino acids on BDNF that are within 3.9 Å of a glutamic acid residue on PEG-PLE are visualized in stick mode. (**D**) Magnified picture of the squared area shown in (**C**). Two hydrogen atoms on Arginine 69 of BDNF are shown to be located within 2 Å of oxygen atoms on PEG-PLE.

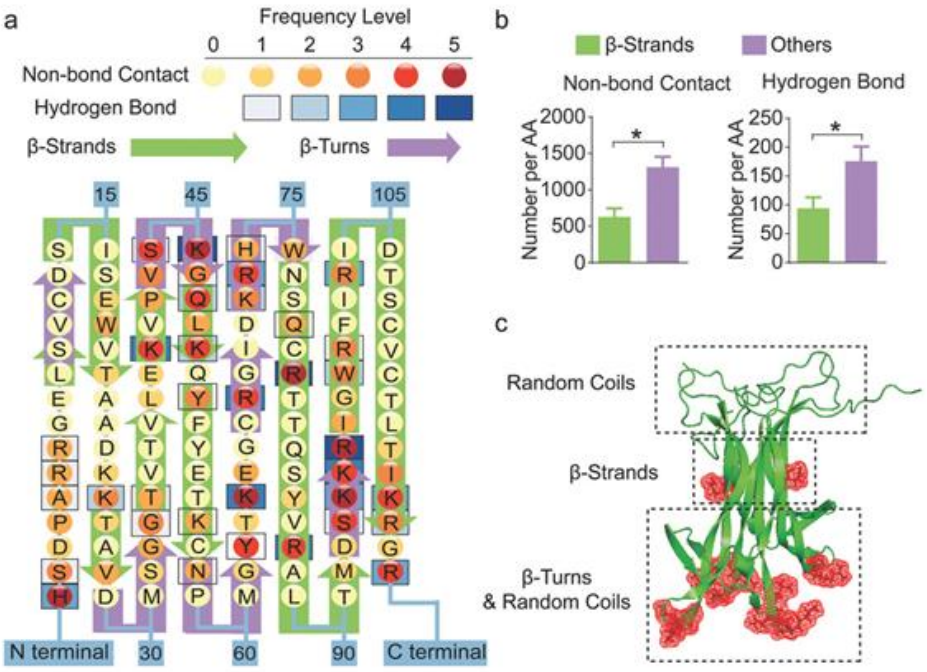


**Figure 2.6 Binding sites with PEG-PLE primarily locate in regions that are rich in random coil and β-turn structures of BDNF.**

(**a**) Frequency map of BDNF-polymer interactions on each amino acid of BDNF. The frequency levels of hydrogen bonds and nonbonding contacts are determined separately based on their total counts (summarized in **Table 2.1**) in the trajectories obtained from four independent simulations with one BDNF dimer and one PEG-PLE chain. (**b**) Quantification of BDNF–polymer interaction occurring on β-strands versus other structural domains. The result is presented as the number of occurrences averaged by the number of amino acids (denoted by AA in the figure) forming each structural domain. "*" denotes statistical significance between two groups ($P < 0.05$). (**c**) Cartoon visualization of a BDNF dimer molecule with illustrations of predominant structural domains at each part of the protein. The red meshes represent amino acids that are actively involved in the binding between BDNF and its receptor, TrkB.

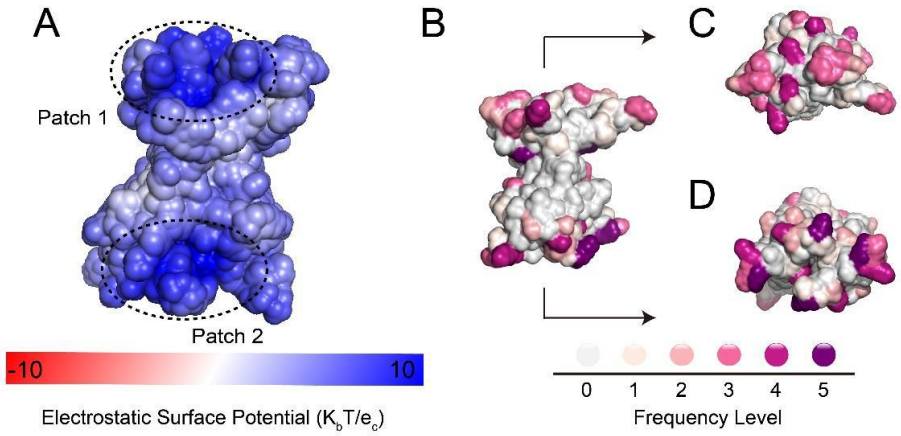


**Figure 2.7 Identification of charge patches on BDNF and 3D density map of BDNF binding with PEG-PLE.**

(**A)** Electrostatic potential of BDNF plotted on the solvent-accessible surface. Potential surfaces are visualized ($-5K_bT/e_c$ (red) and $+5K_bT/e_c$ (blue) around a BDNF dimer molecule at pH 7.0, calculated with APBS tool 2.1. The two major cationic cavities are highlighted with the dashed circles. (**B**) 3D-Heatmap of BDNF-polymer hydrogen bonds on each amino acid of BDNF. Frequency levels were defined in the same way as shown in Figure 3; (**C**) Top view of (**B**); (**D**) Bottom view of (**B**) Frequency levels in (**B**, **C**, and **D**) are defined as described in **Table 2.1**.

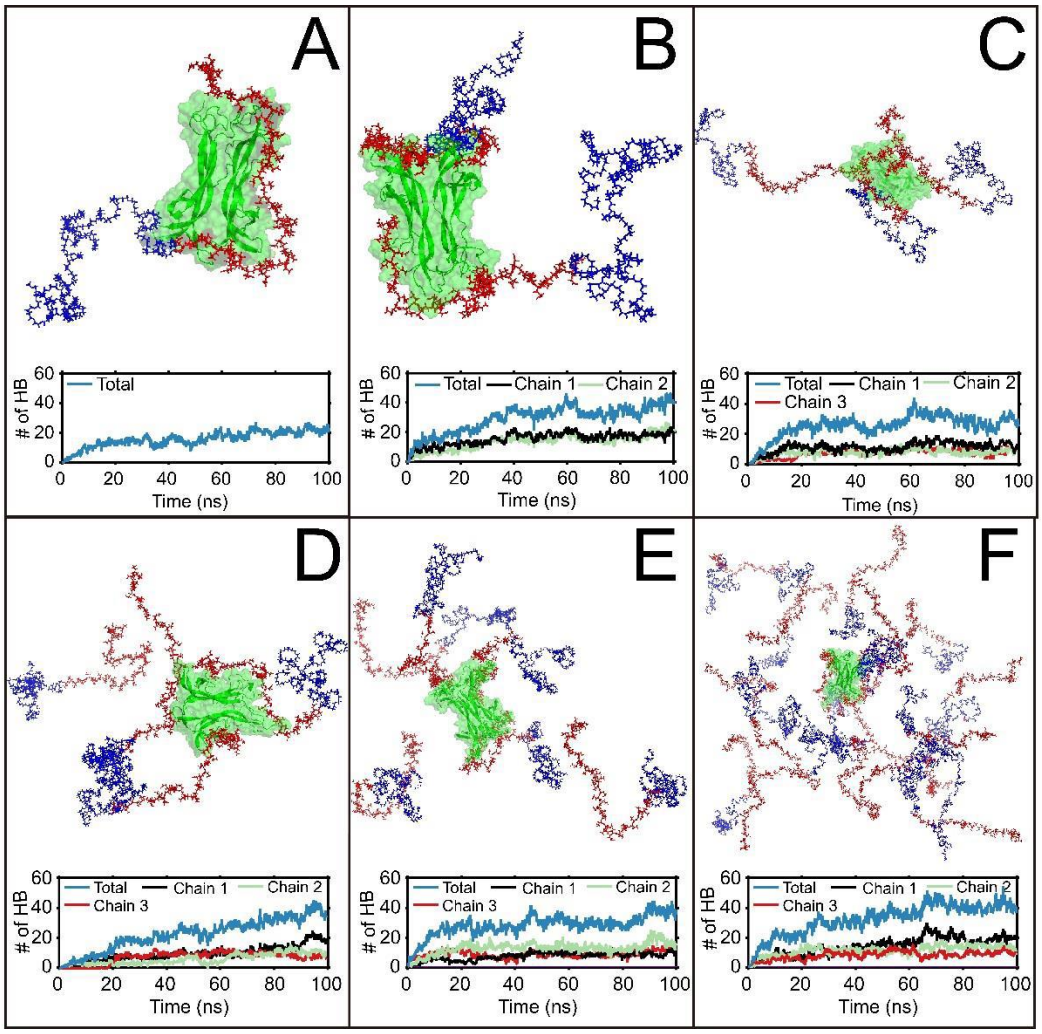


**Figure 2.8 Molecular dynamics simulation of 1 BDNF molecule binding to different number of PEG-PLE chains.**

(**A-F**) Final frames of simulations with 1 BDNF molecule binding to 1, 2, 3, 4, 6, and 20 PEG-PLE chains, respectively. The number of hydrogen bonds occurred during the simulation were plotted against time: blue curves represent the total number of hydrogen bonds between BDNF and all polymer chains in the simulation; black, green, and red curves each represent the number of hydrogen bonds formed between BDNF and one single polymer chain. Green: cartoon and surface illustrations of a BDNF dimer molecule; Blue: stick illustration of PEG; Red: stick illustration of PLE. The number of hydrogen bonds formed was plotted as a function of simulation time under each graph. In all simulations, a maximum number of 3 polymer chains were observed to be able to form hydrogen bonds with the BDNF dimer.

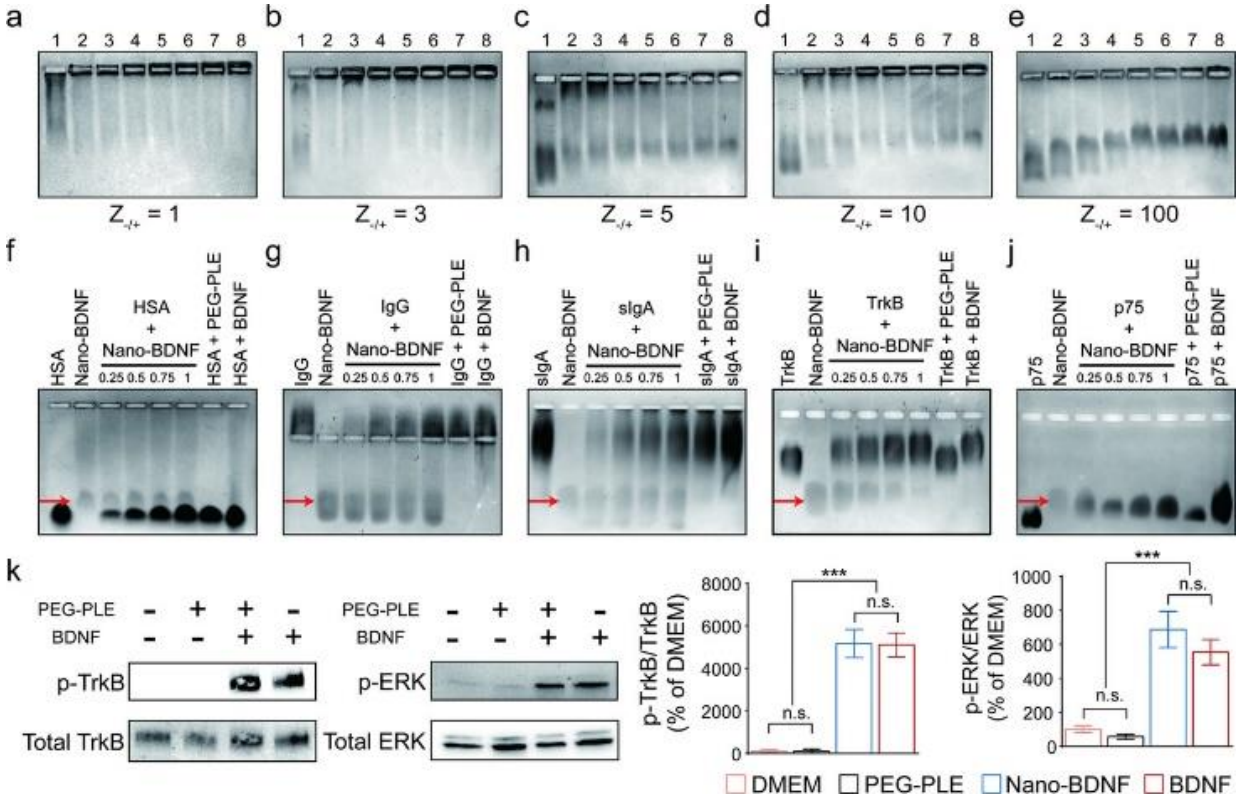


**Figure 2.9 Nano-BDNF prevents BDNF from binding with nasal defensive proteins, while readily releasing active BDNF upon incubation with the BDNF receptors, TrkB and p75NTR.**

(**a–e**) Nano-BDNF samples of different Z–/+ values were prepared in NaCl solutions before horizontal agarose gel electrophoresis. The concentration of NaCl in the Nano-BDNF samples gradually increased from lane 1 to lane 8 (0, 0.15, 0.30, 0.45, 0.60, 0.75, 0.90, and 1.05 M, respectively). The amount of free BDNF in each experimental condition can be estimated by the intensities of staining at the edge of the respective loading well. (**f-j**) The nasal mucosal proteins (**f**) HSA, (**g**) IgG, (**h**) sIgA, and BDNF receptors (**i**) TrkB, (**j**) p75NTR, were incubated with Nano-BDNF (Z–/+ = 200) in lactated ringer's solution (LR) for 30 min before subjected to horizontal agarose gel electrophoresis. From left to right, lane 1: Competitor; lane 2: Nano-BDNF; lane 3: Competitor incubated with Nano-BDNF (molar ratio 0.25: 1); lane 4: Competitor incubated with Nano-BDNF (molar ratio 0.5: 1); lane 5: Competitor incubated with Nano-BDNF (molar ratio 0.75: 1); lane 6: Competitor incubated with Nano-BDNF (molar ratio 1:1); lane 7: Competitor incubated with PEG-PLE (same amounts as in lane 6); lane 8: Competitor incubated

with native BDNF (molar ratio 1:1). Red arrows indicate the location of Nano-BDNF bands in each graph. (**k**) Western blots showing the level of TrkB receptor phosphorylation at the site of Tyrosine 515 as well as the level of ERK phosphorylation in vitro after treatment with (from left to right) DMEM, PEG-PLE, Nano-BDNF, or BDNF for 5 min at 37 °C (n = 6). Quantification of band density was presented by the ratio of phosphorylated TrkB over total TrkB. Data were analyzed with unpaired Student's t-test between each two groups; *** denotes $p < 0.001$ and n.s. denotes no significant difference.

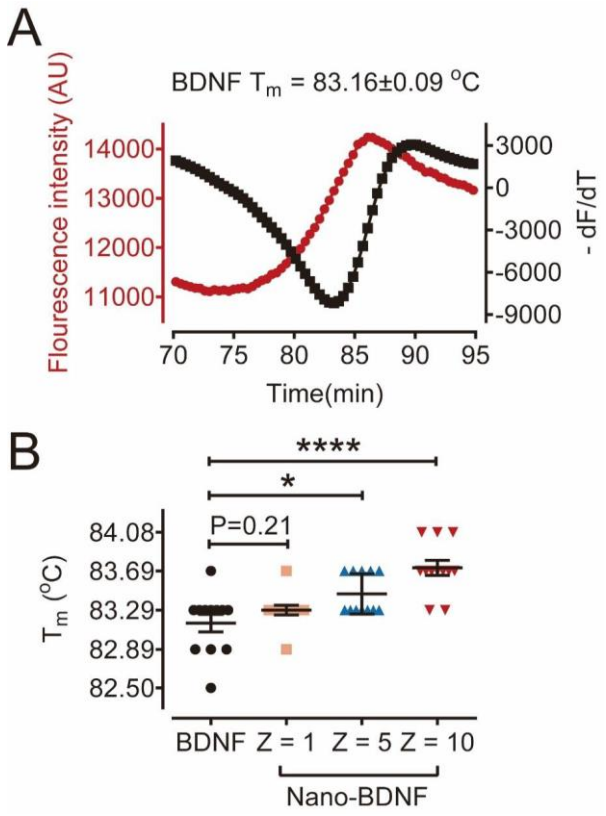


**Figure 2.10 Protein thermal shift assay.**

(**A**) A representative graph demonstrating the melting curve of native BDNF in the proprietary assay buffer in the Protein Thermal Shift™ Dye Kit. The red dots denote fluorescent signal intensity (left Y-axis), and the black triangles denote the negative first-order derivative of fluorescent signal intensity (right Y-axis) in the temperature range of 70°C to 95°C. The $T_m$ of native BDNF was determined to be 83.16 ± 0.09°C as described in the methods section. (**B**) Scatter bar plot summarizing the $T_m$ value of native BDNF and Nano-BDNF at Z-/+ = 1, 5, and 10 (n = 12). Symbols above the horizontal lines denote significance levels compared to the native BDNF group, and are indicated by * ($P < 0.05$) and **** ($P < 0.0001$). This experiment was performed in 10mM phosphate buffer, pH = 7.4.

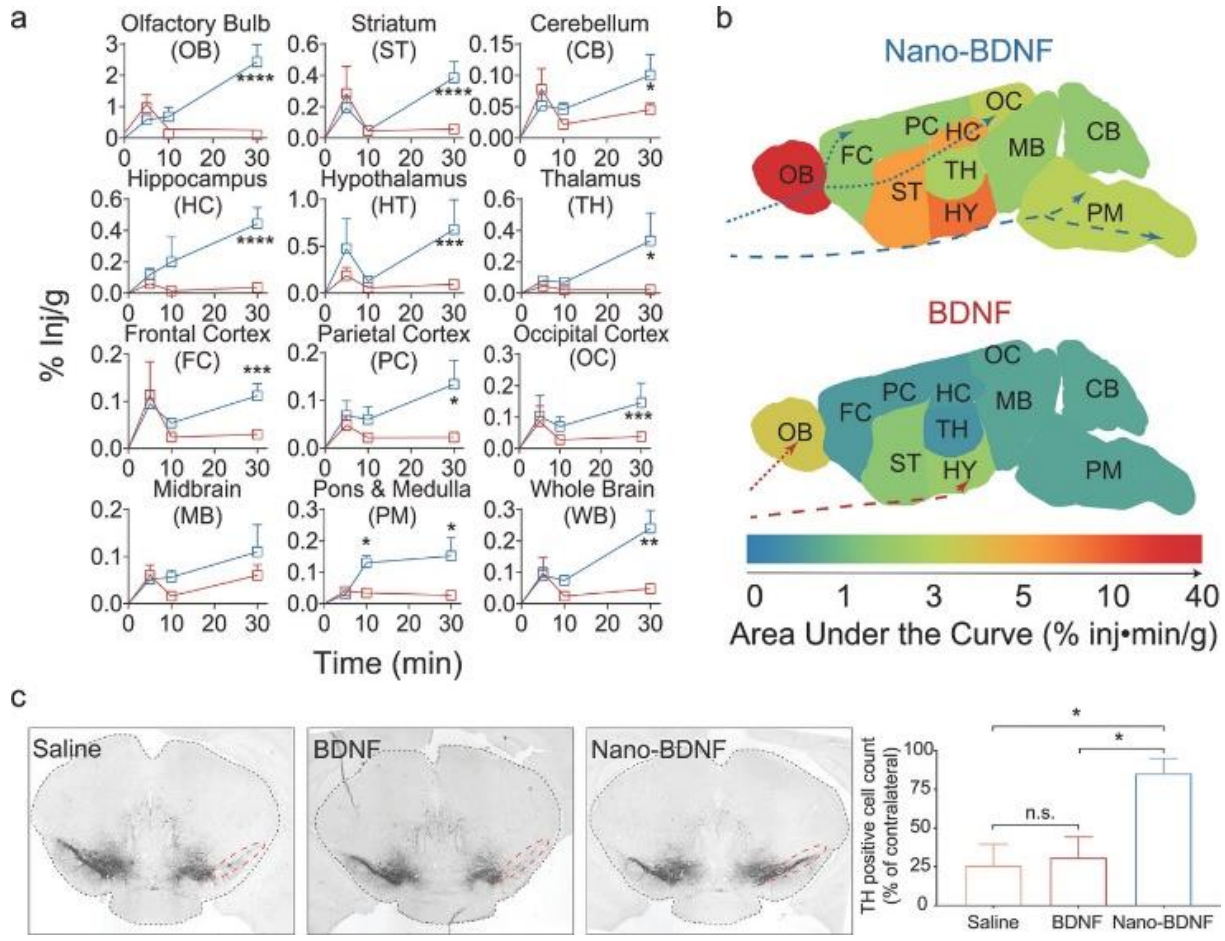


**Figure 2.11 Nano-BDNF significantly improves concentration of therapeutic BDNF in different regions of the brain and proves neuroprotective in a rodent neuroinflammation model.**

(**a**) Significant differences in BDNF concentration were detected in multiple brain regions over a period of 30 min following INB administration of either Nano-BDNF (blue curve) or native BDNF (red curve). (**b**) Heat maps demonstrating the area under the curve (AUC) of BDNF or Nano-BDNF detected in different brain regions over 30 min after INB administration. The traversing trajectories of Nano-BDNF (blue) and native BDNF (red) are shown for both the olfactory pathway (dotted lines) and the trigeminal pathway (dashed lines) based on descriptions in the literature. (**c**) Coronal brain sections at 2.7 ± 0.1 mm posterior bregma, where dopaminergic neuronal loss was observed in ipsilateral substantia nigra induced by intrastriatal LPS injection. Lesions were observed in animals (n = 3) treated with saline (left lane) as well as in those treated with native BDNF (middle lane). In the animals treated with

Nano-BDNF, there was significantly less dopaminergic neuronal loss compared to the other two groups. Quantification of TH-positive cells in the SN area (indicated by red dotted lines) of each brain after treatment was performed as described in the Experimental Section. The numbers are normalized as % of TH-positive cells in the SN area of the contralateral hemisphere on the same brain. Data were analyzed with unpaired Student's t-test between each two groups; * denotes $p < 0.05$, ** denotes $p < 0.01$, *** denotes $p < 0.001$, **** denotes $p < 0.0001$, and n.s. denotes no significant difference.

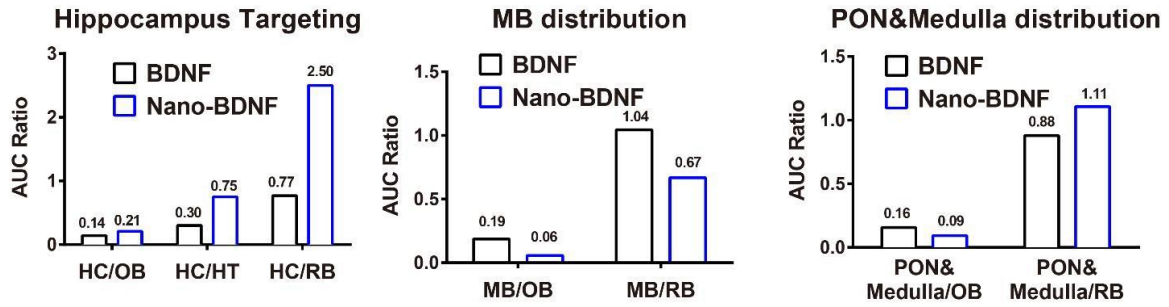


**Figure 2.12 Nano-BDNF distribution in different brain regions after INB delivery compared to native BDNF.**

Data present AUC ratios for the hippocampus (HC), pons (PON) and medulla, and midbrain (MB) vs. olfactory bulb (OB), hypothalamus (HT), and "rest of the brain" (RB) defined as all brain regions excluding HC and brainstem.

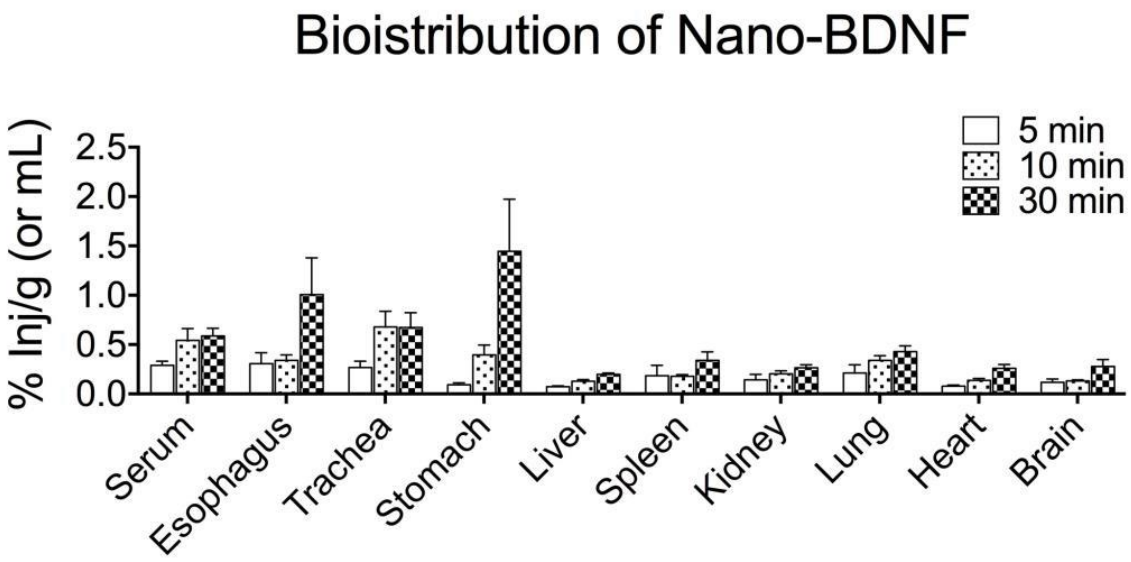


**Figure 2.13 Biodistribution of Nano-BDNF following INB delivery.**

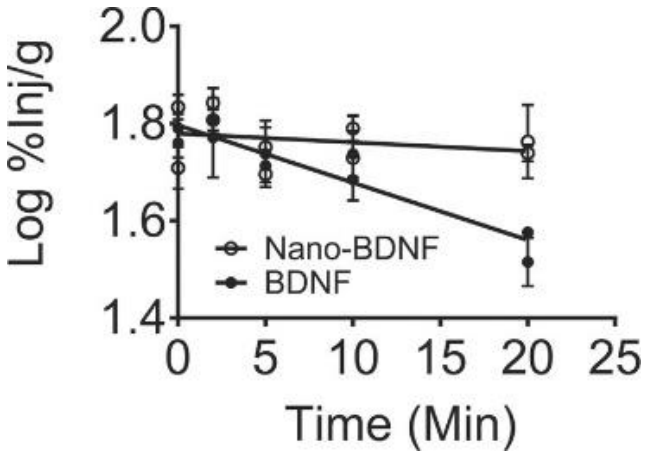


**Figure 2.14 Nano-BDNF inhibits BDNF efflux from the brain to the blood.**

Brain efflux curves of $^{125}$I-BDNF or $^{125}$I-Nano-BDNF after ICV injection showing the rate of efflux, as indicated by the slopes of the lines were −0.012 ± 0.0014 (r2 = 0.89, n = 26) for BDNF and −0.0018 ± 0.0023 (r2 = 0.07, n = 30) for Nano-BDNF, respectively. Both slopes were significantly nonzero and differences between the slopes are extremely significant.

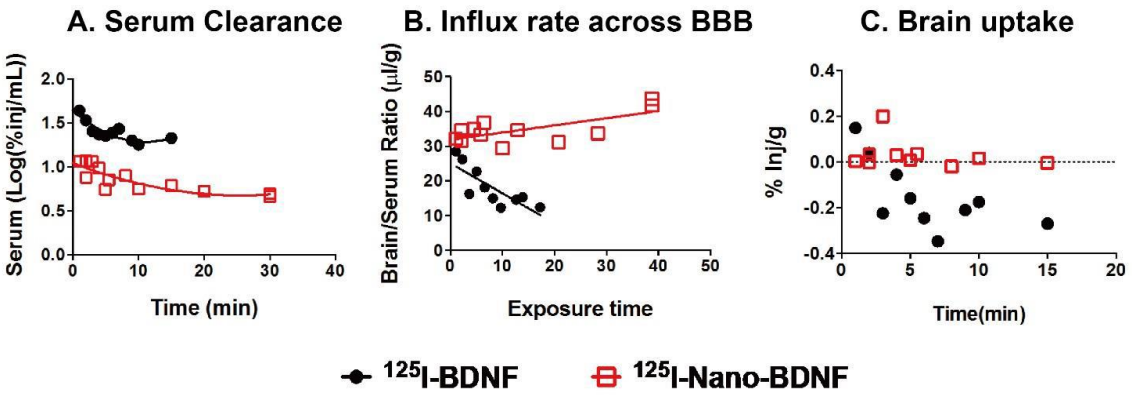


**Figure 2.15 Brain PK of IV Nano-BDNF.**

(**A**) Nano-BDNF clears from the circulation similarly to native BDNF; (**B)** Nano-BDNF displays net influx (Ki = 0.84 uL/g.min) into the brain, whereas native BDNF displays a net efflux from brain to the blood; (**C**) Nano-BDNF displays higher brain uptake than native BDNF, as shown by AUC of 2.96 for Nano-BDNF vs 0.54 for native BDNF. The native BDNF or Nano-BDNF were injected IV at a single dose of 0.5 µg/mouse.

**Table 2.1 Reference chart for the frequency levels shown in Figure 2.6 and Figure S5.**

| *Frequency level* | *Count_NC* | *Count_HB* |
|---|---|---|
| *0* | 0 - 100 | 0 - 100 |
| *1* | 100 - 1000 | 100 - 1000 |
| *2* | 1000 - 5000 | 1000 - 2000 |
| *3* | 5000 - 10000 | 2000 - 3000 |
| *4* | 10000 - 20000 | 3000 - 4000 |
| *5* | > 20000 | > 4000 |

Count_NC denotes the total number of non-bonding contacts.
Count_HB denotes the total number of hydrogen bonds formed across the entire process of the four simulation experiments.

**Table 2.2 Summary of BDNF AUC values (%inj·min/g) in different brain regions).**

| Region | BDNF | Nano-BDNF | Ratio |
|---|---|---|---|
| **Olfactory** | 5.094 | 34.32 | 6.7 |
| **Striatum** | 1.860 | 4.923 | 2.6 |
| **Frontal Cortex** | 0.8850 | 2.033 | 2.3 |
| **Hypothalamus** | 2.145 | 9.588 | 4.5 |
| **Hippocampus** | 0.7300 | 7.229 | 9.9 |
| **Thalamus** | 0.6150 | 4.419 | 7.2 |
| **Parietal Cortex** | 0.6200 | 2.261 | 3.6 |
| **Occipital Cortex** | 0.9400 | 2.593 | 2.8 |
| **Cerebellum** | 0.9200 | 1.704 | 1.9 |
| **Midbrain** | 0.9500 | 1.929 | 2.0 |
| **Pons** | 0.7917 | 3.220 | 4.1 |
| ***Whole Brain** | 1.020 | 3.550 | 3.5 |
| ****Brainstem** | 0.7289 | 2.905 | 4.0 |
| **Serum** | 4.835 | 3.088 | 0.6 |

Whole brain AUC was calculated as the weight-averaged AUC of all the brain regions listed above (except brainstem).

Brainstem AUC was calculated as the weight-averaged AUC of midbrain and pons regions

## CHAPTER 3: PEG-FREE POLYION COMPLEX NANOCARRIERS FOR BRAIN DERIVED NEUROTROPHIC FACTOR[3]

### 3.1 Summary

Many therapeutic formulations incorporate poly(ethylene glycol) (PEG) as a stealth component to minimize early clearance. PEG is immunogenic and susceptible to accelerated clearance after multiple administrations. Here, we present two novel reformulations of a polyion complex (PIC), originally comprised of poly(ethylene glycol)$_{113}$-b-poly(glutamic acid)$_{50}$ (PEG-PLE) and brain derived neurotrophic factor (BDNF), termed Nano-BDNF (Nano-BDNF PEG-PLE). We replace the PEG based block copolymer with two new polymers, poly(sarcosine)$_{127}$-b-poly(glutamic acid)$_{50}$ (PSR-PLE) and poly(methyl-2-oxazolines)$_{38}$-*b*-poly(oxazolepropanoic acid)$_{27}$-*b*-(poly(methyl-2-oxazoline)$_{38}$ (PMeOx-PPaOx-PMeOx) which are driven to association with BDNF via electrostatic interactions and hydrogen bonding to form a PIC. Formulation using a microfluidic mixer yields small and narrowly disperse nanoparticles which associate following similar principles. Additionally, we demonstrate that encapsulation does not inhibit access by the receptor kinase, which effects BDNF's physiologic benefits. Finally, we investigate the formation of nascent nanoparticles through a series of characterization experiments and isothermal titration experiments which show the effects of pH in the context of particle self-assembly. Our findings indicate that thoughtful reformulation of PEG based, therapeutic PICs

[3]Part of this chapter has previously been published as an article in *Pharmaceutics*, proper attribution is as follows: *Fay, J.M.; Lim, C.; Finkelstein, A.; Batrakova, E. V; Kabanov, A. V PEG-Free Polyion Complex Nanocarriers for Brain-Derived Neurotrophic Factor*. *Pharmaceutics* ***2022****, 14, 1391, doi:10.3390/pharmaceutics14071391.*. Editorial decisions were made for formatting coherence, though the best efforts were made to keep the original text

with non-PEG alternatives can be accomplished without compromising the self-assembly of the PIC.

### 3.2 Introduction

Nanoformulations incorporating poly(ethylene glycol) (PEG) coronas have enabled immune evasion and the subsequent delivery of packaged therapeutic agents [102,238]. However, despite PEG's status as the "gold standard" stealth polymer, several issues have been identified. Accelerated clearance after repeat administration of stealth nanoparticles due to elicitation of antibodies has long been noted in the literature [154]. Furthermore, possibly due to the ubiquity of PEG in pharmaceutical products and consumer goods, much of the population has existing α-PEG antibodies [157], which could yield accelerated clearance of PEG based pharmaceutical agents or allergic reactions to critical therapies. Recent reports of possible allergic reactions to PEG in the Pfizer and Moderna vaccines against SARS-COVID-2 have brought an already expansive body of work to the forefront of the scientific consciousness [158–161,239]. PEG's prevalence in modern therapeutics and immunogenicity can combine to create a population level problem as an increasing number of widely distributed therapies incorporate PEG.

Many groups, our own included, have presented a number of novel nanoformulations whereby small molecules, nucleic acids, and proteins are protected by PEG coronas. In one particular example, we presented a polyion complex (PIC) comprised of poly(ethylene glycol)$_{113}$-b-poly(glutamic acid)$_{50}$ (PEG-PLE) and brain-derived neurotrophic factor (BDNF), termed Nano-BDNF PEG-PLE, as a therapeutic candidate for the treatment of neurodegenerative diseases [71,106]. BDNF has demonstrated great promise in treating animal models of several diseases including ischemic stroke [106], Alzheimer's disease [196], Parkinson's disease [71,240], etc. [202]. However, delivery of BDNF to the brain or across the blood-brain barrier (BBB) remains difficult, despite BDNF's ubiquity in the body. Endogenous trans-BBB transporters are quickly saturated, serum half life is short, and direct administration of BDNF to

the brain is attenuated by rapid efflux [71,186]. Nano-BDNF PEG-PLE nanoparticles effectively mediated the delivery of BDNF to its target receptor after intranasal to brain administration [71]. Additionally, we have demonstrated that Nano-BDNF PEG-PLE presents clear benefits over unformulated BDNF in the treatment of Parkinson's disease and ischemic stroke models in mice while preserving BDNF's circulation and residence in affected areas [71,106].

PEG is a long, flexible, and hydrophilic polymer which can comprise a corona which entropically exclude opsonins from penetrating into the nanoparticle and interacting with the therapeutic cargo [150,155,241]. Similar polymers have shown the same stealth effect allowing nanoparticles to circulate longer and minimizing unwanted clearance or surface fouling [168,169,174]. Work from our own lab and others has identified a variety of polymers which recapitulate the long, hydrophilic, and flexible nature of PEG [43,66,135,136,164,174,242]. In particular, our group has extensive experience utilizing poly(2-oxazolines) which present a useful platform for the production of functionalized block copolymers [171,174–176,178,181,243,244]. Convenient extension of polymers using living-cationic-ring-opening-polymerization (LCROP) enables precise control of block length and organization. Several advancements using polyoxazoline constructs to form drug carrying nanoparticles which demonstrate a stealth effect similar to PEGylated liposomes or PICs have been presented [135,171,174–178,180,181,244,245]. Similarly, other groups have used poly(sarcosine) (PSR), another flexible and hydrophilic polymer, to similar effect in non-fouling surfaces and stealth nanoparticles [162–164,166–168,246].

Here we introduce two types of PIC's similar to the original Nano-BDNF PEG-PLE but free of PEG. A nanoparticle comprised of BDNF and poly(sarcosine)$_{127}$-b-poly(glutamic acid)$_{50}$ (Nano-BDNF PSR-PLE) and a series of nanoparticles comprised of BDNF and poly(methyl-2-oxazolines)$_x$-*b*-poly(oxazolepropanoic acid)$_y$-*b*-(poly(methyl-2-oxazoline)$_z$ (PMeOx$_x$-PPaOx$_y$-PMeOx$_z$) (B1-5) (Nano-BDNF B1-5) are presented. We examine the formulation of several Nano-BDNF species and present two nanoparticles which are small and narrowly dispersed. We also

pursue a deeper understanding of the thermodynamics of association between BDNF and our various polymers as well as their behavior to demonstrate similarity between our three chosen polymers. Finally, we consider the application of the nanoparticles to cells stably transfected with tropomyosin receptor kinase B (TrkB), the primary receptor for BDNF [188], in order to assure that we do not prohibit activation of the desired target. In conclusion, we present two novel non-PEG formulations which demonstrate similarity to the original Nano-BDNF PEG-PLE formulation in morphology, activity, and thermodynamic behavior with potential for therapeutic effect in neurological diseases.

## 3.3 Materials and methods

### 3.3.1 Materials

Methyl triflate, 2-methyl-2-oxazoline, methoxycarboxyethyl-2-oxazoline, and piperidine were obtained from Sigma Aldrich. Dialysis membrane with molecular weight cut off [MWCO] 3,500 was purchased from Spectra/Pore. The following materials were purchased from Thermo/Fisher: WhatMan Anotop 0.025 μm non-sterile filters, 25 gauge 0.5 inch, long blunt needle (Strategic Applications inc.), 40% acrylamide 29:1, TEMED, Ammonium persulphate, Malvern Folded Cap Cells, DLS cuvettes (Malvern Pananalytical, Malvern, UK), radioimmunoprecipitation assay buffer, HALT protease and phosphatase inhibitor cocktail, SuperSignal™ West Pico PLUS Chemiluminescent Substrate, iBRIGHT prestained protein ladder, Geneticin™ Selective Antibiotic (G418 Sulfate), Neurobasal Media, B27 supplement, Glutamax 100X, acetonitrile, potassium carbonate, diethyl ether, methanol, agarose tablets, and sodium hydroxide. BDNF was obtained from Novoprotein which later became Bon Opus Biosciences. PSR-PLE was obtained from Peptide Solutions LLC. Colorado calf serum was obtained from the Colorado Serum Company. We obtained Bio-Safe Coomassie Stain and Native Sample buffer for protein gels 4X from Bio-Rad Hercules, CA, USA.

### 3.3.2 Polymer synthesis

Under dry and inert conditions achieved in MBraun glovebox with N2 atmosphere, 1 molar equivalent of the polymerization initiator, methyl triflate (MeOTf), and 10 or 30 molar equivalents of 2-methyl-2-oxazoline (MeOx) were dissolved in 2 mL of acetonitrile (ACN). The mixture was sealed and moved to react in a microwave for 15 min at 150 W and 130 °C. After cooling, the solution was returned to dry and inert conditions where 10 or 30 molar equivalents of the monomer for the second block, methoxycarboxyethyl-2-oxazoline (MestOx), were added. The mixture was sealed and moved to the microwave following the same procedure as above. After cooling, the procedure was repeated with 10 or 30 molar equivalents of MeOx. Polymerization was terminated by adding 3 molar equivalents of piperidine and microwaving for 1 hour at 150 W and 40°C. An excess of $K_2CO_3$ was added to ensure complete cessation of the reaction. The solution was stirred overnight, filtered through a 0.45 μm filter, precipitated in diethyl ether, collected, and freeze dried. The product was dissolved in methanol and 0.1 N NaOH was added to 1 molar equivalent NaOH with the methyl ester group on the poly(MestOx) block of the copolymer to convert to PPaOx. The resultant solution was allowed to react for 2 hours at 80°C. The solution was then dialyzed against distilled water using a dialysis membrane (Spectra/Pore; molecular weight cut off [MWCO] 3,500), product was freeze dried for storage until use.

### 3.3.3 Polymer characterization by $^1$H NMR

Copolymers were suspended in deuterated methanol (MeOD) and $^1$H nuclear magnetic resonance (NMR) spectra were obtained using an INOVA 400 NMR machine. Data were analyzed using MestReNova (11.0). Spectra were calibrated using the MeOD solvent signal at 4.78 ppm. The number average molecular weight was determined by calculating the ratio of the initiator and each repeating unit.

### 3.3.4 Preparation of PIC by manual mixing

The formulation was manufactured as described previously in Jiang et al. [71] Briefly, a concentrated solution of a block copolymer (0.1, 1, or 10 mg/mL) in a specified buffer was added dropwise to the BDNF solution ([BDNF] =1 mg/mL); each drop interspersed with a gentle vortex for 10 seconds. The solution was then diluted to the desired concentration using the buffer and vortexed for another 30 seconds, after which the solution was incubated for 30 min at room temperature.

### 3.3.5 Preparation of PIC using a microfluidic mixer

Separate solutions of BDNF and copolymer in a specified buffer were prepared at 2X the desired end concentrations. We used either phosphate buffered saline (PBS) (10 mM $NaH_2HPO_4$, 1.8 mM $KH_2PO_4$, 2/7 mM KCl, 137 mM NaCl, pH 7.4)) or lactate buffered Ringer's solution (LR) (100 mM NaCl, 3.7 mM KCl, 1.3 mM $CaCl_2$, 1.2 mM $MgCl_2$, 28 mM $NaHCO_3$, 20 mM $NaC_3H_5O_3$, pH 7.4). The BDNF and copolymer solutions were loaded into 1 mL syringes which were then connected to the microfluidic mixer apparatus (**Figure 3.1**) described previously [71]. The solutions were each injected into the mixer at 50 µL/min to mix at a 1/1 volume ratio. The first 100 µL were discarded to allow only properly mixed samples to be collected before experiments.

### 3.3.6 Nanoparticle size, dispersity, and zeta potential

Nano-BDNF was prepared at the desired $Z_{-/+}$ ratio. The particle size and polydispersity index (PDI) were analyzed by dynamic light scattering (DLS) using the Zetasizer Nano ZS (Malvern Instruments Ltd.) with a scattering angle of 173° at RT. For all DLS measurements, the BDNF concentration was 0.05 mg/mL. Unless specified otherwise, the DLS sizes are reported as intensity weighted (z-averaged) diameters. The nanoparticle tracking analysis (NTA) was performed using the NanoSight NS500 (Malvern Panalytical) or Zetaview (ParticleMetrix). All samples were prepared at BDNF concentration 0.005 mg/mL. For the measurements of particle

size and distribution using the NanoSight NS500, the samples were stored on ice and allowed to return to RT prior to use. Readings were taken under flow for 60 s at 20 μL/s using the syringe pump. For the measurements of particle size, distribution, and zeta potential using the Zetaview, the samples were prepared at BDNF concentration 0.005 mg/mL and analyzed either immediately or incubated at RT for various times. Before the measurements, these samples were diluted 10X. Both NanoSight NS500 and Zetaview are reported as number-weighted diameters.

Transmission electron microscopy (TEM) measurements were obtained using samples prepared using the microfluidic mixer at $Z_{-/+} = 5$ in 10 mM phosphate, pH 7.4. Images were taken using a ThermoFisher Talos F200X at an accelerating voltage of 200kV in TEM mode. Samples were drop cast on a TEM formvar carbon grid then stained using aqueous 2% Uranyl Acetate solution. Image processing was performed using Velox then analyzed using ImageJ.

### 3.3.7 Horizontal agarose gel electrophoresis (HAGE)

Agarose gels (0.5 % wt.) were prepared using 20 mM MOPS buffer, containing 2 mM sodium acetate, pH 7.4 which was also used as the running buffer. Nano-BDNF was manually prepared as described above in LR solution, at a concentration of 0.075 mg/mL and volume of 18 μL. The sample was diluted 2X with Native Loading Buffer, pH 6.8 (Bio-Rad) and 35 μL of the final solution were loaded into the wells. Electrophoresis was performed with a constant voltage of 80 V for 1 hour. The gel was washed in deionized water 2X and stained using Biosafe Coomassie Stain (Bio-Rad) for at least 1 hour. Destain was performed using DI water until the gel was mostly clear. Images were taken using the FluorChem E machine (ProteinSimple).

### 3.3.8 Isothermal titration calorimetry (ITC)

BDNF and polymer solutions were dialyzed against 10 mM phosphate, pH 7.4, 10 mM phosphate, pH 5.8, or 10 mM sodium acetate, pH 5.0 overnight with at least two buffer changes. BDNF was diluted to 10 μM and the polymers were diluted to the indicated concentrations then stored on ice. Samples were loaded into the MicroCal PEAQ-ITC machine (Malvern Panalytical)

and stored at 4°C in the tray. The cell and syringe were kept at 25°C and the experiment was performed at 25°C. The polymer was added in 2 μL steps except for the first addition which was 0.2 μL. The cell was allowed to incubate for 3 minutes between each step. Data analysis was performed using the MicroCal ITC analysis software in Origin.

### 3.3.9 Potentiometric titration of polymers

Polymers were solubilized in 10 mL of nitrogen flushed deionized $H_2O$ and a 1.1 molar equivalent aliquot of 1.1 M HCl was added to the 10 mL of polymer solution at a concentration of 500 μM ionizable units. 50 mM NaOH was added in 10 μL increments, the pH was allowed to stabilize (~1 min dwell time), and readings were taken using an Oaklon ion 700 pH meter with Fisherbrand™ accumet™ glass electrode.

### 3.3.10 Cell culture

NIH 3T3 cells stably transfected with TrkB (NIH 3T3 TrkB) were cultured in GlutaMax DMEM supplemented with 10% calf serum, G418 (100 μg/mL), penicillin (100 μg/mL), and streptomycin (100 μg/mL). Cells were cultured at 37°C in a humidified $CO_2$ (5%) incubator.

### 3.3.11 BDNF stimulation

The NIH 3T3 TrkB cells were plated at $5x10^5$ cells/well on 6-well plates 24 hours before treatment. Five hundred nanograms of BDNF or equivalent amount of Nano-BDNF was added to the wells then incubated for 5 min at 37°C in the incubator. Formulations were prepared via microfluidic mixing at $Z_{-/+} = 5$ in cell culture media. Media was removed and replaced with radioimmunoprecipitation assay buffer with HALT™ proteinase and phosphatase inhibitors (ThermoFisher), then the plate was moved to 4°C and agitated using a plate shaker. Material was collected and separated into supernatant and pellet. The supernatant was measured for protein concentration by the BCA assay, then 25 μg of protein was loaded into each well and electrophoresed through a 12.5% SDS-PAGE gel, transferred to PVDF membrane, and visualized via horseradish peroxidase (Supersignal™ West Pico Plus Chemiluminescent Substrate)

following standard western blotting procedures. The following antibodies were used to visualize their cognate proteins: Phospho-p44/42 MAPK (Erk1/2) (Thr202/Tyr204) Antibody (CST 9101), p44/42 MAPK (Erk1/2) Antibody (CST 9102), Anti-Rabbit HRP (CST 7074S).

## 3.4 Results

### 3.4.1. Manufacture and characterization of poly(2-oxazoline) block copolymers

Previous work demonstrated that BDNF readily associated with the negatively charged PEG-PLE diblock copolymer to form stable nanoparticles [71,106]. Pursuant to our objective of replacing PEG with alternative polymers, we produced four block copolymers using LCROP as described previously [247] (**Figure 3.2**). The new polymers were designed as anionic A-B-A type block copolymers composed of hydrophilic uncharged PMeOx (A block) and negatively charged PPaOx (B block). The amounts of monomers, ten or thirty in each step, added during synthesis were selected to produce four variations of PMeOx-PPaOx-PMeOx with the following patterns: short-short-short, short-long-short, long-short-long, and long-long-long (**Figure 3.4**). Structure and length ratio were confirmed via $^{1}$H-NMR (**Figure 3.2, 3.3**). As an alternative approach to formulating BDNF, we used an anionic PSR-PLE di-block copolymer that was available commercially with a similar structure to the original PEG-PLE polymer used in our previous study (**Figure 3.4**).

### 3.4.2. Nano-BDNF candidate winnowing

The length and structure of the copolymer blocks can drastically affect self-assembly of block copolymers with proteins or other cargo for delivery [11]. In addition, the mode of mixing is of paramount importance for formulation of PIC that can form non-equilibrium, slowly transitioning aggregates [65,66]. This is characteristic of PIC's that contain proteins or peptides, such as BDNF, that can self-aggregate because of intermolecular hydrophobic interactions or hydrogen bonding. To quickly identify which block copolymers are most suitable for formulation, we adopted a winnowing strategy. Towards that end, we formulated Nano-BDNF in

10 mM Hepes, pH 7.4 to interrogate block copolymer-protein interaction and identify which copolymers yield relatively small, narrowly dispersed particles.

The ionic strength, salt identity, and pH are all expected to strongly affect the formation of the PIC particles. Initial formulation in minimal conditions of only HEPES buffer allows us to identify which copolymers form stable PICs with BDNF in the near absence of salts. We initiated by manually formulating Nano-BDNF in 10 mM HEPES, pH 7.4, by mixing each copolymer and BDNF. In addition to the effects of buffer components, the ratios in which copolymer and protein are mixed may strongly affect the formation of particles in terms of size, dispersity, stability, etc. [71] The mixing ratio between carboxyl groups of copolymer and amino groups of BDNF is defined here as follows:

$$\boldsymbol{Z_{-/+}} = \frac{[\boldsymbol{Copolymer}]*(\boldsymbol{degree\ of\ polymerization\ of\ ionic\ block})}{[\boldsymbol{BDNF}]*(\boldsymbol{44\ positive\ charges})}, \qquad (1)$$

Each PIC was formulated at several $Z_{-/+}$ ratios (1, 2, 5, 10). We assessed the size and dispersity of the particles using DLS over two days. The poly(2-oxazoline) tri-block copolymers showed major differences in their propensity to associate with BDNF. While we observed particle formation in all cases, copolymers B2 and B5 yielded particle populations that were generally smaller and more uniform (**Figure 3.5-3.17**). In both cases the particle sizes were under 200 nm and the PDI was from 0.2 to 0.3 (except for 24 h time point for B2 that show an unexpectedly high PDI). Formulation with B1 formed larger aggregates (200 to 350 nm) and B3 produced highly disperse particles (PDI from 0.5 to 0.8). Therefore, we disregarded those copolymers in future studies and focused on B2 and B5. We noted that the formulations containing B2 and B5 (at several $Z_{-/+}$ ratios 2, 5, 10) were variable and poorly reproducible, indicating the capricious nature of the manual mixing. Nano-BDNF formulated with PSR-PLE was also not greatly amenable to the formulation at this initial stage as mixing formed highly disperse PIC particles (**Figure 3.5, Figure 3.6**). However, we continued optimization using PSR-PLE due to similarity to the structure of PEG-PLE used in Jiang, et al [71].

The effects of low molecular-mass electrolytes on PICs have been noted in the literature such that different salts can affect particle formation, size, and dispersity [11]. To assess these effects in our systems we opted for the simple addition of 150 mM NaCl to a 10 mM HEPES, pH 7.4 solution. Nano-BDNF was prepared using B2, B5, and PSR-PLE via manual mixing. We did not observe a decisive advantage using any one copolymer under these conditions, B2 yielded small particles with very high polydispersity, PSR-PLE yielded very large but narrowly disperse particles, and B5 was a mix (**Figure 3.18**). Most notably, the particles formed at higher Z-/+ ratios using B5 and PSR-PLE (**Figure 3.16 E, F, I**) were smaller and less dispersed than in the absence of added salt. It may be that the addition of NaCl allowed ion exchange and facilitated packing. The number weighted particle size for B2 was negligible compared to the intensity weighted particle size indicating only small number of aggregates existed that in the presence of salt (**Figure 3.17 A, B, C**).

To select the best copolymers to continue optimization, we altered formulation methodology to include microfluidic mixing, which has yielded decreased particle size and dispersity in past publications [71,248,249]. B2, B5, and PSR-PLE were incorporated into Nano-BDNF using microfluidic mixing in 10 mM HEPES, pH 7.4 with no elementary salt added. We measured size and dispersity using DLS and NTA (**Figure 3.19**). Using microfluidic mixing we generally observed smaller and less disperse particles (**Figure 3.19**) when compared to manual formulation in the same buffer (**Figure 3.5-3.15**). PSR-PLE particles formed using this technique considerably decreased the size and narrowed dispersity compared to manual mixing (**Figure 3.5**). This result is consistent with previous work where Nano-BDNF formulated with PEG-PLE yielded smaller, more narrowly disperse particles when formulated using the same microfluidic mixer. Considering the totality of our results (**Figure 3.5-3.19**) we elected to pursue formulation with PSR-PLE and B5. These two nanoparticle formulations, like the original PEG-PLE based Nano-BDNF, had nearly spherical shape as determined by TEM (**Figure 3.20**).

### 3.4.3 Preparation of Nano-BDNF particles suitable for injection

The final stage of optimization was to prepare Nano-BDNF in isotonic solutions formulated with saline that are commonly used for in vivo injections. We selected PBS and LR for formulation and prepared Nano-BDNF in these buffers using copolymers B5 and PSR-PLE via microfluidic mixing. We analyzed the resultant particles size and distribution right after preparation (**Figure 3.21**) and over time (**Figure 3.22**). Right after mixing, B5 formed the smallest, least disperse particle population when formulated in PBS at $Z_{-/+} = 5$. However, the formulations in the LR were still promising since Nano-BDNF B5 at $Z_{-/+} = 2$ and Nano-BDNF PSR-PLE at $Z_{-/+} = 5$ both yielded particles with sizes less than 120 nm and with RSD under 30. When size and dispersity were measured over time, we found the LR solution yielded smaller sizes and narrower dispersity for both Nano-BDNF B5 and Nano-BDNF PSR-PLE over several hours using the NTA Zetaview (**Figure 3.22**). Therefore, we used LR buffer for the next experiments.

### 3.4.4 HAGE visualization of Nano-BDNF

After optimizing the formulation of Nano-BDNF PSR-PLE and Nano-BDNF B5, we visualized their formation and migration through an agarose gel matrix. Jiang, et al. [71] demonstrated that Nano-BDNF PEG-PLE, formulated at excess of polyanion, yielded complexes with a negative overcharge that migrated BDNF towards the cathode despite the protein's intrinsic net positive charge. Nano-BDNF formulated with PSR-PLE and B5 behaved similarly, such that little or no migration was observed at $Z_{-/+} < 5$, whereas higher $Z_{-/+}$ ($Z_{-/+} = 5, 10$) formulations yielded distinct bands migrating towards cathode (**Figure 3.23**). Notably, as in Jiang, et al. [71] the free BDNF or Nano-BDNF complexes at $Z_{-/+} < 1$ remained in the wells with little apparent movement towards anode. We believe that the HAGE approach is unable to distinguish the free protein and complexes formed at deficiency of the copolymer because it is known that BDNF can bind to agarose and is also prone to aggregation [216]. In the complexes formed at lower mixing ratio, the BDNF molecule may not be completely masked by the bound

copolymer and partially exposed. On the other hand, the mobility of the complexes formed at higher $Z_{-/+}$ may indicate not only the overcharging but also complete masking of the BDNF by the copolymer that inhibits the aggregation and/or binding to agarose.

### 3.4.5 Zeta-potential characterization of Nano-BDNF

As an unambiguous method for characterization of Nano-BDNF complexes at both low and high mixing ratios, we used the NTA Zetaview machine which directly measures the particle size and zeta potential in the same samples, and additionally reports the calculated dispersity as well as concentration of the particles (**Figure 3.24**). For this study we used three block copolymers, PEG-PLE, PSR-PLE and B5, and prepared the PICs by the microfluidic mixing. The overall pattern of behavior of the complexes in 10 mM sodium phosphate, pH 7.4 was very similar for all three copolymers. We were able to observe the formation of the nanosized complexes at $Z_{-/+}$ as low as 0.25 (**Figure 3.24 A, B**). These complexes were already net negatively charged at low $Z_{-/+}$ ratio but increased in the absolute value of the charge with further addition of anionic copolymer (**Figure 3.24 C**). For all three copolymers, as the $Z_{-/+}$ increased above 0.5, the concentration of the particles sharply decreased by over 10 times (with no precipitation observed) (**Figure 3.24 D**). This phenomenon could be explained by the increased binding of the copolymer to BDNF upon increase of $Z_{-/+}$, which promotes self-assembly of PICs with higher molecular masses and higher aggregation numbers of BDNF and copolymer. In contrast, at low $Z_{-/+}$ we may be observing formation of nascent complexes which have lower molecular masses and aggregation numbers. This assumption is only partially supported by the particle size measurements (**Figure 3.24 A**). While there was a distinct trend for increases in the sizes of Nano-BDNF PEG-PLE and B5, no increases in the particle size were apparent in the case of PSR-PLE. However, the discussed transitions in the PICs may be masked by the shape effects which are not accounted for by our size measurement technique.

The self-assembly and overcharging effects in nano-BDNF must be dependent on the degree of ionization of the reacting anionic block copolymer. To test this, we conducted the same

experiment at pH 5.0 (**Figure 3.24 E-H**) using a 10 mM sodium acetate buffer, where the polyanions have lower ionization degree (**Figure 3.25, Table S1**). In this case, the complexes formed at $Z_{-/+}$ = 0.25 appeared to have positive charge, which gradually decreased as the amount of the anionic copolymer increased (**Figure 3.24 G**). Interestingly, there was an increase in the concentration of the nanoparticles, most distinct in the cases of PEG-PLE and PSR-PLE, which suggests transition to PICs with lower molecular mass and aggregation numbers, i.e., opposite to what is seen at pH 7.4.

### 3.4.6 Effects of pH on polymer ionization

Understanding the effects of pH on our polymers is critical in the characterization of our complex systems. We characterized the degree of ionization for each polymer and calculated the $pK_a$ values to better understand the effects of our perturbations of the system. We fitted the modified Henderson Hasselbalch equation using the least squares fit in Microsoft Excel to our degree of ionization data and thus obtained predicted values at pH 5.0, 5.8, and 7.4.

$$\alpha(pH) = \frac{1}{10^{n(pK_a - pH)} + 1}, \quad (2)$$

Where α is the degree of ionization, $pK_a$ is an effective $pK_a$ and n is the Hill coefficient [250,251].

After obtaining the titration curve, we identified a region of low ionization which would serve as an effective point zero for tracking the molar ratio of added base (γ) as compared to the concentration of ionizable units ($c_m$):

$$\gamma = \frac{[NaOH]}{c_m}, \quad (3)$$

The $c_m$ is the concentration of the carboxylic groups from the repeating units of the anionic block copolymers the numbers of which were previously determined by the $^1$H NMR spectra (B5) or provided by the manufacturer (PEG-PLE, PSR-PLE).

We used the relationship (3) whereby we can relate the degree of ionization (α) to (γ) as comes from charge neutralization:

$$\alpha = \gamma + \frac{[H^+]-[OH^-]}{c_m}, \quad (4)$$

This was then fitted using a least squares analysis using the relationship between pH and α (2). Results can be found in **Figure 3.25** and **Table 3.1.**

### 3.4.7 Thermodynamic analysis of BDNF-polyanion association

To further investigate the phenomena observed in the previous experiment, we used ITC to measure the heat released as we added copolymer to BDNF. Our experiments were designed to keep the BDNF concentration constant as the anionic block copolymer increased step by step. The copolymer concentrations were adjusted to keep the number of polyacid repeating units uniform across different copolymers. Thus, the x-axis in our thermograms correlates to the $Z_{-/+}$ ratio rather than the molar ratio. For clarity, $Z_{-/+}$ ratio equal 1 corresponds to the polyanion/BDNF molar ratio 0.88 for both PEG-PLE and PSR-PLE and 1.63 for B5 due to the differences in the degrees of polymerization of the polyanion blocks of these copolymers (**Figure 3.2**). Addition of each copolymer dropwise to a well containing BDNF yielded exothermic reactions (**Figure 3.26**). Notably, none of the integrated ITC curves had a simple sigmoidal shape that would be expected for a simple single set of identical sites (SSIS) model for the molecules binding [252]. In fact, for each of the copolymers there was a sharp minimum observed at $Z_{-/+}$ between 0.25 and 0.5. The heat effects level off to the baseline at $Z_{-/+}$ between 0.5 and 0.8. Notably, the pattern of heat release is like what might be expected of multiple ligands binding a transition metal [252]. In our system, this curve might be due to initial formation of nascent PICs formed at low $Z_{-/+}$ which further self-assemble into mature Nano-BDNF nanoparticle as more block copolymer is added.

To further validate the relationship between these processes and the charge ratio of the reacting components in the mixture, we again decreased the pH value of the system, keeping all other parameters the same. Although the overall shape of the curves did not change, at pH 5.0 the minimum in integrated ITC curves shifted to higher $Z_{-/+}$ between 0.5 and 0.8 and the

saturation region to $Z_{-/+}$ between 1.5 and 2.0 (**Figure 3.27**, Also see **Table 3.2** for comparison of plot features at different pH). The polyanionic blocks (PLE and PPaOx) in our block copolymers undergo ionization in the range from pH 4 to pH 8 (**Figure 3.25, Table 3.1**). The shift of the position of the minimum in integrated ITC curves is consistent with a decrease in the amount of ionized carboxylic groups in the reacting polyacids that takes place at lower pH, and is indicative of the electrostatic nature of the polyion coupling reactions in this $Z_{-/+}$ range. Interestingly, at pH 5.8 no such shift in the integrated ITC curves minimum and level off regions was observed (**Figure 3.28**), which is probably explained by cooperative stabilization of the PICs as will be discussed below. The overall magnitude of the exothermic heat effects seen at the integrated ITC curves minima differed for block copolymers and were notably smaller for B5, for which the heat release dramatically decreased at lower pH (**Table 3.2**).

### 3.4.8 Stimulation of the TrkB pathway

The potential therapeutic application of BDNF is premised on the effective stimulation of the TrkB kinase pathway which effects neuropotentiation, neuron survival, and repair [188,202]. Nanoformulation entails the possibility of making BDNF unavailable to the receptor TrkB. We applied Nano-BDNF to NIH 3T3 cells stably transfected with TrkB and measured the phosphorylation of a downstream kinase, extracellular signal-regulated kinase 1/2 (Erk). BDNF, Nano-BDNF B5 $Z_{\pm}$=2, and Nano-BDNF PSR-PLE $Z_{\pm}$=5 stimulated the phosphorylation of Erk compared to the total Erk present in the cell (**Fig 3.29**). The availability of BDNF was acceptable and indicates that neither of our novel Nano-BDNF formulations inhibits TrkB signaling.

## 3.5 Discussion

The well-established immunogenicity of PEG and the high frequency of endogenous α-PEG antibodies indicate a dire need for alternative drug encapsulation technologies with comparable or lower immunogenic profiles [154,157–160]. A recent study identified anaphylaxis

caused by the COVID-19 vaccines which was disproportionally prevalent in women, most likely influenced by higher exposure in household products containing PEG [161,239]. Both poly(sarcosine) and poly(methyl-2-oxazolines) have demonstrated physical, protective, and stealth characteristics similar to PEG [43,164,167–169,174,175,246]. Critically, these alternative polymers do not currently have such extensive applications across several industries which limits exposure for most of the population. Both poly(sarcosine) and poly(oxazolines) are relatively simple to manufacture and functionalize or are commercially available. Poly(oxazolines) in particular are a broad class of molecules that allow for hydrophobic, charged, and otherwise reactive moieties to be included in polymer structures [171,174,178,253]. Other work has taken advantage of the variety of poly(oxazoline) functional groups including as the stealth portion of the nanoparticles [171,175,177,178,247,254]. Additionally, LCROP allows excellent control over the length and order of blocks which are easily assessed using $^{1}$H NMR to determine structure as demonstrated in the results section.

The original Nano-BDNF formulation using PEG-PLE, described in Jiang, et al. and Harris, et al., demonstrated promising effects in disease models [71,106]. Indeed, the simple self-assembly made similar nanoparticles especially persuasive to attempt to reformulate. Our motivation was not necessarily to improve over the prior PEG-PLE based composition but rather to explore and provide reasonable alternatives in which PEG is substituted by a similarly non-fouling and biocompatible polymer. Our candidate molecules with non-PEG protective blocks were suggested by their similarity to original formulation, especially in the context of the associative block. A winnowing strategy eliminated the polymers which yielded poorly formed or inconsistent particles and we found that optimal particles were formed in the same buffer as Nano-BDNF PEG-PLE.

We implemented microfluidic mixing throughout our study to prepare the complexes. The small-scale batch formulation by manual mixing carries the inherent drawback of batch-by-batch variation due to non-uniform mixing. We overcome this limitation by extensive use of

microfluidic mixing which, in addition to improving reproducibility, decreases size and narrows dispersity by mixing the components in a controlled manner. Microfluidic mixing has become an increasingly common technique, especially in formulation of lipid nanoparticles [249]. Furthermore, in our experience, the dispersity of PICs is improved through application of this technology and consistency across batches is also improved [71]. Here, our choice of a reusable, simple, cheap, in house designed mixer indicates that even low-level implementation of these technologies can improve the consistency and quality of formulations.

Nanoformulation carries inherent risk of deactivation of an intended therapy, especially for signaling molecules which must access and bind to a target receptor. Here we demonstrate that despite inclusion of the BDNF into the PICs at the excess of the copolymers, both our re-formulated Nano-BDNF variants remain active with respect to TrkB signaling pathway in cells. This has been previously reported by us for Nano-BDNF PEG-PLE and the mechanism was demonstrated [71]. Specifically, we have previously shown that while the complexes remain stable in the presence of salt and serum proteins (human serum albumin, IgG, secreted IgA), the TrkB receptor can readily abstract the BDNF molecule, presumably due to higher affinity to the BDNF active site compared to the anionic block copolymer. In this case, TrkB can access and bind BDNF which yields a signaling cascade that we monitor via Erk phosphorylation. We believe that we observe activation of the receptor with the reformulated Nano-BDNF particles that proceeds via similar mechanism as was reported before [71]. Moreover, based on prior molecular modeling analysis [71], the polyanion binds to the same active site as the TrkB thereby competitively masking this site in the absence of the specific receptor. Therefore, this class of PICs is particularly well suited for delivery of BDNF and possibly other neurotrophins. Non-covalent interactions allow some reorganization and may enable a receptor with strong, specific binding to access the signaling molecule. Conversely, the preferential binding with the anionic blocks of the copolymers protects from opsonization [71,106].

Our study also provides new insight on the complexation of the BDNF with anionic block copolymers. Using the highly efficient, multi-utility nanoparticle tracking technique, we confirm the formation of the PICs at the deficiency of the anionic block copolymers. Based on the patterns of the particle zeta potential and concentration, we propose that these complexes form initially as the nascent species that reorganize into mature Nano-BDNF particles as the amounts of the added anionic block copolymers ($Z_{-/+}$ ratio) increase. An independent ITC experiment confirms the distinct processes at lower and higher $Z_{-/+}$ ratios. The processes of polymer coupling at the block copolymer deficiency at lower $Z_{-/+}$ are strongly exothermic which results in appearance of the deep minima in the integrated curve. This exothermic effect vanished as the amount of the block copolymer increased at higher $Z_{-/+}$. The data from our ITC experiments were not easily fit by SSIS models or a two-step model like DNA condensation [252,255,256]. However, the ITC pattern observed for complexation of net cationic BDNF with our polyanions appears to qualitatively mirror that previously observed for the binding of DNA with polycations as reported by us and Kataoka [255,257].

There are, however, notable differences. First, our systems display strongly exothermic effects while the DNA and polycation binding is endothermic. Second, the magnitude of our effect, although varying for different polyanions, is at least one order of magnitude greater than the effects observed for DNA and polycation binding. The small enthalpic effects observed for DNA and polycation binding are typical for entropy driven processes due to the counterion release [257], and could also be compounded by the conformational transitions due to the DNA condensation [255]. In our case, BDNF displays 44 unique, positively charged Lys and Arg residues on its exterior and based on the prior molecular modeling binding of the polycarboxylic acid to it involves formation of multiple hydrogen bonds [71]. The hydrogen bond formation is an exothermic process which is consistent with our observation [258].

Unsurprisingly, the complexation is dependent on pH which alters ionization of the polyacid. In the supplement we provided the titration results and ionization characteristics of all

three anionic block copolymer used in our work. As we decrease the pH to 5.0, the degree of ionization decreases dramatically, and the characteristics of the complexes change. By the nanoparticle tracking technique we observe formation of positively charged species at low amounts of the added anionic block copolymers ($Z_{-/+}$ ratio). We also observe changes in the ITC patterns where the amount of the block copolymer required in the exothermic binding increases. The greatest effects appear with the poly(oxazoline) block copolymer B5, which has the highest value of $pK_a$. This suggests strong effect of the polyanion ionization in the formation of Nano-BDNF complexes. However, we would like to point out that the direct quantitative relation of the degree of ionization of the weak polyelectrolytes to polyion complexation should be done with caution because of the cooperative stabilization of the ionized forms [259]. Specifically, in the discussed pH range the BDNF molecule is positively charged, and binding to it can stabilize the ionized forms of the polycarboxylic acids even at low pH (a phenomenon we cannot demonstrate here by potentiometric titration because of prohibitive costs). This may explain why we do not see much change in the ITC results at pH 5.8. Most importantly, our current findings suggest that by carefully selecting pH during the manufacturing processes, the properties of polyelectrolyte formulations of neurotrophins can be optimized. Overall, deeper understanding of the physics which dictate nanoparticle formation and how varying conditions affect formulation can yield valuable insight to how future polyelectrolyte complex formulations are designed or reformulated.

In conclusion, we demonstrate the suitability of two novel polymers to substitute for PEG-PLE in reformulations of Nano-BDNF that are free of PEG. Particles of similar size and properties are formed through simple, microfluidic mixing. Overall, we demonstrate that by preserving the specific attributes of the associative and protective blocks, we can produce nanoparticles that behave in a similar manner. The new results are instrumental for the design of future formulations of neurotrophins for clinical use

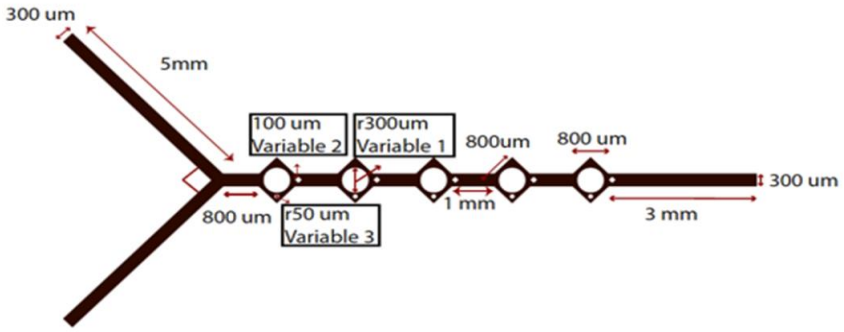


**Figure 3.1 Schematics showing configuration and dimensions of the mixer used for microfluidics formulation.**

Reproduced with permission from Jiang et al. [71]: Much of our work is dependent on the application of an in house designed microfluidic mixer by which we can exert control over the rate of mixing through the device. We introduced this device in the previous report of the precedent work [71] where we observed much improved formulation of Nano-BDNF PEG-PLE.

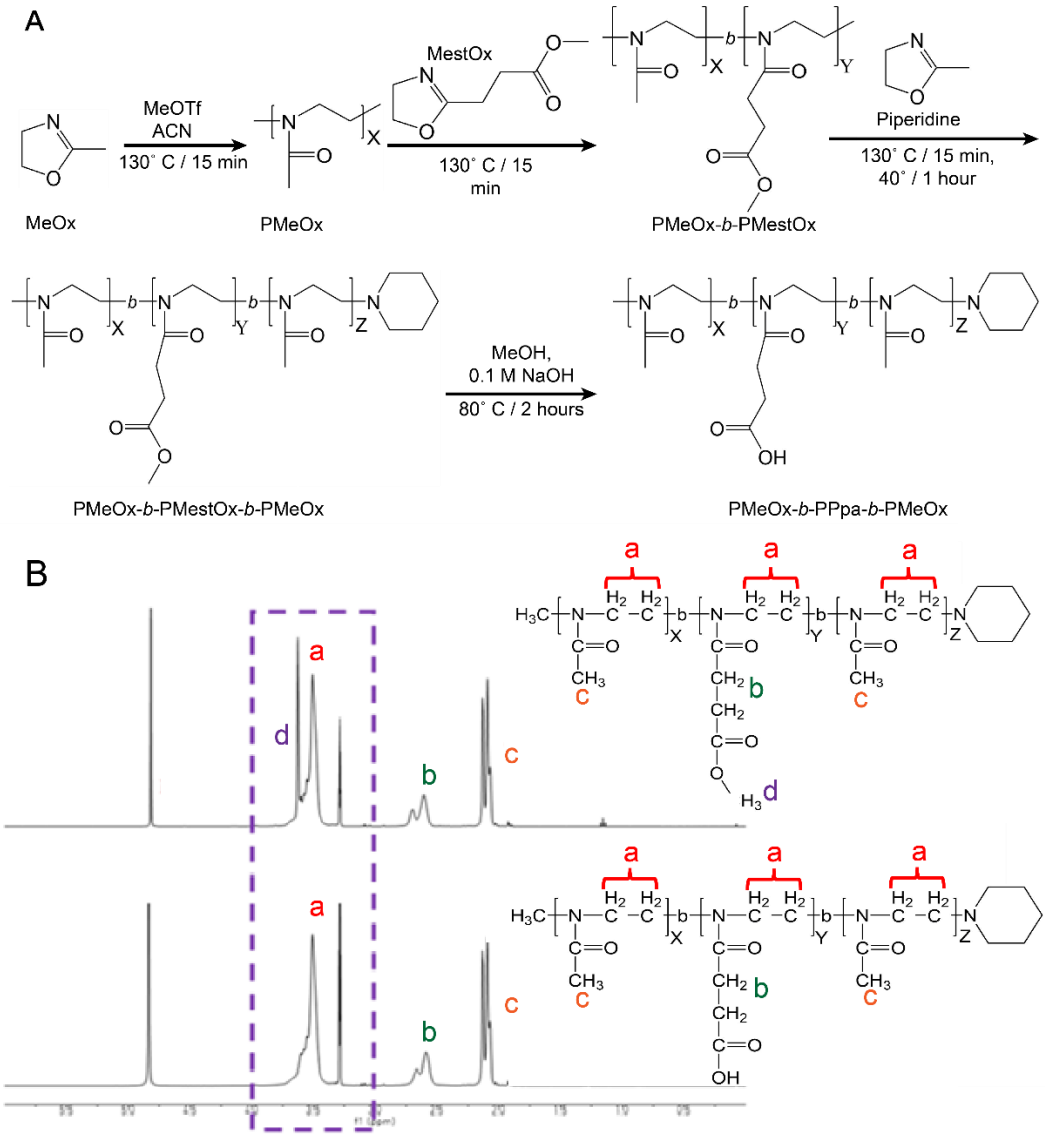


**Figure 3.2 Polymer synthesis and characterization.**

**(A)** Synthesis scheme for the preparation of poly(2-oxazoline) tri-block copolymers via LCROP. Briefly, the initiator, MeOTf, was reacted with MeOx in ACN for 15 min at 130°C followed by sequential polymerization of subsequent blocks in ACN for 15 min each then termination with piperidine reacted for 1 hour at 40°C. The protective methyl group on the MestOx block was removed by reacting with NaOH in MeOH for 2 hours at 80°C. **(B)** $^{1}$H-NMR peak assignments of PMeOx-*b*-MestOx-*b*-PMeOx and PMeOx-*b*-PPaOx-*b*-PMeOx. Note the elimination of peak **(d)** representing the deprotection of the hydroxyl group on the middle block. Peaks (a,b, and c)

present no change during deprotection. Spectra of the four polymers produced can be found in **Figure 3.3**.

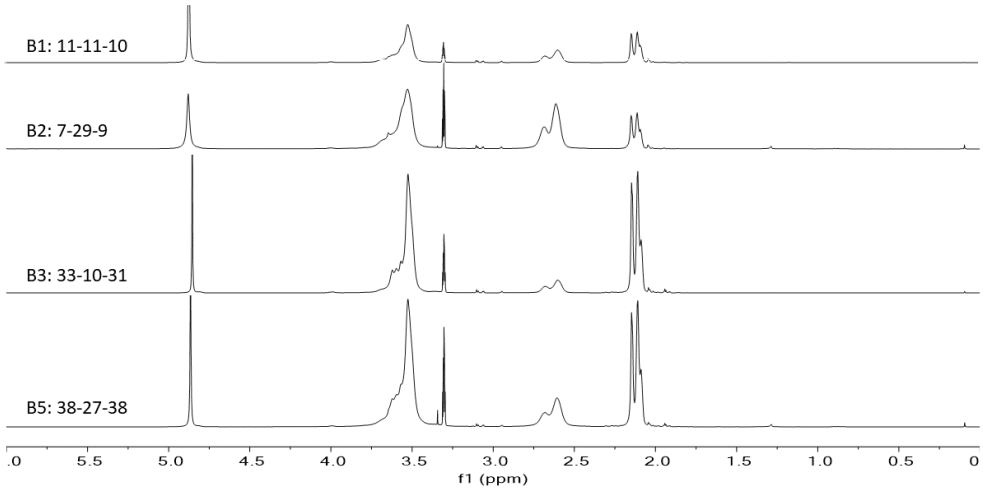


**Figure 3.3 $^{1}$H NMR spectra of the four PMeOx-PPaOx-PMeOx polymers.**

Polymers were dissolved in deuterated methanol and analyzed in a INOVA 400 NMR machine.

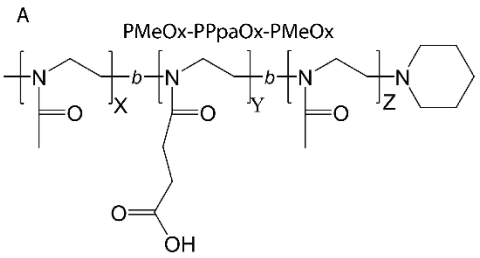


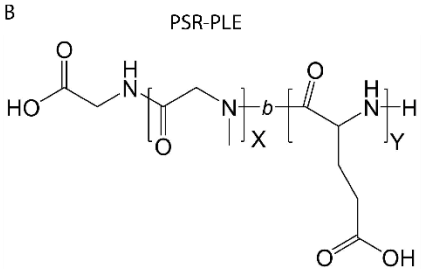


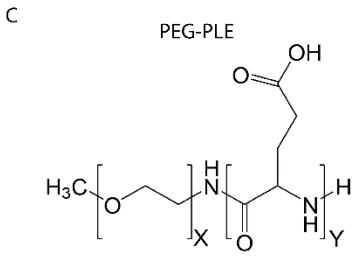


D

| Polymer Blocks | Designation | X | Y | Z | MW |
|---|---|---|---|---|---|
| PMeOx-PPpaOx-PMeOx | B1 | 11 | 11 | 10 | 3358 |
| | B2 | 7 | 29 | 9 | 5507 |
| | B3 | 33 | 10 | 31 | 7183 |
| | B5 | 38 | 27 | 38 | 10321 |
| PSR-PLE | | 127 | 50 | NA | 12800 |
| PEG-PLE | | 113 | 50 | NA | 13000 |

**Figure 3.4 Block copolymer structures (A-C), and molecular characteristics (D).**

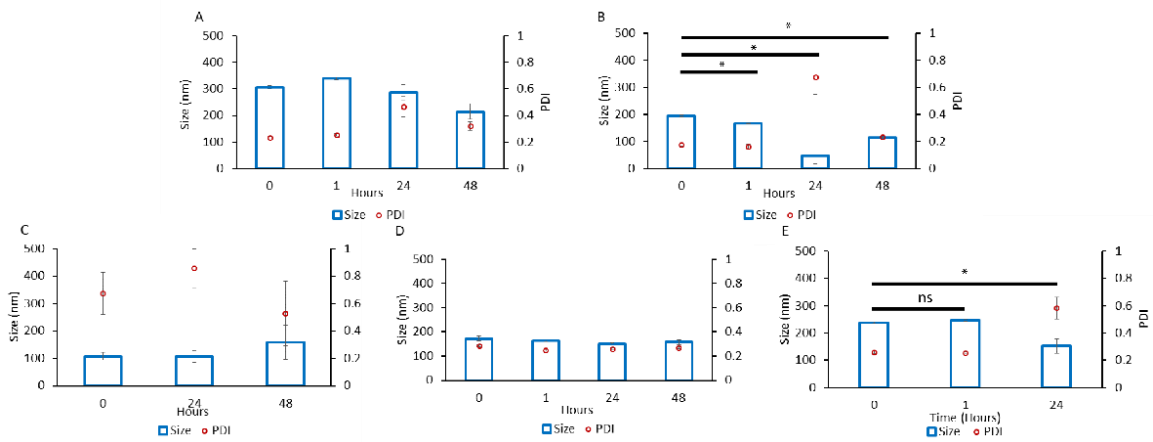


**Figure 3.5 Particle size and dispersity of Nano-BDNF.**

The complexes were prepared by manual mixing of the solutions of BDNF and **(A)** B1, **(B)** B2, **(C)** B3, **(D)** B5, or **(E)** PSR-PLE in 10 mM HEPES, pH 7.4. The component charge ratio was $Z_{-/+}$ = 1 **(B-E)** or $Z_{-/+}$ = 2 **(A)**. The DLS measurements were carried out for up to 48 hours. Values are mean ± SEM, * $p < 0.05$, ns = no significance. unmarked plots do not show statistically significant differences. Statistical significance was established using an unpaired two tailed Student's t-test.

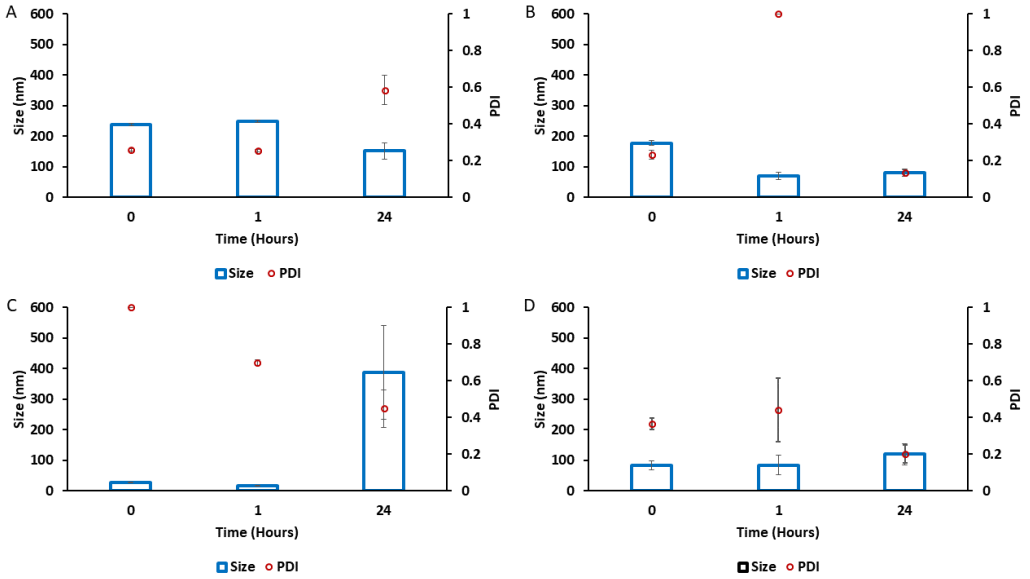


**Figure 3.6 Intensity weighted particle size and dispersity of Nano-BDNF PSR-PLE.** The complexes were prepared by manual mixing of the solutions of BDNF and PSR-PLE in 10 mM HEPES, pH 7.4 at the $Z_{-/+}$ ratios of (**A**) 1, (**B**) 2, (**C**) 5, and (**D**) 10. The DLS measurements were carried out for up to 48 hours. Values are mean ± SEM.

.

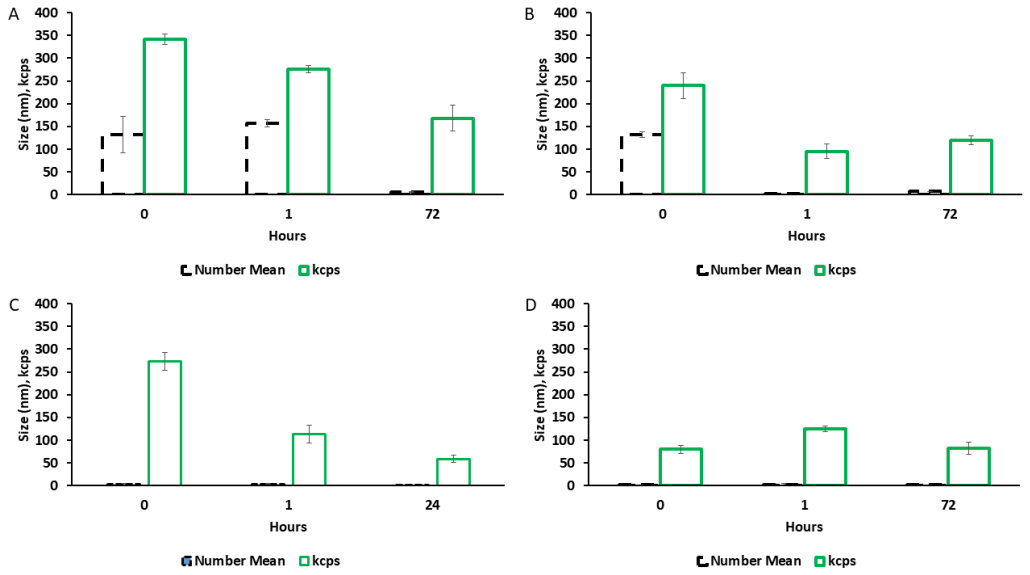


**Figure 3.7 Number weighted particle size and kilocount per second of Nano-BDNF PSR-PLE measurements in DLS of the same samples as shown Figure 3.6.**

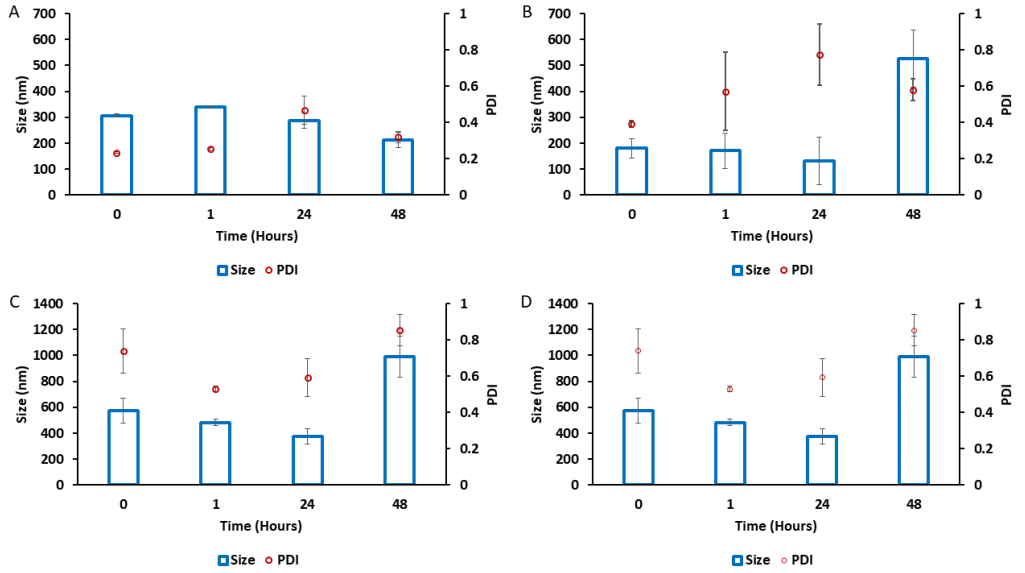


**Figure 3.8 Intensity weighted particle size and dispersity of Nano-BDNF B1.**

The complexes were prepared by manual mixing of the solutions of BDNF and PSR-PLE in 10 mM HEPES, pH 7.4 at the $Z_{-/+}$ ratios of (**A**) 1, (**B**) 2, (**C**) 5, and (**D**) 10. The DLS measurements were carried out for up to 48 hours. Values are mean ± SEM.

.

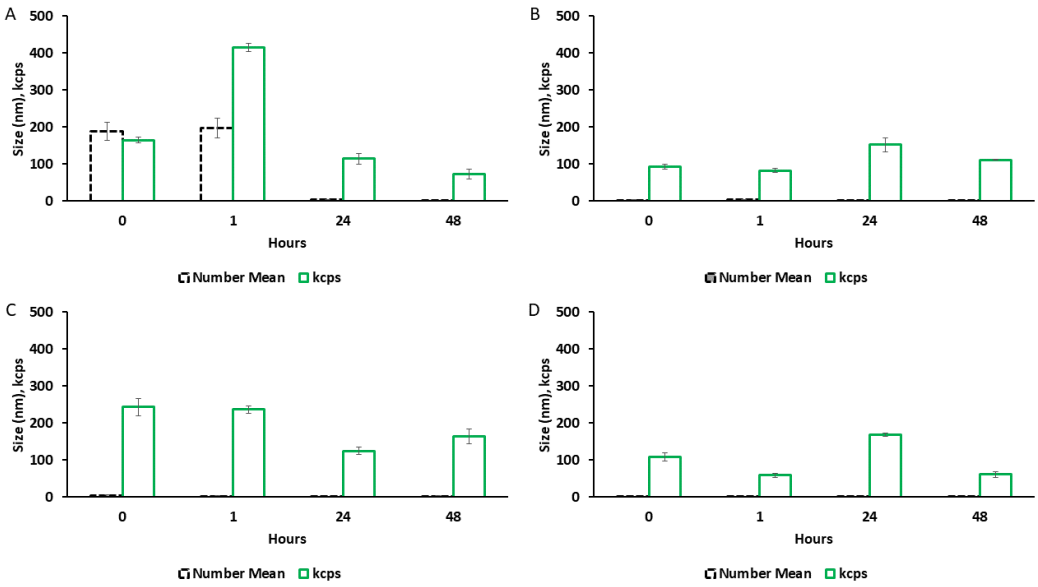


**Figure 3.9 Number weighted particle size and kilocount per second of Nano-BDNF B1 measurements in DLS of the same samples as shown Figure 3.8.**

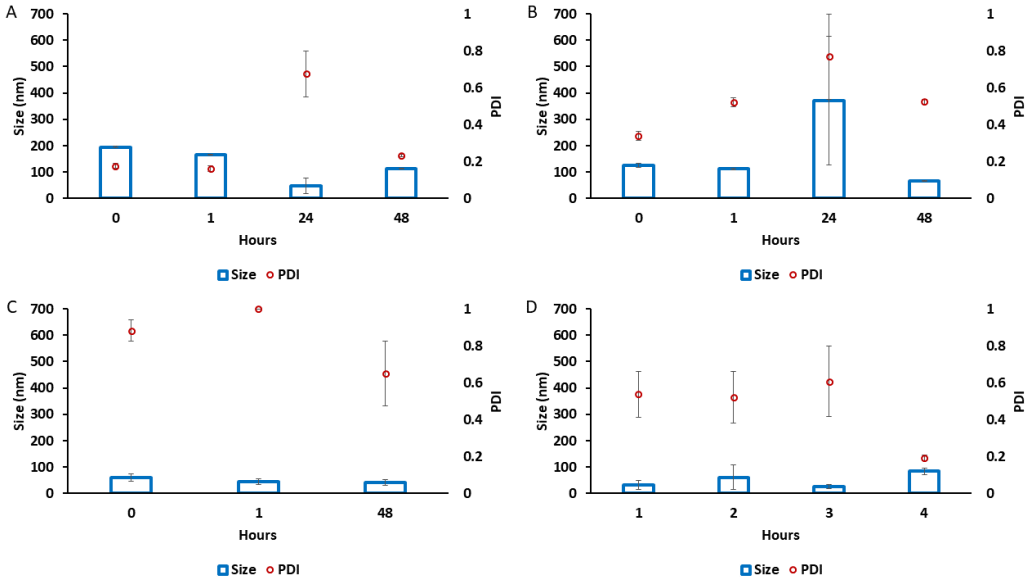


**Figure 3.10 Intensity weighted particle size and dispersity of Nano-BDNF B2.**

The complexes were prepared by manual mixing of the solutions of BDNF and PSR-PLE in 10 mM HEPES, pH 7.4 at the $Z_{-/+}$ ratios of (**A**) 1, (**B**) 2, (**C**) 5, and (**D**) 10. The DLS measurements were carried out for up to 48 hours. Values are mean ± SEM.

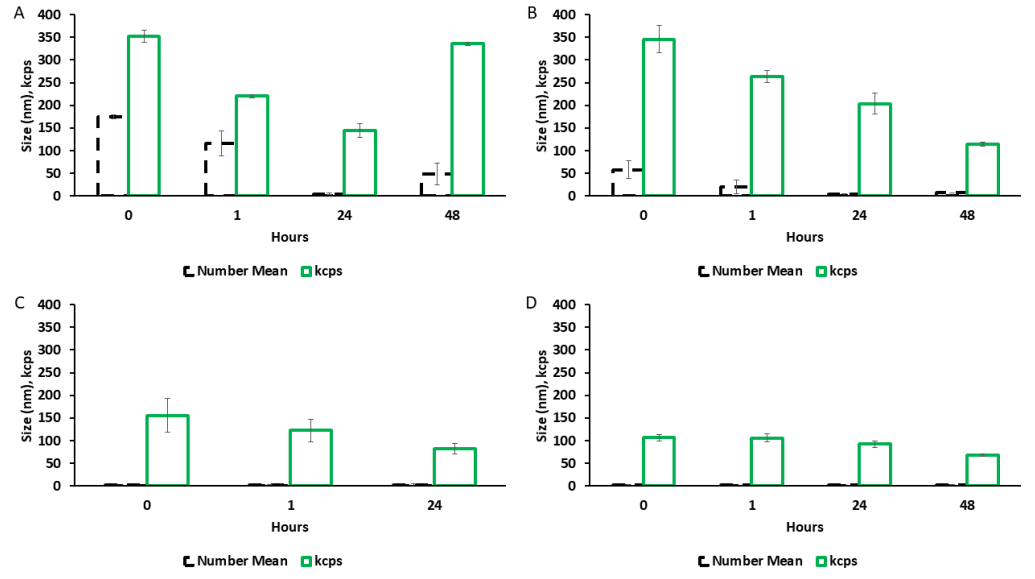


**Figure 3.11 Number weighted particle size and kilocount per second of Nano-BDNF B2 measurements in DLS of the same samples as shown Figure 3.10.**

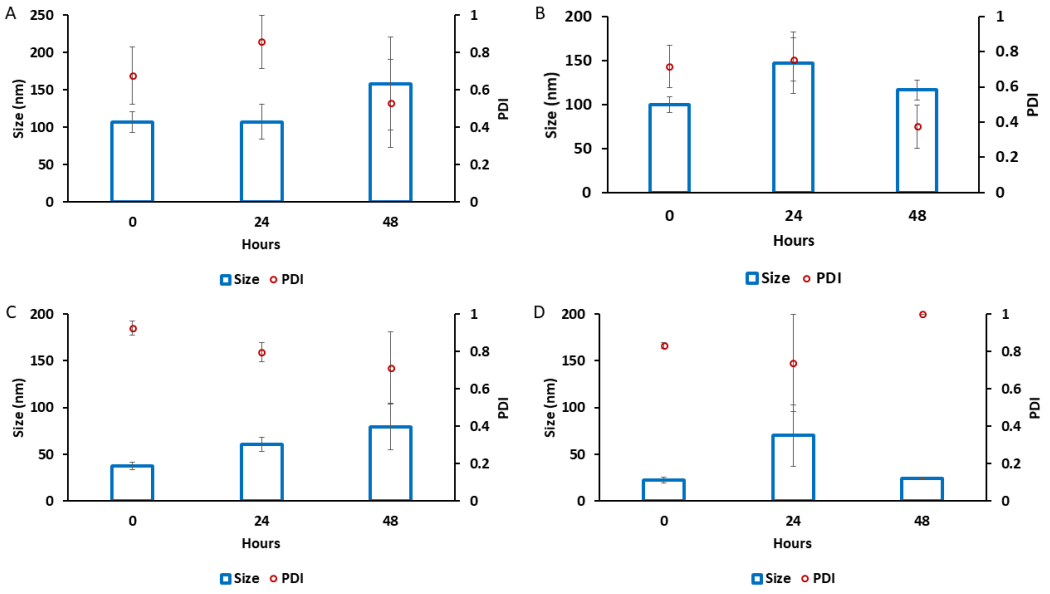


**Figure 3.12 Intensity weighted particle size and dispersity of Nano-BDNF B3.**

The complexes were prepared by manual mixing of the solutions of BDNF and PSR-PLE in 10 mM HEPES, pH 7.4 at the $Z_{-/+}$ ratios of (**A**) 1, (**B**) 2, (**C**) 5, and (**D**) 10. The DLS measurements were carried out for up to 48 hours. Values are mean ± SEM.

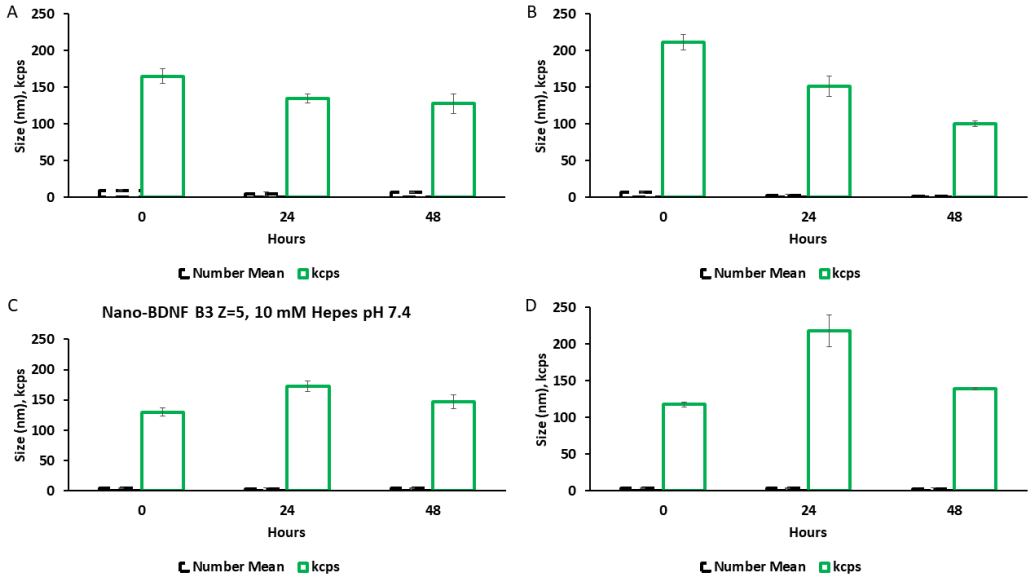


**Figure 3.13 Number weighted particle size and kilocount per second of Nano-BDNF B3 measurements in DLS of the same samples as shown Figure 3.12.**

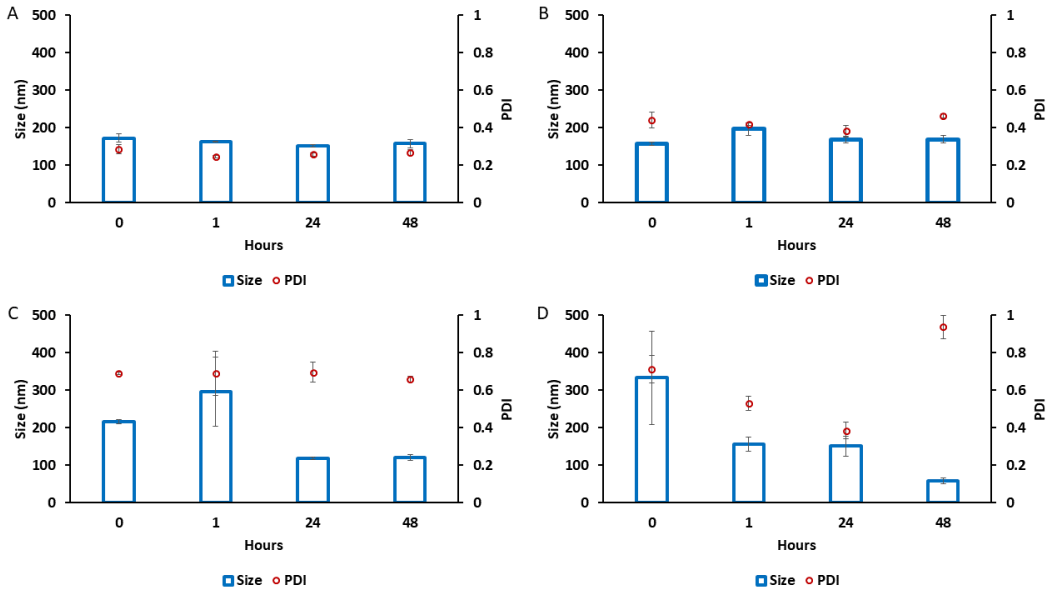


**Figure 3.14 Intensity weighted particle size and dispersity of Nano-BDNF B5.**

The complexes were prepared by manual mixing of the solutions of BDNF and PSR-PLE in 10 mM HEPES, pH 7.4 at the $Z_{-/+}$ ratios of (**A**) 1, (**B**) 2, (**C**) 5, and (**D**) 10. The DLS measurements were carried out for up to 48 hours. Values are mean ± SEM.

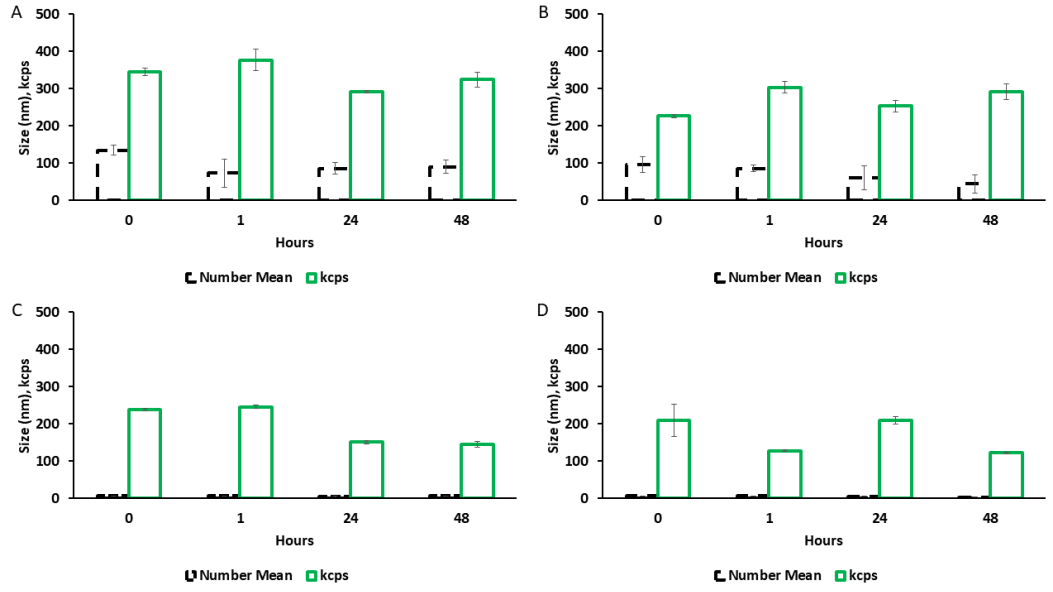


**Figure 3.15 Number weighted particle size and kilocount per second of Nano-BDNF B5 measurements in DLS of the same samples as shown Figure 3.14.**

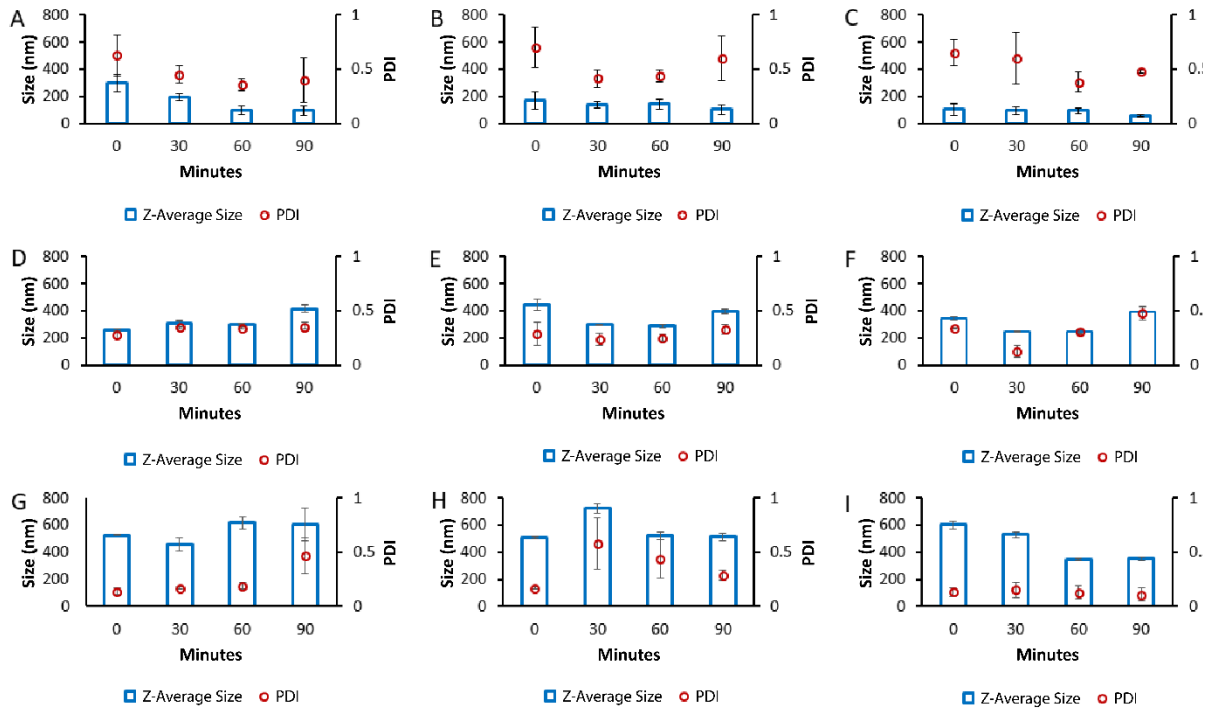


**Figure 3.16 Intensity weighted particle size and dispersity of Nano-BDNF in the presence of small-molecular mass electrolyte.**

Nano-BDNF (**A**) B2 $Z_{-/+}$=1, (**B**) B2 $Z_{-/+}$=2, (**C**) B2 $Z_{-/+}$=5, (**D**) B5 $Z_{-/+}$=1, (**E**) B5 $Z_{-/+}$=2, (**F**) B5 $Z_{-/+}$=5, (**G**) PSR-PLE $Z_{-/+}$=1, (**H**) PSR-PLE $Z_{-/+}$=2, and (**I**) PSR-PLE $Z_{-/+}$=5 were prepared in 10 mM HEPES, 150 mM NaCl, pH 7.4 via manual mixing. The particles were measure for size and dispersity over 90 minutes using the Malvern Zetasizer DLS machine. Values are mean ± SEM.

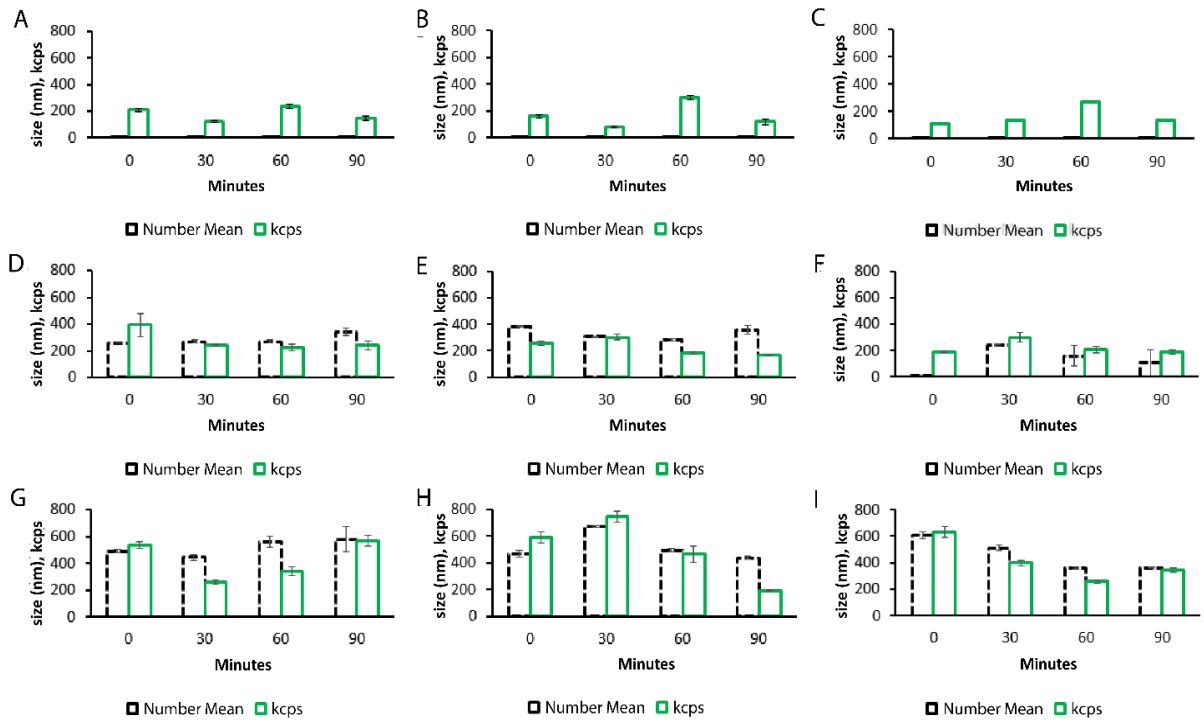


**Figure 3.17 Number weighted particle size and kilocount of Nano-BDNF in the presence of small-molecular mass electrolyte measured by DLS of the same samples as shown Figure 3.16.**

Nano-BDNF (A) B2 Z-/+=1, (B) B2 Z-/+=2, (C) B2 Z-/+=5, (D) B5 Z-/+=1, (E) B5 Z-/+=2, (F) B5 Z-/+=5, (G) PSR-PLE Z-/+=1, (H) PSR-PLE Z-/+=2, and (I) PSR-PLE Z-/+=5 were prepared in 10 mM HEPES, 150 mM NaCl, pH 7.4 via manual mixing. The particles were measure for size and dispersity over 90 minutes using the Malvern Zetasizer DLS machine. Values are mean ± SEM.

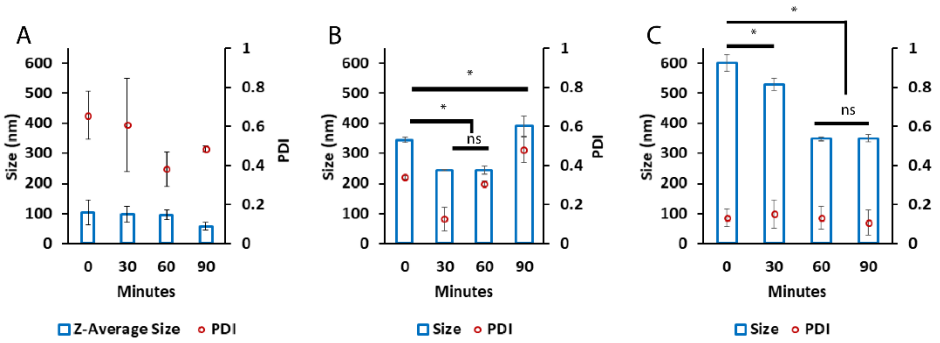


**Figure 3.18 Particle size and dispersity of Nano-BDNF in the presence of small-molecular mass electrolyte.**

All Nano-BDNF samples were prepared at $Z_{\pm} = 5$ by manual mixing of the solutions of BDNF and **(A)** B2, **(B)** B5, or **(C)** PSR-PLE in 10 mM HEPES, pH 7.4, 150 mM NaCl. The DLS measurements were carried out for over 2 hours. Values are mean ± SEM, * $p < 0.05$, ns = no significance, unmarked plots do not show statistically significant differences. Statistical significance was established using an unpaired two tailed Student's t-test.

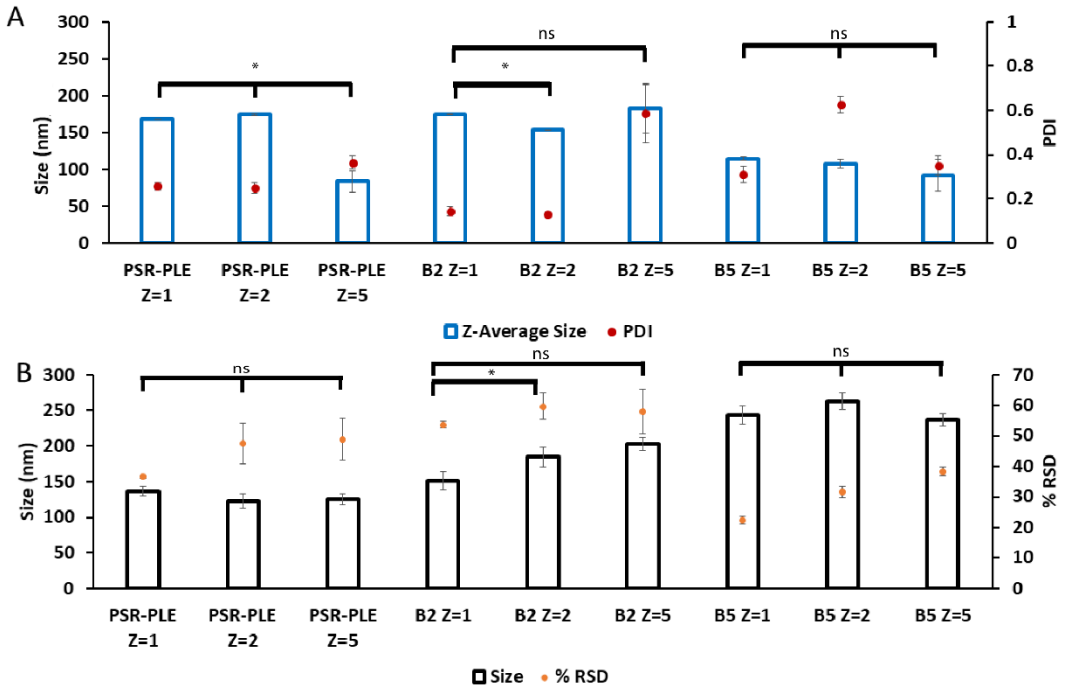


**Figure 3.19 Particle size and dispersity of Nano-BDNF prepared by microfluidic mixing.**

Nano-BDNF samples were prepared in 10 mM Hepes, pH 7.4 at various $Z_{-/+}$ ratios. The complexes were characterized by **(A)** DLS or **(B)** NTA using Nanosight NS500**.** Values are mean ± SEM, * $p < 0.05$, ns = no significance, unmarked plots do not show statistically significant differences. Statistical significance was established using an unpaired two tailed Student's t-test

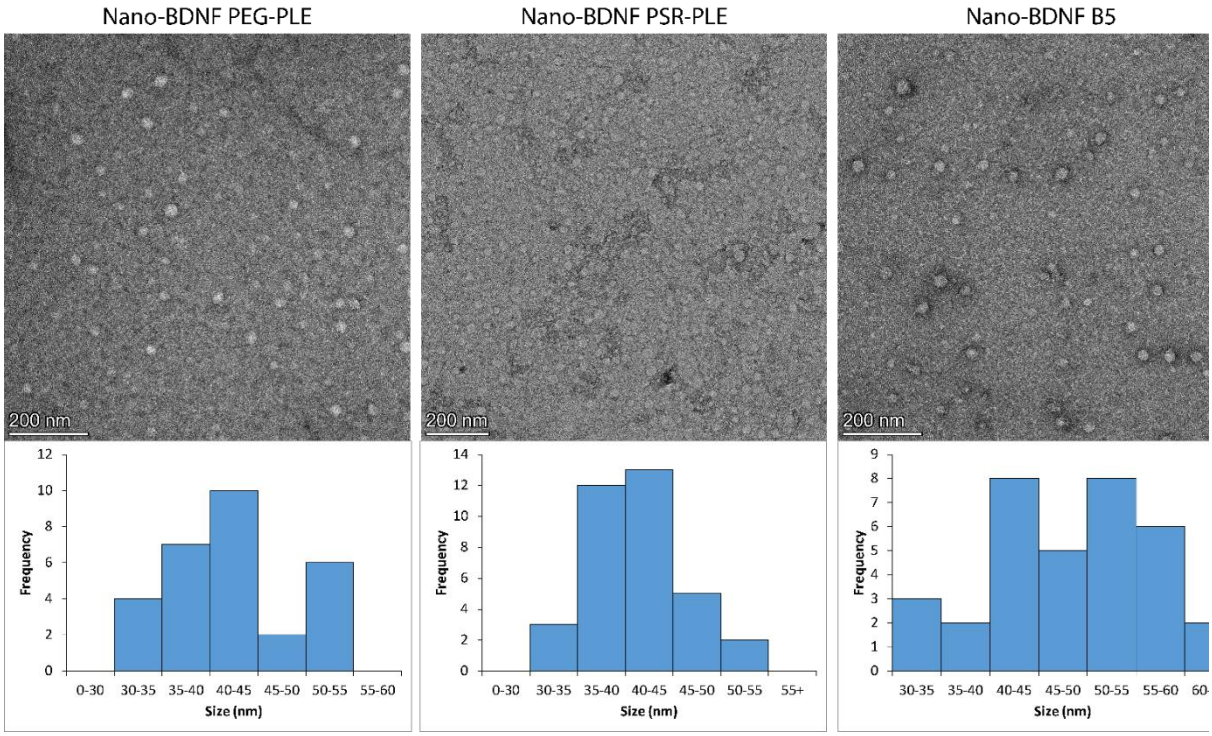


**Figure 3.20 Transmission electron microscopy (TEM) visualization of mixer formulated Nano-BDNF in 10 mM phosphate, pH 7.4.**

Representative images of Nano-BDNF formulations ($Z_{-/+} = 5$) are show such that the scale bar is 200 nm. Histograms of measured sizes are included underneath the correlated image.

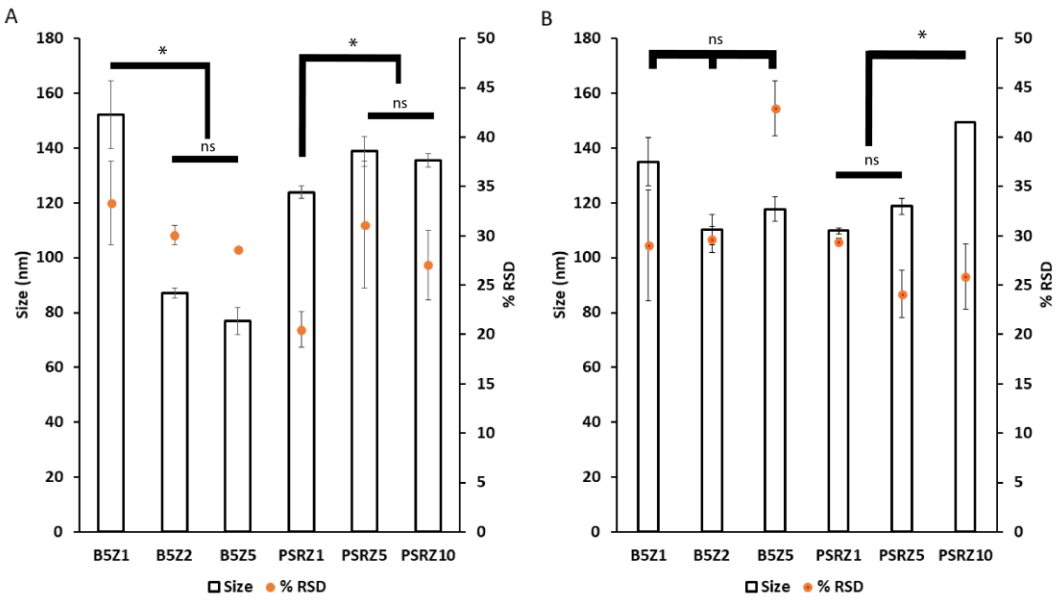


**Figure 3.21 Particle size and distribution of Nano-BDNF samples in isotonic solutions.**

The complexes were prepared by microfluidic mixing in **(A)** PBS and **(B)** LR. The measurements were carried out within 10 min after mixing at RT. The NTA measurements were carried out using Nanosight NS500. Values are mean ± SEM, * $p < 0.05$, ns = no significance, unmarked plots do not show statistically significant differences. Statistical significance was established using an unpaired two tailed Student's t-test.

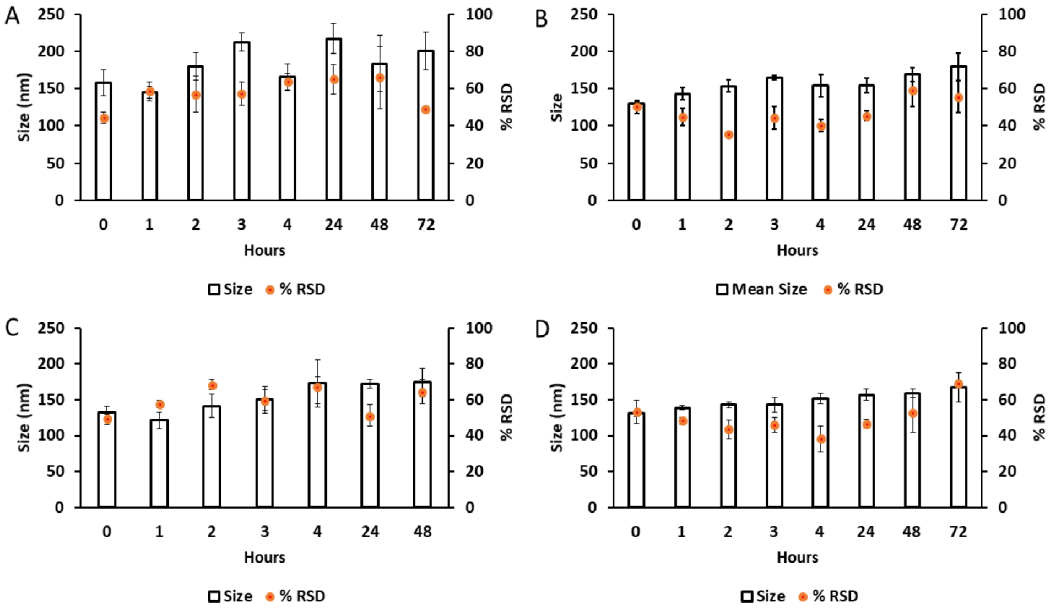


**Figure 3.22 Particle size and distribution of mixer formulated Nano-BDNF.**

Particle size and distribution of mixer formulated Nano-BDNF in (**A,C**) PBS and (**B,D**) LR solution over time. (**A,B**) Nano-BDNF PSR-PLE $Z_{-/+}$=5 and (**C,D**) Nano-BDNF B5 $Z_{-/+}$=5 were analyzed at the indicated times using the Zetaview machine. Data is presented as mean ± SEM.

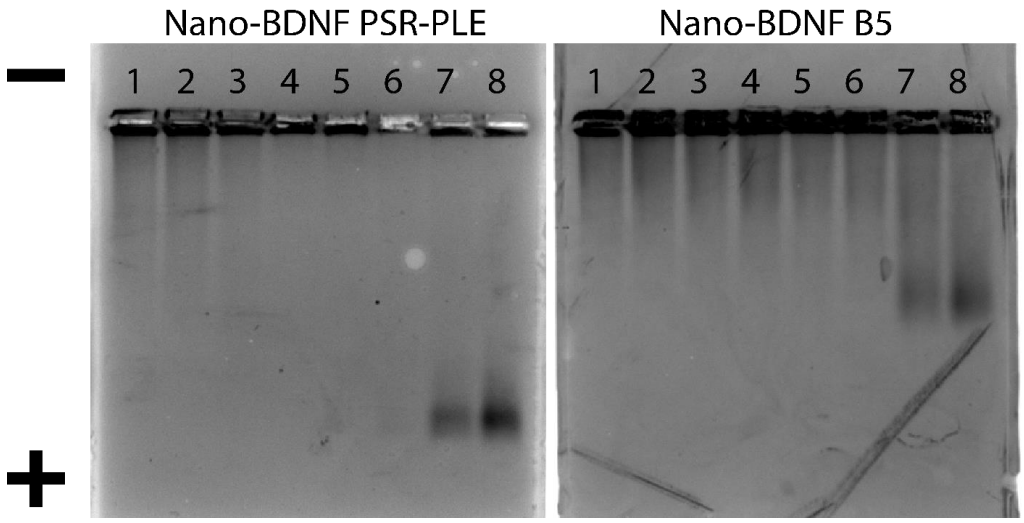


**Figure 3.23 HAGE analysis of Nano-BDNF.**

The complexes were prepared in LR by manual mixing of BDNF with respective copolymers. Lanes 1 through 8 correspond to BDNF alone (lane 1), and Nano-BDNF prepared at various $Z_{-/+}$: 0.1 (lane 2), 0.25 (lane 3), 0.50 (lane 4), 0.75 (lane 5), 1.0 (lane 6), 5.0 (lane 7), 10.0 (lane 8). The protein bands were visualized by Coomassie blue staining.

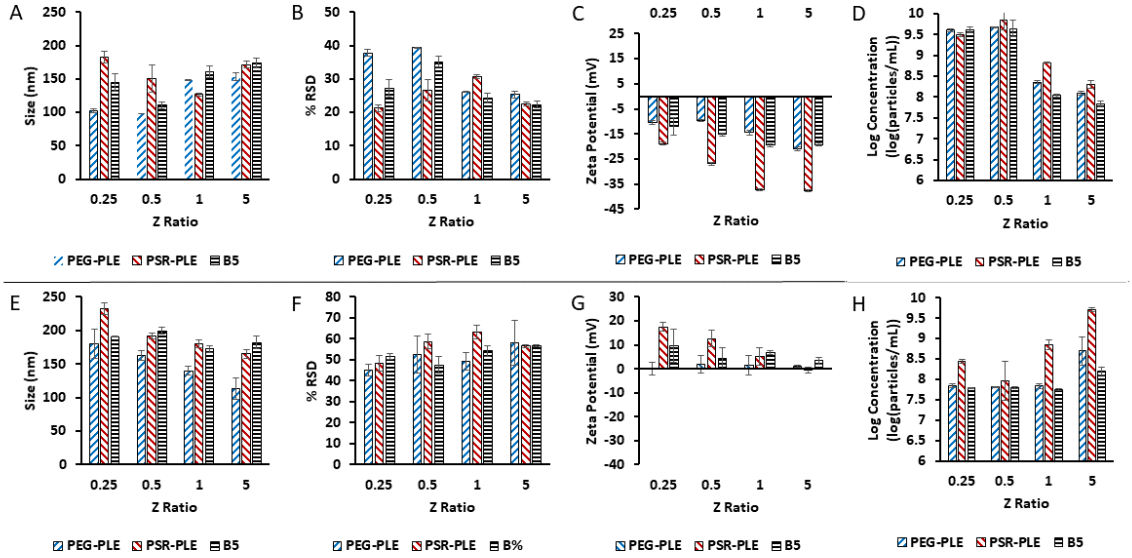


**Figure 3.24 Particle characterization by (A, E) size, (B, F) dispersity, (C, G) zeta potential, and (D-H) concentration.**

Nano-BDNF was formulated in **(A-D)** 10 mM sodium phosphate, pH 7.4 and **(E-F)** 10 mM sodium acetate, pH 5.0 at room temperature using PEG-PLE, PSR-PLE or B5. Values are mean ± SEM

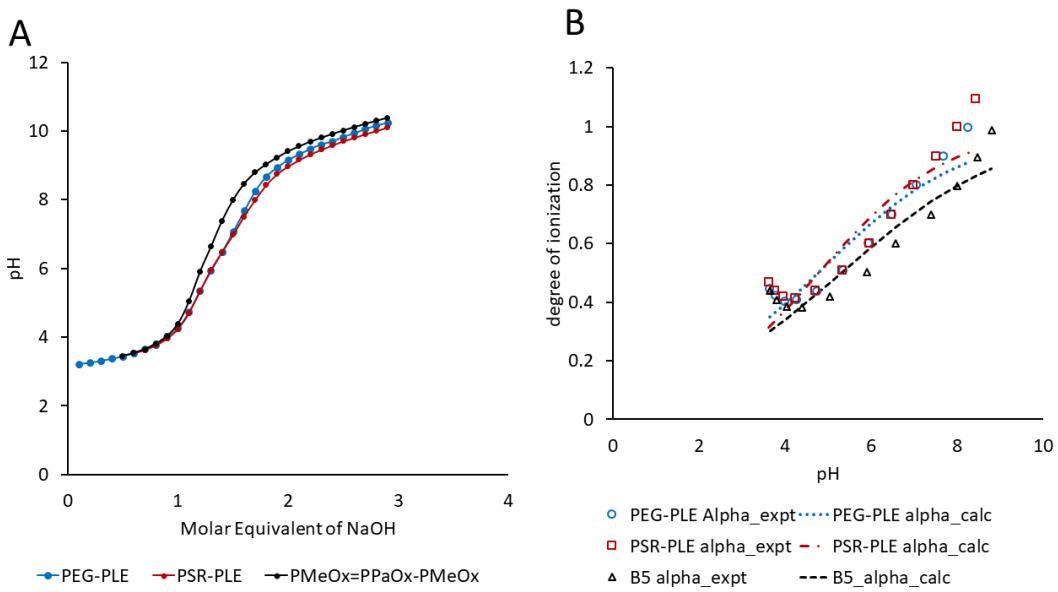


**Figure 3.25 Titration of Block Copolymers.**

(**A**) The curves of pH titration using NaOH and (**B**) the degree of ionization for the three block copolymers. The degree of ionization was determined experimentally from the titration data or fitted to the experimental data.

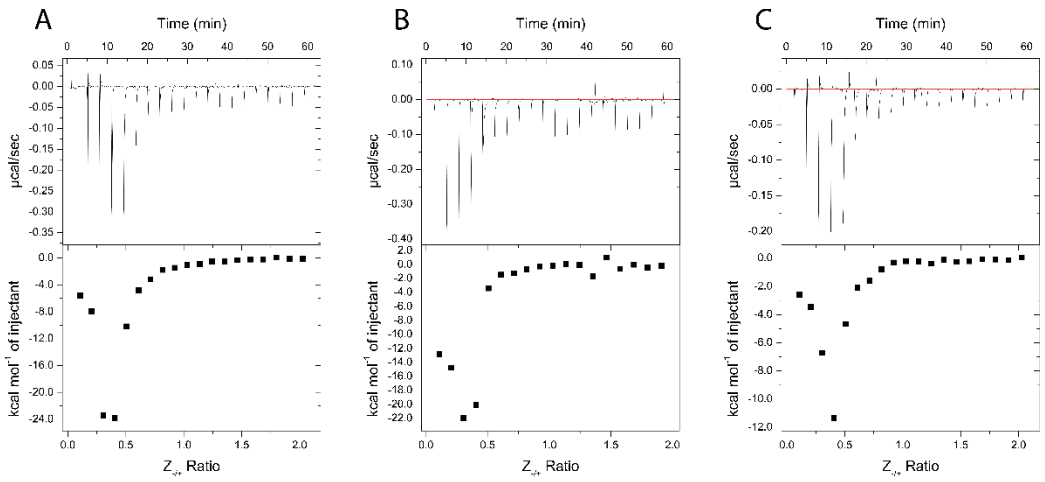


**Figure 3.26 ITC thermograms of Nano-BDNF formation in 10 mM sodium phosphate buffer, pH 7.4.**

The holding cell was filled with 200 µL of 10 µM BDNF at 25°C. **(A)** 88 µM PEG-PLE **(B)** 88 µM PSR-PLE, and **(C)** 162 µM B5 were injected in 2 µL increments with a 3 min dwell time between each injection. Top: time dependence of the heat supplied to the sample cell for each injection of the block copolymer into the BDNF solution. Bottom - integrated ITC curves for the block copolymer binding with BDNF as a function of the charge ratio Z-/+.

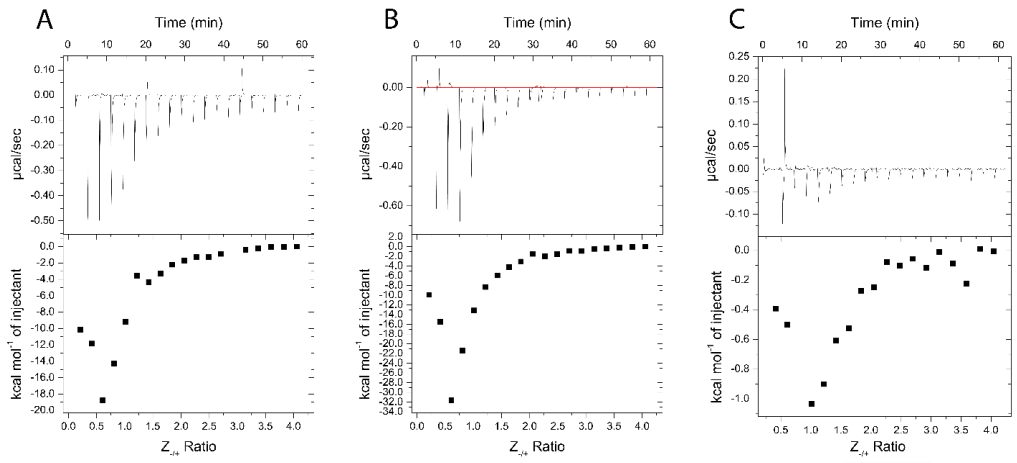


**Figure 3.27 ITC thermograms of Nano-BDNF formation in 10 mM sodium acetate buffer, pH 5.0.**

The holding cell was filled with 200 µL of 10 µM BDNF in at 25°C. (**A**) 88 µM PEG-PLE **(B)** 88 µM PSR-PLE, and **(C)** 162 µM B5 were injected in 2 µL increments with a 3 min dwell time between each injection. Top: time dependence of the heat supplied to the sample cell for each injection of the block copolymer into the BDNF solution. Bottom - integrated ITC curves for the block copolymer binding with BDNF as a function of the charge ratio Z-/+.

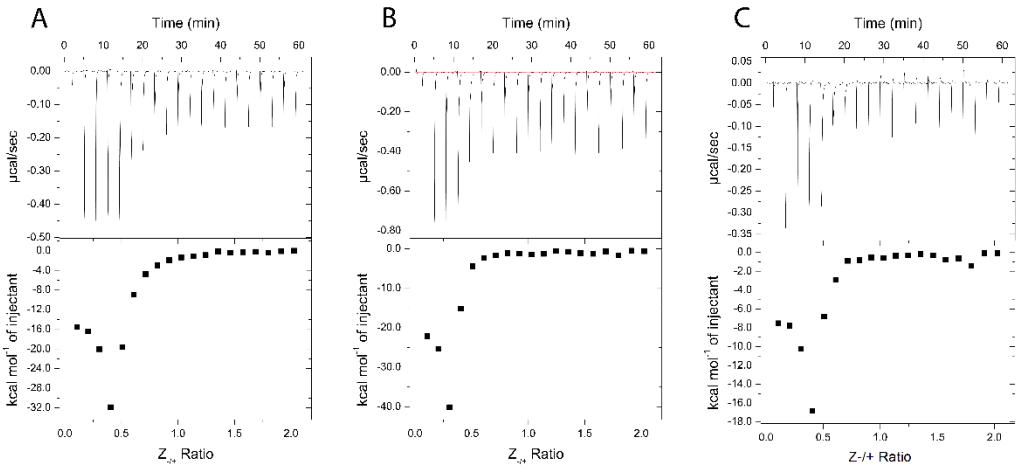


**Figure 3.28 ITC thermograms of Nano-BDNF formation in 10 mM sodium phosphate buffer, pH 5.8.**

The holding cell was filled with 200 µL of 10 µM BDNF in at 25°C. (**A**) 88 µM PEG-PLE (**B**) 88 µM PSR-PLE, and (**C**) 162 µM B5 E were injected in 2 µL increments with a 3 min dwell time between each injection. Top: time dependence of the heat supplied to the sample cell for each injection of the block copolymer into the BDNF solution. Bottom - integrated ITC curves for the block copolymer binding with BDNF as a function of the charge ratio $Z_{-/+}$.

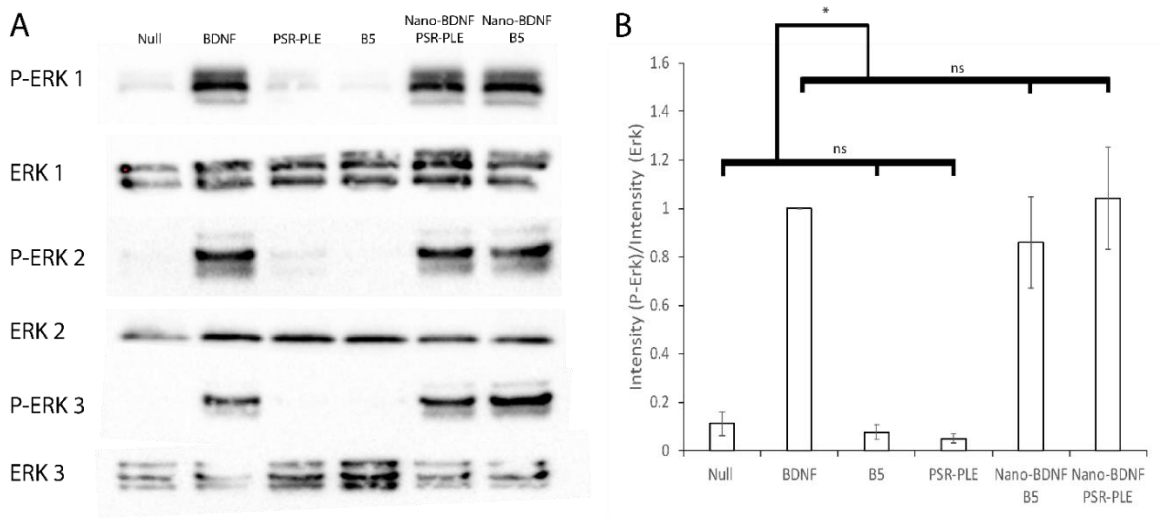


**Figure 3.29 Stimulation of the TrkB Pathway by application of BDNF and Nano-BDNF formulations to NIH 3T3 TrkB cells.**

For each experiment (1-3), cultured cells were stimulated with 500 ng/mL of BDNF, equivalent amount of nano-BDNF formulated in media at $Z_{-/+} = 5$, or polymer alone. **(A)** Erk or P-Erk was detected using α-Erk or α-P-Erk via western blot. **(B)** The adjusted total lane volume (measured in signal intensity) of each lane on the blots was determined then the ratio of p-ErK/Erk was calculated. All values were normalized to the BDNF sample and averaged. Experiments were done in triplicate from the point of cell culture. Values are mean ± SEM, * $p < 0.05$, ns = no significance. Statistical significance was established using an unpaired two tailed Student's t-test.

**Table 3.1 The calculated effective pKa values and degrees of ionization at critical pH values[a].**

| Block Copolymer | Effective $pK_a$ | Hill coefficient, *n* | Degree of Ionization, α | | |
|---|---|---|---|---|---|
| | | | pH 5.0 | pH 5.8 | pH 7.4 |
| PEG-PLE | 4.75 | 0.25 | 0.54 | 0.65 | 0.82 |
| PSR-PLE | 4.78 | 0.29 | 0.54 | 0.66 | 0.85 |
| B5 | 5.29 | 0.22 | 0.46 | 0.56 | 0.74 |

[a] Effective pKa and α are defined here from the fitted modified Henderson Hasselbalch equation

**Table 3.2. Critical Z-/+ values of in the analysis of ITC thermograms.**

| Block Copolymer | $Z_{-/+}$ of the curve minimum | | | $Z_{-/+}$ of the curve saturation | | |
|---|---|---|---|---|---|---|
| | pH 7.4 | pH 5.8 | pH 5.0 | pH 7.4 | pH 5.8 | pH 5.0 |
| PEG-PLE | 0.4 | 0.4 | 0.6 | 0.9 | 1.0 | 2.2 |
| PSR-PLE | 0.4 | 0.3 | 0.6 | 0.6 | 0.6 | 2.0 |
| B5 | 0.4 | 0.4 | 1.0 | 0.9 | 0.7 | 2.2 |

## CHAPTER 4: CONCLUSIONS AND FUTURE DIRECTION

The eventual goal of the work described in this dissertation is twofold. First, we intend to develop a viable therapeutic candidate for the treatment of neurologic diseases. Second, given the initial development of Nano-BDNF PEG PLE described in chapter 2, to improve upon and diversify the therapeutic formulations available for administration. We have presented work which significantly advances both aims by developing Nano-BDNF and then by reformulating using two novel polymers which do not contain PEG.

We have demonstrated that simple mixing is sufficient to produce a reasonably small, spherical, and narrowly dispersed PIC comprised of PEG-PLE and BDNF. Moreover, the protein is stabilized after administration to mouse models and more efficacious than naked BDNF. My primary contributions to that work lay in the analysis of protein-polymer association, demonstrating that the PEG-PLE/BDNF complexation is driven by electrostatic interactions, especially at the charged poles and stabilized by a hydrogen bonding network. Furthermore, we showed that BDNF can be generally protected by the PIC micelle until it encounters specific binders which outcompete the PIC polymers. Finally, in collaboration with Dr. Vinod, I introduced this microfluidic mixer and demonstrated improved formulation of Nano-BDNF PEG-PLE.

The improvement observed with introduction of the microfluidic mixer as well as the already prevalent concerns about PEG inspired us to initiate the project described in Chapter 3, whereby we introduce two PEG-free polymers and successfully complex them with BDNF. We also explore the complexation through a more physics oriented lens, demonstrating extreme similarity as well as recapitulation of known physical processes observed in PECs. We also

present a process which may be used to reformulate other non-covalent PICs for macromolecular encapsulation.

Moving forward with Nano-BDNF, there are clear next steps which would be required to validate the therapeutic efficacy of our novel PICs. First, it would be wise to perform a pharmacokinetic study of where the particle goes, the rate of clearance, and how various routes of administration affect its distribution in healthy mice. After identifying the best protocol for a given application such as injury repair, supplementing for a neurodevelopmental disorder, or promoting neuron survival in a neurodegenerative disease, a disease or disorder model can be chosen. Due to the wide applicability of BDNF, there are a plethora of models to choose from though close, long term collaborations suggest either Parkinson's disease or ischemic stroke. Nano-BDNF PEG-PLE has already demonstrated considerable effect in an ischemic stroke model and preliminary results in a Parkinson's disease model. Ischemic stroke is particular persuasive due to its commonality, the well-defined model, and previous results with Nano-BDNF PEG-PLE. Alternatively, Alzheimer's disease is also convincing for the high incidence, devastating effects, and lack of therapeutic options.

Finally, a major portion of our work focuses on substituting PMeOx and PSR for PEG. We thoroughly review the issues with PEG in the introduction and it is clear that alternatives are needed. Diversifying the formulations for known, effective, PEGylated drugs should become a priority in the pharmaceutical industry. Current PEG sensitive populations are small. However, continued heavy use of PEG will increase this population especially with pharmaceutical agents designed to stimulate the immune system. Availability of equivalent alternatives may overcome issues of PEG resistance and provide options for patients who cannot take PEG drugs.

## REFERENCES


1. Bungenberg de Jong, H.G.; Kruyt, H.R. Coacervation (Partial Miscibility in Colloid Systems). *Proc. R. Acad. Amsterdam* **1929**, *32*, 849–856.
2. de Jong, H.G.B.; Dekker, W.A.L.; Winkler, K.C. Complex Relationships in Lyophilic Colloidal Systems. III. A. Examples of Complex and Autocomplex Flocculi. B. The "Salt Solubility" of Globulins at the Isoelectric Point. *Recl. des Trav. Chim. des Pays-Bas* **2010**, *53*, 607–621, doi:10.1002/recl.19340530705.
3. de Jong, H.L.B.; Klaar, W.J.; Sumner, C.G. Colloid Chemistry of Gliadin Separation Phenomena. *Trans. Faraday Soc.* **1932**, *28*, 27, doi:10.1039/tf9322800027.
4. Overbeek, J.T.G.; de Jong, H.G.B. Colloid Science. In; Kruyt, H.R., Ed.; Elsevier Publishing Company: New york, Amsterdam, London, Brussels, 1949; pp. 184–480.
5. Oparin, A.I.; Synge, A. *The Origin of Life on Earth*; Academic Press: New York, 1957;
6. Deng, N.N. Complex Coacervates as Artificial Membraneless Organelles and Protocells. *Biomicrofluidics* **2020**, *14*, 1–6, doi:10.1063/5.0023678.
7. Morawetz, H.; Hughes, W.L. The Interaction of Proteins with Synthetic Polyelectrolytes. I. Complexing of Bovine Serum Albumin. *J. Phys. Chem.* **1952**, *56*, 64–69, doi:10.1021/j150493a014.
8. BERDICK, M.; MORAWETZ, H. The Interaction of Catalase with Synthetic Polyelectrolytes. *J. Biol. Chem.* **1954**, *206*, 959–971, doi:10.1016/s0021-9258(19)50866-3.
9. Peterson, E.A.; Sober, H.A. Chromatography of Proteins. I. Cellulose Ion-Exchange Adsorbents. *J. Am. Chem. Soc.* **1956**, *78*, 751–755, doi:10.1021/ja01585a016.
10. Miller, I.R.; Bach, D. Interaction of DNA with Heavy Metal Ions and Polybases: Cooperative Phenomena. *Biopolymers* **1968**, *6*, 169–179, doi:10.1002/bip.1968.360060202.
11. Kabanov, V.A. Polyelectrolyte Complexes in Solution and in Bulk. *Russ. Chem. Rev.* **2005**, *74*, 3–20, doi:10.1070/RC2005v074n01ABEH001165.
12. Zezin, A.B.; Lutsenko, V. V.; Rogacheva, V.B.; Aleksina, O.A.; Kalyuzhnaya, R.I.; Kabanov, V.A.; Kargin, V.A. Cooperative Interaction of Synthetic Polyelectrolytes in Aqueous Solution. *Polym. Sci. U.S.S.R.* **1972**, *14*, 857–865, doi:10.1016/0032-3950(72)90083-4.
13. Tsuchida, E. The Formation of Higher Structure through Hydrophobic Interaction of Interpolymer Complexes. *Die Makromol. Chemie* **1974**, *175*, 603–611, doi:10.1002/macp.1974.021750221.
14. Kharenko, A. V.; Starikova, Y.A.; Lutsenko, V. V.; Zezin, A.B. Study of Cooperative Reactions of Oligo- and Polyphosphates with Polybases. *Polym. Sci. U.S.S.R.* **1976**, *18*, 1837–1843, doi:10.1016/0032-3950(76)90316-6.
15. Papisov, I.M.; Litmanovich, A.A. Specificity of Cooperative Interactions between Simple Synthetic Macromolecules and Its Connection with Chain Length. *Polym. Sci. U.S.S.R.* **1977**, *19*, 830–837, doi:10.1016/0032-3950(77)90236-2.
16. Kharenko, O.A.; Kharenko, A. V.; Kasaikin, V.A.; Zeizin, A.B.; Kabanov, V.A. The

Structure of Non-Stoichiometric, Water Soluble Polyelectrolyte Complexes. *Polym. Sci. U.S.S.R.* **1979**, *21*, 3009–3017, doi:10.1016/0032-3950(79)90135-7.

17. Kharenko, O.A.; Kharenko, A. V.; Kalyuzhnaya, R.I.; Izumrudov, V.A.; Kasaikin, V.A.; Zezin, A.B.; Kabanov, V.A. Non-Stoichiometric Polyelectrolyte Complexes: New, Water Soluble Macromolecular Compounds. *Polym. Sci. U.S.S.R.* **1979**, *21*, 3002–3008, doi:10.1016/0032-3950(79)90134-5.

18. Michaels, A.S.; Mir, L.; Schneider, N.S. A Conductometric Study of Polycation-Polyanion Reactions in Dilute Aqueous Solution. *J. Phys. Chem.* **1965**, *69*, 1447–1455, doi:10.1021/j100889a003.

19. Izumrudov, V.A.; Kharenko, O.A.; Kharenko, A. V.; Gulyayeva, Z.G.; Kasaikin, V.A.; Zesin, A.B.; Kabanov, V.A. Behaviour of Non-Stoichiometric Polyelectrolyte Complexes in Aqueous Salt Solutions. *Polym. Sci. U.S.S.R.* **1980**, *22*, 767–776, doi:10.1016/0032-3950(80)90405-0.

20. Kharenko, O.A.; Izumrudov, V.A.; Kharenko, A.V.; Kasaikin, V.A.; Zezin, A.B.; Kabanov, V.A. Association and Dissociation Processes in Solutions of Non-Stoichiometric Polyelectrolyte Complexes. *Polym. Sci. U.S.S.R.* **1980**, *22*, 247–254, doi:10.1016/0032-3950(80)90441-4.

21. Kharenko, A.V.; Neverova, Y.A.; Kalyuzhnaya, R.I.; Zezin, A.B.; Kabanov, V.A. Structure and Properties of Polyelectrolyte Complexes—Products of Incomplete Reactions between Poly-N,N-Dimethylaminoethyl Methacrylate and Polyphosphates and Polyacrylates. *Polym. Sci. U.S.S.R.* **1981**, *23*, 2268–2277, doi:10.1016/0032-3950(81)90253-7.

22. Mustafayev, M.I.; Kabanov, V.A. Soluble Ternary Complex of Poly-4-Vinylpyridine, Bovine Serum Albumin and Copper. *Polym. Sci. U.S.S.R.* **1981**, *23*, 299–304, doi:10.1016/0032-3950(81)90169-6.

23. Gulyayeva, Z.G.; Zansokhova, M.F.; Razvodovskii, Y.F.; Yefimov, V.S.; Zezin, A.B.; Kabanov, V.A. Oligomeric Ionenes and Their Reactions with Synthetic Polyacids. *Polym. Sci. U.S.S.R.* **1983**, *25*, 1436–1443, doi:10.1016/0032-3950(83)90080-1.

24. Izumrudov, V.A.; Savitskii, A.P.; Bakeev, K.N.; Zezin, A.B.; Kabanov, A. V A Fluorescence Quenching Study of Interpolyelectrolyte Reactions. *Makromol. Chem., Rapid Commun.* **1984**, *714*, 709–714, doi:10.1002/marc.1984.030051102.

25. Kabanov, V.A.; Zezin, A.B.; Izumrudov, V.A.; Bronich, T.K.; Bakeev, K.N. Cooperative Interpolyelectrolyte Reactions. *Die Makromol. Chemie* **1985**, *13*, 137–155, doi:10.1002/macp.1985.020131985111.

26. Izumrudov, V.A.; Bronich, T.K.; Zezin, A.B.; Kabanov, V.A. The Kinetics and Mechanism of Intermacromolecular Reactions in Polyelectrolyte Solutions. *J. Polym. Sci. Polym. Lett. Ed.* **1985**, *23*, 439–444, doi:10.1002/pol.1985.130230808.

27. Bakeev, K.N.; Izumrudov, V.A.; Kuchanov, S.I.; Zezin, A.B.; Kabanov, V.A. Kinetics and Mechanism of Interpolyelectrolyte Exchange and Addition Reactions. *Macromolecules* **1992**, *25*, 4249–4254, doi:10.1021/ma00043a003.

28. Izumrudov, V.A.; Bronich, T.K.; Saburova, O.S.; Zezin, A.B.; Kabanov, V.A. The Influence of Chain Length of a Competitive Polyanion and Nature of Monovalent Counterions on the Direction of the Substitution Reaction of Polyelectrolyte Complexes. *Macromol. Chem., Rapid Commun.* **1988**, *12*, 7–12, doi:10.1002/marc.1988.030090102.

29. Kabanov, A. V.; Kabanov, V.A. DNA Complexes with Polycations for the Delivery of Genetic Material into Cells. *Bioconjug. Chem.* **1995**, *6*, 7–20, doi:10.1021/bc00031a002.

30. Kabanov, A. V.; Bronich, T.K.; Kabanov, V.A.; Yu, K.; Eisenberg, A. Soluble Stoichiometric Complexes from Poly( N -Ethyl-4-Vinylpyridinium) Cations and Poly(Ethylene Oxide)- Block -Polymethacrylate Anions. *Macromolecules* **1996**, *29*, 6797–6802, doi:10.1021/ma960120k.

31. Harada, A.; Kataoka, K. Formation of Polyion Complex Micelles in an Aqueous Milieu from a Pair of Oppositely-Charged Block Copolymers with Poly(Ethylene Glycol) Segments. *Macromolecules* **1995**, *28*, 5294–5299, doi:10.1021/ma00119a019.

32. Stuart, M.A.C.; Besseling, N.A.M.; Fokkink, R.G. Formation of Micelles with Complex Coacervate Cores. *Langmuir* **1998**, *14*, 6846–6849, doi:10.1021/la980778m.

33. Voets, I.K.; de Keizer, A.; Cohen Stuart, M.A. Complex Coacervate Core Micelles. *Adv. Colloid Interface Sci.* **2009**, *147–148*, 300–318, doi:10.1016/j.cis.2008.09.012.

34. Kabanov, A. V.; Chekhonin, V.P.; Alakhov, V.Y.; Batrakova, E. V.; Lebedev, A.S.; Melik-Nubarov, N.S.; Arzhakov, S.A.; Levashov, A. V.; Morozov, G. V.; Severin, E.S.; et al. The Neuroleptic Activity of Haloperidol Increases after Its Solubilization in Surfactant Micelles. Micelles as Microcontainers for Drug Targeting. *FEBS Lett.* **1989**, *258*, 343–345, doi:10.1016/0014-5793(89)81689-8.

35. Kabanov, A. V.; Batrakova, E. V.; Melik-Nubarov, N.S.; Fedoseev, N.A.; Dorodnich, T.Y.; Alakhov, V.Y.; Chekhonin, V.P.; Nazarova, I.R.; Kabanov, V.A. A New Class of Drug Carriers: Micelles of Poly(Oxyethylene)-Poly(Oxypropylene) Block Copolymers as Microcontainers for Drug Targeting from Blood in Brain. *J. Control. Release* **1992**, *22*, 141–157, doi:10.1016/0168-3659(92)90199-2.

36. Hwang, D.; Ramsey, J.D.; Kabanov, A. V. Polymeric Micelles for the Delivery of Poorly Soluble Drugs: From Nanoformulation to Clinical Approval. *Adv. Drug Deliv. Rev.* **2020**, *156*, 80–118, doi:10.1016/j.addr.2020.09.009.

37. Kabanov, A. V.; Vinogradov, S. V.; Suzdaltseva, Y.G.; Alakhov, V.Y. Water-Soluble Block Polycations as Carriers for Oligonucleotide Delivery. *Bioconjug. Chem.* **1995**, *6*, 639–643, doi:10.1021/bc00036a001.

38. Kataoka, K.; Togawa, H.; Harada, A.; Yasugi, K.; Matsumoto, T.; Katayose, S. Spontaneous Formation of Polyion Complex Micelles with Narrow Distribution from Antisense Oligonucleotide and Cationic Block Copolymer in Physiological Saline. *Macromolecules* **1996**, *29*, 8556–8557, doi:10.1021/ma961217+.

39. Vinogradov, S. V; Bronich, T.K.; Kabanov, A. V Self-Assembly of Polyamine–Poly(Ethylene Glycol) Copolymers with Phosphorothioate Oligonucleotides. *Bioconjug. Chem.* **1998**, *9*, 805–812, doi:10.1021/bc980048q.

40. Harada, A.; Kataoka, K. Chain Length Recognition: Core-Shell Supramolecular Assembly from Oppositely Charged Block Copolymers. *Science (80-. ).* **1999**, *283*, 65–67, doi:10.1126/science.283.5398.65.

41. Gebhart, C.L.; Kabanov, A. V. Evaluation of Polyplexes as Gene Transfer Agents. *J. Control. Release* **2001**, *73*, 401–416, doi:10.1016/S0168-3659(01)00357-1.

42. Kakizawa, Y.; Harada, A.; Kataoka, K. Environment-Sensitive Stabilization of Core-Shell Structured Polyion Complex Micelle by Reversible Cross-Linking of the Core through

Disulfide Bond [13]. *J. Am. Chem. Soc.* **1999**, *121*, 11247–11248, doi:10.1021/ja993057y.

43. Gao, S.; Holkar, A.; Srivastava, S. Protein – Polyelectrolyte Complexes and Micellar Assemblies. *Polymers (Basel).* **2019**, *11*, doi:10.3390/polym11071097.

44. Putnam, D.; Zelikin, A.N.; Izumrudov, V.A.; Langer, R. Polyhistidine-PEG:DNA Nanocomposites for Gene Delivery. *Biomaterials* **2003**, *24*, 4425–4433, doi:10.1016/S0142-9612(03)00341-7.

45. Kanayama, N.; Fukushima, S.; Nishiyama, N.; Itaka, K.; Jang, W.D.; Miyata, K.; Yamasaki, Y.; Chung, U. il; Kataoka, K. A PEG-Based Biocompatible Block Catiomer with High Buffering Capacity for the Construction of Polyplex Micelles Showing Efficient Gene Transfer toward Primary Cells. *ChemMedChem* **2006**, *1*, 439–444, doi:10.1002/cmdc.200600008.

46. Miyata, K.; Oba, M.; Nakanishi, M.; Fukushima, S.; Yamasaki, Y.; Koyama, H.; Nishiyama, N.; Kataoka, K. Polyplexes from Poly(Aspartamide) Bearing 1,2-Diaminoethane Side Chains Induce PH-Selective, Endosomal Membrane Destabilization with Amplified Transfection and Negligible Cytotoxicity. *J. Am. Chem. Soc.* **2008**, *130*, 16287–16294, doi:10.1021/ja804561g.

47. Chan, L.Y.; Khung, Y.L.; Lin, C.Y. Preparation of Messenger RNA Nanomicelles via Non-Cytotoxic PEG-Polyamine Nanocomplex for Intracerebroventicular Delivery: A Proof-of-Concept Study in Mouse Models. *Nanomaterials* **2019**, *9*, doi:10.3390/nano9010067.

48. Yoshinaga, N.; Naito, M.; Tachihara, Y.; Boonstra, E.; Osada, K.; Cabral, H.; Uchida, S. PEGylation of MRNA by Hybridization of Complementary PEG-RNA Oligonucleotides Stabilizes MRNA without Using Cationic Materials. *Pharmaceutics* **2021**, *13*, doi:10.3390/pharmaceutics13060800.

49. Kim, A.; Miura, Y.; Ishii, T.; Mutaf, O.F.; Nishiyama, N.; Cabral, H.; Kataoka, K. Intracellular Delivery of Charge-Converted Monoclonal Antibodies by Combinatorial Design of Block/Homo Polyion Complex Micelles. *Biomacromolecules* **2016**, *17*, 446–453, doi:10.1021/acs.biomac.5b01335.

50. Lee, Y.; Ishii, T.; Cabral, H.; Kim, H.J.; Seo, J.H.; Nishiyama, N.; Oshima, H.; Osada, K.; Kataoka, K. Charge-Conversional Polyionic Complex Micelles-Efficient Nanocarriers for Protein Delivery into Cytoplasm. *Angew. Chemie - Int. Ed.* **2009**, *48*, 5309–5312, doi:10.1002/anie.200900064.

51. Jiang, Y.; Arounleut, P.; Rheiner, S.; Bae, Y.; Kabanov, A. V.; Milligan, C.; Manickam, D.S. SOD1 Nanozyme with Reduced Toxicity and MPS Accumulation. *J. Control. Release* **2015**, *231*, 38–49, doi:10.1016/j.jconrel.2016.02.038.

52. Koide, A.; Kishimura, A.; Osada, K.; Jang, W.D.; Yamasaki, Y.; Kataoka, K. Semipermeable Polymer Vesicle (PICsome) Self-Assembled in Aqueous Medium from a Pair of Oppositely Charged Block Copolymers: Physiologically Stable Micro-/Nanocontainers of Water-Soluble Macromolecules. *J. Am. Chem. Soc.* **2006**, *128*, 5988–5989, doi:10.1021/ja057993r.

53. Kishimura, A.; Koide, A.; Osada, K.; Yamasaki, Y.; Kataoka, K. Encapsulation of Myoglobin in PEGylated Polyion Complex Vesicles Made from a Pair of Oppositely Charged Block Ionomers: A Physiologically Available Oxygen Carrier. *Angew. Chemie - Int. Ed.* **2007**, *46*, 6085–6088, doi:10.1002/anie.200701776.

54. Wibowo, A.; Osada, K.; Matsuda, H.; Anraku, Y.; Hirose, H.; Kishimura, A.; Kataoka, K.

Morphology Control in Water of Polyion Complex Nanoarchitectures of Double-Hydrophilic Charged Block Copolymers through Composition Tuning and Thermal Treatment. *Macromolecules* **2014**, *47*, 3086–3092, doi:10.1021/ma500314d.

55. Perry, S.L.; Leon, L.; Hoffmann, K.Q.; Kade, M.J.; Priftis, D.; Black, K. a.; Wong, D.; Klein, R. a.; Pierce, C.F.; Margossian, K.O.; et al. Chirality-Selected Phase Behaviour in Ionic Polypeptide Complexes. *Nat. Commun.* **2015**, *6*, 6052, doi:10.1038/ncomms7052.

56. Marciel, A.B.; Chung, E.J.; Brettmann, B.K.; Leon, L. Bulk and Nanoscale Polypeptide Based Polyelectrolyte Complexes. *Adv. Colloid Interface Sci.* **2017**, *239*, 187–198, doi:10.1016/j.cis.2016.06.012.

57. Sueyoshi, D.; Anraku, Y.; Komatsu, T.; Urano, Y.; Kataoka, K. Enzyme-Loaded Polyion Complex Vesicles as in Vivo Nanoreactors Working Sustainably under the Blood Circulation: Characterization and Functional Evaluation. *Biomacromolecules* **2017**, *18*, 1189–1196, doi:10.1021/acs.biomac.6b01870.

58. Hori, M.; Cabral, H.; Toh, K.; Kishimura, A.; Kataoka, K. Robust Polyion Complex Vesicles (PICsomes) under Physiological Conditions Reinforced by Multiple Hydrogen Bond Formation Derived by Guanidinium Groups. *Biomacromolecules* **2018**, *19*, 4113–4121, doi:10.1021/acs.biomac.8b01097.

59. Heuberger, L.; Korpidou, M.; Eggenberger, O.M.; Kyropoulou, M.; Palivan, C.G. Current Perspectives on Synthetic Compartments for Biomedical Applications. *Int. J. Mol. Sci.* **2022**, *23*, 5718, doi:10.3390/ijms23105718.

60. Solomatin, S. V.; Bronich, T.K.; Bargar, T.W.; Eisenberg, A.; Kabanov, V.A.; Kabanov, A. V. Environmentally Responsive Nanoparticles from Block Ionomer Complexes: Effects of PH and Ionic Strength. *Langmuir* **2003**, *19*, 8069–8076, doi:10.1021/la030015l.

61. Chelushkin, P.S.; Lysenko, E.A.; Bronich, T.K.; Eisenberg, A.; Kabanov, V.A.; Kabanov, A. V. Polyion Complex Nanomaterials from Block Polyelectrolyte Micelles and Linear Polyelectrolytes of Opposite Charge: 1. Solution Behavior. *J. Phys. Chem. B* **2007**, *111*, 8419–8425, doi:10.1021/jp0674221.

62. Hofs, B.; Voets, I.K.; De Keizer, A.; Cohen Stuart, M.A. Comparison of Complex Coacervate Core Micelles from Two Diblock Copolymers or a Single Diblock Copolymer with a Polyelectrolyte. *Phys. Chem. Chem. Phys.* **2006**, *8*, 4242–4251, doi:10.1039/b605695d.

63. Park, J.S.; Akiyama, Y.; Yamasaki, Y.; Kataoka, K. Preparation and Characterization of Polyion Complex Micelles with a Novel Thermosensitive Poly(2-Isopropyl-2-Oxazoline) Shell via the Complexation of Oppositely Charged Block Ionomers. *Langmuir* **2007**, *23*, 138–146, doi:10.1021/la061431j.

64. Li, L.; Srivastava, S.; Andreev, M.; Marciel, A.B.; De Pablo, J.J.; Tirrell, M. V. Phase Behavior and Salt Partitioning in Polyelectrolyte Complex Coacervates. *Macromolecules* **2018**, *51*, 2988–2995, doi:10.1021/acs.macromol.8b00238.

65. Chelushkin, P.S.; Lysenko, E.A.; Bronich, T.K.; Eisenberg, A.; Kabanov, V.A.; Kabanov, A. V. Polyion Complex Nanomaterials from Block Polyelectrolyte Micelles and Linear Polyelectrolytes of Opposite Charge. 2. Dynamic Properties. *J. Phys. Chem. B* **2008**, *112*, 7732–7738, doi:10.1021/jp8012877.

66. Li, Y.; Bronich, T.K.; Chelushkin, P.S.; Kabanov, A. V. Dynamic Properties of Block Ionomer Complexes with Polyion Complex Cores. *Macromolecules* **2008**, *41*, 5863–

5868, doi:10.1021/ma702671w.

67. Harada, A.; Kataoka, K. Effect of Charged Segment Length on Physicochemical Properties of Core-Shell Type Polyion Complex Micelles from Block Ionomers. *Macromolecules* **2003**, *36*, 4995–5001, doi:10.1021/ma025737i.

68. Voets, I.K.; De Keizer, A.; Cohen Stuart, M.A.; Justynska, J.; Schlaad, H. Irreversible Structural Transitions in Mixed Micelles of Oppositely Charged Diblock Copolymers in Aqueous Solution. *Macromolecules* **2007**, *40*, 2158–2164, doi:10.1021/ma0614444.

69. Priftis, D.; Laugel, N.; Tirrell, M. Thermodynamic Characterization of Polypeptide Complex Coacervation. *Langmuir* **2012**, *28*, 15947–15957, doi:10.1021/la302729r.

70. Fu, J.; Schlenoff, J.B. Driving Forces for Oppositely Charged Polyion Association in Aqueous Solutions: Enthalpic, Entropic, but Not Electrostatic. *J. Am. Chem. Soc.* **2016**, *138*, 980–990, doi:10.1021/jacs.5b11878.

71. Jiang, Y.; Fay, J.M.; Poon, C.D.; Vinod, N.; Zhao, Y.; Bullock, K.; Qin, S.; Manickam, D.S.; Yi, X.; Banks, W.A.; et al. Nanoformulation of Brain-Derived Neurotrophic Factor with Target Receptor-Triggered-Release in the Central Nervous System. *Adv. Funct. Mater.* **2018**, *28*, 1–11, doi:10.1002/adfm.201703982.

72. Fay, J.M.; Lim, C.; Finkelstein, A.; Batrakova, E. V; Kabanov, A. V PEG-Free Polyion Complex Nanocarriers for Brain-Derived Neurotrophic Factor. *Pharmaceutics* **2022**, *14*, 1391, doi:10.3390/pharmaceutics14071391.

73. Li, C.; Wang, Y.; Wang, X.; Gao, Z.; Ma, L.; Lu, X.; Cai, Y. Nanostructured Multiphase Condensation of Complex Coacervates in Polymerization-Induced Electrostatic Self-Assembly. *ACS Macro Lett.* **2021**, *10*, 780–785, doi:10.1021/acsmacrolett.1c00308.

74. Ren, J.; Zhang, Y.; Zhang, J.; Gao, H.; Liu, G.; Ma, R.; An, Y.; Kong, D.; Shi, L. PH/Sugar Dual Responsive Core-Cross-Linked PIC Micelles for Enhanced Intracellular Protein Delivery. *Biomacromolecules* **2013**, *14*, 3434–3443, doi:10.1021/bm4007387.

75. Yang, M.; Digby, Z.A.; Schlenoff, J.B. Precision Doping of Polyelectrolyte Complexes: Insight on the Role of Ions. *Macromolecules* **2020**, *53*, 5465–5474, doi:10.1021/acs.macromol.0c00965.

76. Oh, K.T.; Bronich, T.K.; Kabanov, V.A.; Kabanov, A. V Block Polyelectrolyte Networks from Poly(Acrylic Acid) and Poly(Ethylene Oxide): Sorption and Release of Cytochrome C. *Biomacromolecules* **2007**, *8*, 490–497, doi:10.1021/bm060599g.

77. Zhang, Y.; Batys, P.; O'Neal, J.T.; Li, F.; Sammalkorpi, M.; Lutkenhaus, J.L. Molecular Origin of the Glass Transition in Polyelectrolyte Assemblies. *ACS Cent. Sci.* **2018**, *4*, 638–644, doi:10.1002/pol.1957.1202611319.

78. Vishwasrao, H.M.; Master, A.M.; Seo, Y.G.; Liu, X.M.; Pothayee, N.; Zhou, Z.; Yuan, D.; Boska, M.D.; Bronich, T.K.; Davis, R.M.; et al. Luteinizing Hormone Releasing Hormone-Targeted Cisplatin-Loaded Magnetite Nanoclusters for Simultaneous MR Imaging and Chemotherapy of Ovarian Cancer. *Chem. Mater.* **2016**, *28*, 3024–3040, doi:10.1021/acs.chemmater.6b00197.

79. Banani, S.F.; Lee, H.O.; Hyman, A.A.; Rosen, M.K. Biomolecular Condensates: Organizers of Cellular Biochemistry. *Nat. Rev. Mol. Cell Biol.* **2017**, *18*, 285–298, doi:10.1038/nrm.2017.7.

80. Schuler, B.; Borgia, A.; Borgia, M.B.; Heidarsson, P.O.; Holmstrom, E.D.; Nettels, D.; Sottini, A. Binding without Folding – the Biomolecular Function of Disordered Polyelectrolyte Complexes. *Curr. Opin. Struct. Biol.* **2020**, *60*, 66–76, doi:10.1016/j.sbi.2019.12.006.

81. Madinya, J.J.; Chang, L.W.; Perry, S.L.; Sing, C.E. Sequence-Dependent Self-Coacervation in High Charge-Density Polyampholytes. *Mol. Syst. Des. Eng.* **2020**, *5*, 632–644, doi:10.1039/c9me00074g.

82. Ladenheim, H.; Morawetz, H. A New Type of Polyampholyte: Poly(4-Vinyl Pyridine Betaine). *J. Polym. Sci.* **1957**, *26*, 251–254, doi:10.1002/pol.1957.1202611319.

83. Neitzel, A.E.; De Hoe, G.X.; Tirrell, M. V. Expanding the Structural Diversity of Polyelectrolyte Complexes and Polyzwitterions. *Curr. Opin. Solid State Mater. Sci.* **2021**, *25*, 100897, doi:10.1016/j.cossms.2020.100897.

84. Paschke, S.; Lienkamp, K. Polyzwitterions: From Surface Properties and Bioactivity Profiles to Biomedical Applications. *ACS Appl. Polym. Mater.* **2020**, *2*, 129–151, doi:10.1021/acsapm.9b00897.

85. Taylor, M.E.; Lounder, S.J.; Asatekin, A.; Panzer, M.J. Synthesis and Self-Assembly of Fully Zwitterionic Triblock Copolymers. *ACS Mater. Lett.* **2020**, *2*, 261–265, doi:10.1021/acsmaterialslett.9b00500.

86. Chuanoi, S.; Anraku, Y.; Hori, M.; Kishimura, A.; Kataoka, K. Fabrication of Polyion Complex Vesicles with Enhanced Salt and Temperature Resistance and Their Potential Applications as Enzymatic Nanoreactors. *Biomacromolecules* **2014**, *15*, 2389–2397, doi:10.1021/bm500127g.

87. Lutz, J.-F.; Ouchi, M.; Liu, D.R.; Sawamoto, M. Sequence-Controlled Polymers. *Science (80-. ).* **2013**, *341*, 13924–13925, doi:10.1126/science.1238149.

88. Lutz, J.F.; Lehn, J.M.; Meijer, E.W.; Matyjaszewski, K. From Precision Polymers to Complex Materials and Systems. *Nat. Rev. Mater.* **2016**, *1*, doi:10.1038/natrevmats.2016.24.

89. Rosales, A.M.; Segalman, R.A.; Zuckermann, R.N. Polypeptoids: A Model System to Study the Effect of Monomer Sequence on Polymer Properties and Self-Assembly. *Soft Matter* **2013**, *9*, 8400–8414, doi:10.1039/c3sm51421h.

90. Perry, S.L.; Leon, L.; Hoffmann, K.Q.; Kade, M.J.; Priftis, D.; Black, K.A.; Wong, D.; Klein, R.A.; Pierce, C.F.; Margossian, K.O.; et al. Chirality-Selected Phase Behaviour in Ionic Polypeptide Complexes. *Nat. Commun.* **2015**, *6*, doi:10.1038/ncomms7052.

91. Chang, L.W.; Lytle, T.K.; Radhakrishna, M.; Madinya, J.J.; Vélez, J.; Sing, C.E.; Perry, S.L. Sequence and Entropy-Based Control of Complex Coacervates. *Nat. Commun.* **2017**, *8*, 1–7, doi:10.1038/s41467-017-01249-1.

92. Tabandeh, S.; Leon, L. Engineering Peptide-Based Polyelectrolyte Complexes with Increased Hydrophobicity. *Molecules* **2019**, *24*, doi:10.3390/molecules24050868.

93. Rumyantsev, A.M.; Jackson, N.E.; Yu, B.; Ting, J.M.; Chen, W.; Tirrell, M. V.; De Pablo, J.J. Controlling Complex Coacervation via Random Polyelectrolyte Sequences. *ACS Macro Lett.* **2019**, *8*, 1296–1302, doi:10.1021/acsmacrolett.9b00494.

94. Rumyantsev, A.M.; Jackson, N.E.; De Pablo, J.J. Polyelectrolyte Complex Coacervates:

Recent Developments and New Frontiers. *Annu. Rev. Condens. Matter Phys.* **2021**, *12*, 155–176, doi:10.1146/annurev-conmatphys-042020-113457.

95. Lytle, T.K.; Chang, L.W.; Markiewicz, N.; Perry, S.L.; Sing, C.E. Designing Electrostatic Interactions via Polyelectrolyte Monomer Sequence. *ACS Cent. Sci.* **2019**, *5*, 709–718, doi:10.1021/acscentsci.9b00087.

96. Kord Forooshani, P.; Lee, B.P. Recent Approaches in Designing Bioadhesive Materials Inspired by Mussel Adhesive Protein. *J. Polym. Sci. Part A Polym. Chem.* **2017**, *55*, 9–33, doi:10.1002/pola.28368.

97. Zhao, Q.; Lee, D.W.; Ahn, B.K.; Seo, S.; Kaufman, Y.; Israelachvili, J.N.; Waite, J.H. Underwater Contact Adhesion and Microarchitecture in Polyelectrolyte Complexes Actuated by Solvent Exchange. *Nat. Mater.* **2016**, *15*, 407–412, doi:10.1038/nmat4539.

98. White, J.D.; Wilker, J.J. Underwater Bonding with Charged Polymer Mimics of Marine Mussel Adhesive Proteins. *Macromolecules* **2011**, *44*, 5085–5088, doi:10.1021/ma201044x.

99. Kim, S.; Huang, J.; Lee, Y.; Dutta, S.; Young Yoo, H.; Mee Jung, Y.; Jho, Y.; Zeng, H.; Hwang, D.S. Complexation and Coacervation of Like-Charged Polyelectrolytes Inspired by Mussels. *Proc. Natl. Acad. Sci. U. S. A.* **2016**, *113*, E847–E853, doi:10.1073/pnas.1521521113.

100. Kang, T.; Banquy, X.; Heo, J.; Lim, C.; Lynd, N.A.; Lundberg, P.; Oh, D.X.; Lee, H.K.; Hong, Y.K.; Hwang, D.S.; et al. Mussel-Inspired Anchoring of Polymer Loops That Provide Superior Surface Lubrication and Antifouling Properties. *ACS Nano* **2016**, *10*, 930–937, doi:10.1021/acsnano.5b06066.

101. Webber, M.J.; Appel, E.A.; Vinciguerra, B.; Cortinas, A.B.; Thapa, L.S.; Jhunjhunwala, S.; Isaacs, L.; Langer, R.; Anderson, D.G. Supramolecular PEGylation of Biopharmaceuticals. *Proc. Natl. Acad. Sci.* **2016**, *113*, 14189–14194, doi:10.1073/pnas.1616639113.

102. Armstrong, J.K. *PEGylated Protein Drugs: Basic Science and Clinical Applications*; Birkhauser: Basel, Switzerland, 2009; ISBN 9783764386788.

103. Leader, B.; Baca, Q.J.; Golan, D.E. Protein Therapeutics: A Summary and Pharmacological Classification. *Nat. Rev. Drug Discov.* **2008**, *7*, 21–39, doi:10.1038/nrd2399.

104. Yu, M.; Wu, J.; Shi, J.; Farokhzad, O.C. Nanotechnology for Protein Delivery: Overview and Perspectives. *J. Control. Release* **2016**, *240*, 24–37, doi:10.1016/j.jconrel.2015.10.012.

105. Shi, D.; Beasock, D.; Fessler, A.; Szebeni, J.; Ljubimova, J.Y.; Afonin, K.A.; Dobrovolskaia, M.A. To PEGylate or Not to PEGylate: Immunological Properties of Nanomedicine's Most Popular Component, Polyethylene Glycol and Its Alternatives. *Adv. Drug Deliv. Rev.* **2022**, *180*, 114079, doi:10.1016/j.addr.2021.114079.

106. Harris, N.M.; Ritzel, R.; Mancini, N.; Jiang, Y.; Yi, X.; Manickam, D.S.; Banks, W.A.; Kabanov, A. V.; McCullough, L.D.; Verma, R. Nano-Particle Delivery of Brain Derived Neurotrophic Factor after Focal Cerebral Ischemia Reduces Tissue Injury and Enhances Behavioral Recovery. *Pharmacol. Biochem. Behav.* **2016**, *150–151*, 48–56, doi:10.1016/j.pbb.2016.09.003.

107. Lee, Y.; Kataoka, K. Biosignal-Sensitive Polyion Complex Micelles for the Delivery of

Biopharmaceuticals. *Soft Matter* **2009**, *5*, 3810, doi:10.1039/b909934d.

108. Sedlák, E.; Fedunová, D.; Veselá, V.; Sedláková, D.; Antalík, M. Polyanion Hydrophobicity and Protein Basicity Affect Protein Stability in Protein-Polyanion Complexes. *Biomacromolecules* **2009**, *10*, 2533–2538, doi:10.1021/bm900480t.

109. Cousin, F.; Gummel, J.; Combet, S.; Boué, F. The Model Lysozyme-PSSNa System for Electrostatic Complexation: Similarities and Differences with Complex Coacervation. *Adv. Colloid Interface Sci.* **2011**, *167*, 71–84, doi:10.1016/j.cis.2011.05.007.

110. Wang, S.; Chen, K.; Li, L.; Guo, X. Binding between Proteins and Cationic Spherical Polyelectrolyte Brushes: Effect of PH, Ionic Strength, and Stoichiometry. *Biomacromolecules* **2013**, *14*, 818–827, doi:10.1021/bm301865g.

111. Xu, X.; Angioletti-Uberti, S.; Lu, Y.; Dzubiella, J.; Ballauff, M. Interaction of Proteins with Polyelectrolytes: Comparison of Theory to Experiment. *Langmuir* **2019**, *35*, 5373–5391, doi:10.1021/acs.langmuir.8b01802.

112. Bourganis, V.; Karamanidou, T.; Kammona, O.; Kiparissides, C. Polyelectrolyte Complexes as Prospective Carriers for the Oral Delivery of Protein Therapeutics. *Eur. J. Pharm. Biopharm.* **2017**, *111*, 44–60, doi:10.1016/j.ejpb.2016.11.005.

113. Alcalá-Barraza, S.R.; Lee, M.S.; Hanson, L.R.; McDonald, A. a; Frey, W.H.; McLoon, L.K. Intranasal Delivery of Neurotrophic Factors BDNF, CNTF, EPO, and NT-4 to the CNS. *J. Drug Target.* **2010**, *18*, 179–190, doi:10.3109/10611860903318134.

114. Oller-Salvia, B.; Sánchez-Navarro, M.A.; Ciudad, S.; Guiu, M.; Arranz-Gibert, P.; Garcia, C.; Gomis, R.R.; Cecchelli, R.; García, J.; Giralt, E.; et al. MiniAp-4: A Venom-Inspired Peptidomimetic for Brain Delivery. *Angew. Chemie - Int. Ed.* **2016**, *55*, 572–575, doi:10.1002/anie.201508445.

115. Kim, A.; Miura, Y.; Ishii, T.; Mutaf, O.F.; Nishiyama, N.; Cabral, H.; Kataoka, K. Intracellular Delivery of Charge-Converted Monoclonal Antibodies by Combinatorial Design of Block/Homo Polyion Complex Micelles. *Biomacromolecules* **2016**, *17*, 446–453, doi:10.1021/acs.biomac.5b01335.

116. Kabanov, V.A.; Evdakov, V.P.; Mustafayev, M.I.; Antipina, A.D. Cooperative Bonding of Serum Albumin by Quaternized Poly-4-Vinylpyridines and Structure of the Complexes Formed. *Mol. Biol.* **1977**, *11*, 582–597.

117. Kabanov, V.A.; Mustafaev, M.I.; Belova, V. V.; Evdakov, V.P. Soluble Complexes of Bovine Serum Albumin with Amphoteric Linear Electrolytes. *Mol. Biol.* **1979**, *12*, 1264–1277.

118. Kabanov, V.A.; Mustafayev, M.I.; Goncharov, V.V. Soluble Complexes of Bovine Serum Albumin with Poly-4-Vinylpyridinium Cations Containing N-Cetyl Side Radicals. *Polym. Sci. U.S.S.R.* **1981**, *23*, 287–298, doi:10.1016/0032-3950(81)90168-4.

119. Margolin, A.L.; Izumrudov, V.A.; Švedas, V.K.; Zezin, A.B.; Kabanov, V.A.; Berezin, I.V. Preparation and Properties of Penicillin Amidase Immobilized in Polyelectrolyte Complexes. *Biochim. Biophys. Acta - Enzymol.* **1981**, *660*, 359–365, doi:10.1016/0005-2744(81)90181-9.

120. Tobío, M.; Gref, R.; Sánchez, A.; Langer, R.; Alonso, M.J. Stealth PLA-PEG Nanoparticles as Protein Carriers for Nasal Administration. *Pharm. Res.* 1998, *15*, 270–275.

121. Harada, A.; Kataoka, K. On-off Control of Enzymatic Activity Synchronizing with

Reversible Formation of Supramolecular Assembly from Enzyme and Charged Block Copolymers [12]. *J. Am. Chem. Soc.* **1999**, *121*, 9241–9242, doi:10.1021/ja9919175.

122. Harada, A.; Kataoka, K. Novel Polyion Complex Micelles Entrapping Enzyme Molecules in the Core. 2. Characterization of the Micelles Prepared at Nonstoichiometric Mixing Ratios. *Langmuir* **1999**, *15*, 4208–4212, doi:10.1021/la981087t.

123. Jaturanpinyo, M.; Harada, A.; Yuan, X.; Kataoka, K. Preparation of Bionanoreactor Based on Core-Shell Structured Polyion Complex Micelles Entrapping Trypsin in the Core Cross-Linked with Glutaraldehyde. *Bioconjug. Chem.* **2004**, *15*, 344–348, doi:10.1021/bc034149m.

124. Kawamura, A.; Harada, A.; Kono, K.; Kataoka, K. Self-Assembled Nano-Bioreactor from Block Ionomers with Elevated and Stabilized Enzymatic Function. *Bioconjug. Chem.* **2007**, *18*, 1555–1559, doi:10.1021/bc070029t.

125. Yuan, X.; Harada, A.; Yamasaki, Y.; Kataoka, K. Stabilization of Lysozyme-Incorporated Polyion Complex Micelles by the ω-End Derivatization of Poly(Ethylene Glycol)–Poly(α,β-Aspartic Acid) Block Copolymers with Hydrophobic Groups. *Langmuir* **2005**, *21*, 2668–2674, doi:10.1021/la0488811.

126. Yuan, X.; Yamasaki, Y.; Harada, A.; Kataoka, K. Characterization of Stable Lysozyme-Entrapped Polyion Complex (PIC) Micelles with Crosslinked Core by Glutaraldehyde. *Polymer (Guildf).* **2005**, *46*, 7749–7758, doi:10.1016/j.polymer.2005.02.121.

127. Lindhoud, S.; Norde, W.; Stuart, M.A.C. Reversibility and Relaxation Behavior of Polyelectrolyte Complex Micelle Formation. *J. Phys. Chem. B* **2009**, *113*, 5431–5439, doi:10.1021/jp809489f.

128. Lindhoud, S.; Voorhaar, L.; Vries, R. De; Schweins, R.; Stuart, M.A.C.; Norde, W. Salt-Induced Disintegration of Lysozyme-Containing Polyelectrolyte Complex Micelles. *Langmuir* **2009**, *25*, 11425–11430, doi:10.1021/la901591p.

129. Lindhoud, S.; De Vries, R.; Schweins, R.; Cohen Stuart, M.A.; Norde, W. Salt-Induced Release of Lipase from Polyelectrolyte Complex Micelles. *Soft Matter* **2009**, *5*, 242–250, doi:10.1039/b811640g.

130. Lindhoud, S.; de Vries, R.; Norde, W.; Stuart, M.A.C. Structure and Stability of Complex Coacervate Core Micelles with Lysozyme. *Biomacromolecules* **2007**, *8*, 2219–2227, doi:10.1021/bm0700688.

131. Lee, Y.; Fukushima, S.; Bae, Y.; Hiki, S.; Ishii, T.; Kataoka, K. A Protein Nanocarrier from Charge-Conversion Polymer in Response to Endosomal PH. *J. Am. Chem. Soc.* **2007**, *129*, 5362–5363, doi:10.1021/ja071090b.

132. Zhang, Y.; Han, K.; Lu, D.; Liu, Z. Reversible Encapsulation of Lysozyme within MPEG-b-PMAA: Experimental Observation and Molecular Dynamics Simulation. *Soft Matter* **2013**, *9*, 8723–8729, doi:10.1039/c3sm50586c.

133. Reichert, C.; Borchard, G. Noncovalent PEGylation, An Innovative Subchapter in the Field of Protein Modification. *J. Pharm. Sci.* **2016**, *105*, 386–390, doi:10.1002/jps.24692.

134. Fay, J.M.; Zhu, C.; Proctor, E.A.; Tao, Y.; Cui, W.; Ke, H.; Dokholyan, N.V. A Phosphomimetic Mutation Stabilizes SOD1 and Rescues Cell Viability in the Context of an ALS-Associated Mutation. *Structure* **2016**, *24*, doi:10.1016/j.str.2016.08.011.

135. Tong, J.; Yi, X.; Luxenhofer, R.; Banks, W.A.; Jordan, R.; Zimmerman, M.C.; Kabanov, A. V Conjugates of Superoxide Dismutase 1 with Amphiphilic Poly(2-Oxazoline) Block Copolymers for Enhanced Brain Delivery: Synthesis, Characterization and Evaluation in Vitro and in Vivo. *Mol. Pharm.* **2013**, *10*, 360–377, doi:10.1021/mp300496x.

136. Jiang, Y.; Brynskikh, A.M.; S-Manickam, D.; Kabanov, A. V. SOD1 Nanozyme Salvages Ischemic Brain by Locally Protecting Cerebral Vasculature. *J. Control. Release* **2015**, *213*, 36–44, doi:10.1016/j.jconrel.2015.06.021.

137. Efremenko, E.N.; Lyagin, I.V.; Klyachko, N.L.; Bronich, T.; Zavyalova, N.V.; Jiang, Y.; Kabanov, A.V. A Simple and Highly Effective Catalytic Nanozyme Scavenger for Organophosphorus Neurotoxins. *J. Control. Release* **2017**, *247*, 175–181, doi:10.1016/j.jconrel.2016.12.037.

138. Zhang, P.; Liu, E.J.; Tsao, C.; Kasten, S.A.; Boeri, M. V.; Dao, T.L.; DeBus, S.J.; Cadieux, C.L.; Baker, C.A.; Otto, T.C.; et al. Nanoscavenger Provides Long-Term Prophylactic Protection against Nerve Agents in Rodents. *Sci. Transl. Med.* **2019**, *11*, doi:10.1126/scitranslmed.aau7091.

139. Li, J.; Anraku, Y.; Kataoka, K. Self-Boosting Catalytic Nanoreactors Integrated with Triggerable Crosslinking Membrane Networks for Initiation of Immunogenic Cell Death by Pyroptosis. *Angew. Chemie - Int. Ed.* **2020**, *59*, 13526–13530, doi:10.1002/anie.202004180.

140. Zhang, X.; Chen, W.; Zhu, X.; Lu, Y. Encapsulating Therapeutic Proteins with Polyzwitterions for Lower Macrophage Nonspecific Uptake and Longer Circulation Time. *ACS Appl. Mater. Interfaces* **2017**, *9*, 7972–7978, doi:10.1021/acsami.6b16413.

141. Batrakova, E. V; Li, S.; Reynolds, A.D.; Mosley, R.L.; Bronich, T.K.; Kabanov, A. V; Gendelman, H.E. A Macrophage - Nanozyme Delivery System for Parkinson ' s Disease. *Bioconjug. Chem.* **2007**, *18*, 1498–1506, doi:10.1021/bc700184b.

142. Brynskikh, A.M.; Zhao, Y.; Mosley, R.L.; Li, S.; Boska, M.D.; Klyachko, N.L.; Kabanov, A. V; Gendelman, H.E.; Batrakova, E. V Macrophage Delivery of Therapeutic Nanozymes in a Murine Model of Parkinson's Disease. *Nanomedicine (Lond).* **2010**, *5*, 379–396, doi:10.2217/nnm.10.7.

143. Zhao, Y.; Haney, M.J.; Mahajan, V.; Reiner, B.C.; Dunaevsky, A.; Mosley, R.L.; Kabanov, A. V; Gendelman, H.E.; Batrakova, E. V Active Targeted Macrophage-Mediated Delivery of Catalase to Affected Brain Regions in Models of Parkinson's Disease. *J. Nanomed. Nanotechnol.* **2011**, *S4*, doi:10.4172/2157-7439.S4-003.

144. Haney, M.J.; Klyachko, N.L.; Zhao, Y.; Gupta, R.; Plotnikova, E.G.; He, Z.; Patel, T.; Piroyan, A.; Sokolsky, M.; Kabanov, A. V.; et al. Exosomes as Drug Delivery Vehicles for Parkinson's Disease Therapy. *J. Control. Release* **2015**, *207*, 18–30, doi:10.1016/j.jconrel.2015.03.033.

145. Haney, M.J.; Zhao, Y.; Harrison, E.B.; Mahajan, V.; Ahmed, S.; He, Z.; Suresh, P.; Hingtgen, S.D.; Klyachko, N.L.; Mosley, R.L.; et al. Specific Transfection of Inflamed Brain by Macrophages: A New Therapeutic Strategy for Neurodegenerative Diseases. *PLoS One* **2013**, *8*, doi:10.1371/journal.pone.0061852.

146. Yi, X.; Yuan, D.; Farr, S.A.; Banks, W.A.; Poon, C.D.; Kabanov, A. V. Pluronic Modified Leptin with Increased Systemic Circulation, Brain Uptake and Efficacy for Treatment of Obesity. *J. Control. Release* **2014**, *191*, 34–46, doi:10.1016/j.jconrel.2014.05.044.

147. Yuan, D.; Yi, X.; Zhao, Y.; Poon, C.D.; Bullock, K.M.; Hansen, K.M.; Salameh, T.S.; Farr, S.A.; Banks, W.A.; Kabanov, A. V. Intranasal Delivery of N-Terminal Modified Leptin-Pluronic Conjugate for Treatment of Obesity. *J. Control. Release* **2017**, *263*, 172–184, doi:10.1016/j.jconrel.2017.03.029.

148. Yuan, D.; Zhao, Y.; Banks, W.A.; Bullock, K.M.; Haney, M.; Batrakova, E.; Kabanov, A. V. Macrophage Exosomes as Natural Nanocarriers for Protein Delivery to Inflamed Brain. *Biomaterials* **2017**, *142*, 1–12, doi:10.1016/j.biomaterials.2017.07.011.

149. Robinson, R.C.; Radziejewski, C.; Stuart, D.I.; Jones, E.Y. Structure of the Brain-Derived Neurotrophic Factor/Neurotrophin 3 Heterodimer. *Biochemistry* **1995**, *34*, 4139–4146, doi:10.1007/s12291-011-0108-4.

150. Abuchowski, A.; Es, T. Van; Palczuk, N.C.; Davis, F.F. Alteration of Immunological Properties of Bovine Serum Albumin by Covalent Attachment of Polyethylene Glycol *. *J. Biol. Chem.* **1977**, *252*, 3578–3581, doi:10.1016/S0021-9258(17)40291-2.

151. Merrill, E.W. Distinctions and Correspondences among Surfaces Contacting Blood. *Ann. N. Y. Acad. Sci.* **1987**, *516*, 196–203.

152. Wang, Y.; Lai, S.K.; Suk, J.S.; Pace, A.; Cone, R. Addressing the PEG Mucoadhesivity Paradox to Engineer Nanoparticles That "Slip" through the Human Mucus Barrier. *Agnew Chem Int Ed Engl* **2008**, *47*, 9726–9729, doi:10.1002/anie.200803526.Addressing.

153. Nance, E.A.; Woodworth, G.F.; Sailor, K.A.; Shih, T.; Xu, Q.; Swaminathan, G.; Xiang, D.; Eberhart, C.; Hanes, J. A Dense Poly(Ethylene Glycol) Coating Improves Penetration of Large Polymeric Nanoparticles within Brain Tissue. *Sci. Transl. Med.* **2012**, *4*, doi:10.1126/scitranslmed.3003594.A.

154. Ishida, T.; Masuda, K.; Ichikawa, T.; Ichihara, M.; Irimura, K.; Kiwada, H. Accelerated Clearance of a Second Injection of PEGylated Liposomes in Mice. *Int. J. Pharm.* **2003**, *255*, 167–174, doi:10.1016/S0378-5173(03)00085-1.

155. Armstrong, J.K. The Occurrence, Induction, Specificity and Potential Effect of Antibodies against Poly(Ethylene Glycol). In *PEGylated Protein Drugs: Basic Science and Clinical Applications*; Veronese, F.M., Ed.; Birkhäuser Basel: Basel, 2009; pp. 147–168 ISBN 978-3-7643-8679-5.

156. Henry, C.E.; Wang, Y.-Y.; Yang, Q.; Hoang, T.; Chattopadhyay, S.; Hoen, T.; Ensign, L.M.; Nunn, K.L.; Schroeder, H.; McCallen, J.; et al. Anti-PEG Antibodies Alter the Mobility and Biodistribution of Densely PEGylated Nanoparticles in Mucus. *Acta Biomater.* **2016**, *43*, 61–70, doi:10.1016/j.actbio.2016.07.019.

157. Yang, Q.; Jacobs, T.M.; McCallen, J.D.; Moore, D.T.; Huckaby, J.T.; Edelstein, J.N.; Lai, S.K. Analysis of Pre-Existing IgG and IgM Antibodies against Polyethylene Glycol (PEG) in the General Population. *Anal. Chem.* **2016**, *88*, 11804–11812, doi:10.1021/acs.analchem.6b03437.

158. Haddad, H.F.; Burke, J.A.; Scott, E.A.; Ameer, G.A. Clinical Relevance of Pre-Existing and Treatment-Induced Anti-Poly ( Ethylene Glycol ) Antibodies. *Regen. Eng. Transl. Med.* **2021**, *8*, 32–42, doi:10.1007/s40883-021-00198-y.

159. Moghimi, S.M. Allergic Reactions and Anaphylaxis to LNP-Based COVID-19 Vaccines. *Mol. Ther.* **2021**, *29*, 898–900, doi:10.1016/j.ymthe.2021.01.030.

160. Risma, K.A.; Edwards, K.M.; Hummell, D.S.; Little, F.F. Potential Mechanisms of Anaphylaxis to COVID-19 MRNA Vaccines. *J. Allergy Clin. Immunol.* **2019**, *147*, 2075-2082.e2, doi:10.1016/j.jaci.2021.04.002.

161. Warren, C.M.; Snow, T.T.; Lee, A.S.; Shah, M.M.; Heider, A.; Blomkalns, A.; Betts, B.; Buzzanco, A.S.; Gonzalez, J.; Chinthrajah, R.S.; et al. Assessment of Allergic and Anaphylactic Reactions to MRNA COVID-19 Vaccines with Confirmatory Testing in a US Regional Health System. *JAMA Netw. Open* **2021**, *4*, 1–15, doi:10.1001/jamanetworkopen.2021.25524.

162. Lau, K.H.A. Peptoids for Biomaterials Science. *Biomater. Sci.* **2014**, *2*, 627–633, doi:10.1039/C3BM60269A.

163. Chan, B.A.; Xuan, S.; Li, A.; Simpson, J.M.; Sternhagen, G.L.; Yu, T.; Darvish, O.A.; Jiang, N.; Zhang, D. Polypeptoid Polymers: Synthesis, Characterization, and Properties. *Biopolymers* **2018**, *109*, 1–25, doi:10.1002/bip.23070.

164. Barz, M.; Luxenhofer, R.; Zentel, R.; Vicent, M.J. Overcoming the PEG-Addiction: Well-Defined Alternatives to PEG, from Structure–Property Relationships to Better Defined Therapeutics. *Polym. Chem.* **2011**, *2*, 1900–1918, doi:10.1039/C0PY00406E.

165. Ostuni, E.; Chapman, R.G.; Liang, M.N.; Meluleni, G.; Pier, G.; Ingber, D.E.; Whitesides, G.M. Self-Assembled Monolayers That Resist the Adsorption of Proteins and the Adhesion of Bacterial and Mammalian Cells. *Langmuir* **2001**, *17*, 6336–6343, doi:10.1021/la010552a.

166. Huesmann, D.; Sevenich, A.; Weber, B.; Barz, M. A Head-to-Head Comparison of Poly(Sarcosine) and Poly(Ethylene Glycol) in Peptidic, Amphiphilic Block Copolymers. *Polym. (United Kingdom)* **2015**, *67*, 240–248, doi:10.1016/j.polymer.2015.04.070.

167. Hu, Y.; Hou, Y.; Wang, H.; Lu, H. Polysarcosine as an Alternative to PEG for Therapeutic Protein Conjugation. *Bioconjug. Chem.* **2018**, *29*, 2232–2238, doi:10.1021/acs.bioconjchem.8b00237.

168. Son, K.; Ueda, M.; Taguchi, K.; Maruyama, T.; Takeoka, S. Evasion of the Accelerated Blood Clearance Phenomenon by Polysarcosine Coating of Liposomes. *J. Control. Release* **2020**, *322*, 209–216, doi:10.1016/j.jconrel.2020.03.022.

169. Luxenhofer, R.; Han, Y.; Schulz, A.; Tong, J.; He, Z.; Kabanov, A. V; Jordan, R. Poly(2-Oxazoline)s as Polymer Therapeutics. *Macromol. Rapid Commun.* **2012**, *33*, 1613–1631, doi:10.1212/WNL.51.3.695.

170. Mero, A.; Pasut, G.; Via, L.D.; Fijten, M.W.M.; Schubert, U.S.; Hoogenboom, R.; Veronese, F.M. Synthesis and Characterization of Poly(2-Ethyl 2-Oxazoline)-Conjugates with Proteins and Drugs: Suitable Alternatives to PEG-Conjugates? *J. Control. Release* **2008**, *125*, 87–95, doi:10.1016/j.jconrel.2007.10.010.

171. Hwang, D.; Ramsey, J.D.; Makita, N.; Sachse, C.; Jordan, R.; Sokolsky-papkov, M.; Kabanov, A. V Novel Poly ( 2-Oxazoline ) Block Copolymer with Aromatic Heterocyclic Side Chains as a Drug Delivery Platform. *J. Control. Release* **2019**, *307*, 261–271, doi:10.1016/j.jconrel.2019.06.037.

172. Zalipsky, S.; Hansen, C.B.; Oaks, J.M.; Allen, T.M. Evaluation of Blood Clearance Rates and Biodistribution of Poly(2-Oxazoline)-Grafted Liposomes. *J. Pharm. Sci.* **1996**, *85*, 133–137, doi:10.1021/js9504043.

173. Woodle, M.C.; Engbers, C.M.; Zalipsky, S. New Amphipatic Polymer-Lipid Conjugates Forming Long-Circulating Reticuloendothelial System-Evading Liposomes. *Bioconjug. Chem.* **1994**, *5*, 493–496, doi:10.1021/bc00030a001.

174. Konradi, R.; Acikgoz, C.; Textor, M. Polyoxazolines for Nonfouling Surface Coatings - A Direct Comparison to the Gold Standard PEG. *Macromol. Rapid Commun.* **2012**, *33*, 1663–1676, doi:10.1002/marc.201200422.

175. Seo, Y.; Schulz, A.; Han, Y.; He, Z.; Bludau, H.; Wan, X.; Tong, J.; Bronich, T.K.; Sokolsky, M.; Luxenhofer, R.; et al. Poly(2-Oxazoline) Block Copolymer Based Formulations of Taxanes: Effect of Copolymer and Drug Structure, Concentration, and Environmental Factors. *Polym. Adv. Technol.* **2015**, *26*, 837–850, doi:10.1002/pat.3556.

176. Hwang, D.; Dismuke, T.; Tikunov, A.; Rosen, E.P.; Kagel, J.R.; Ramsey, J.D.; Lim, C.; Zamboni, W.; Kabanov, A. V; Gershon, T.R.; et al. Poly ( 2-Oxazoline ) Nanoparticle Delivery Enhances the Therapeutic Potential of Vismodegib for Medulloblastoma by Improving CNS Pharmacokinetics and Reducing Systemic Toxicity. *Nanomedicine Nanotechnology, Biol. Med.* **2021**, *32*, 102345, doi:10.1016/j.nano.2020.102345.

177. Hwang, D.; Ramsey, J.D.; Kabanov, A. V Polymeric Micelles for the Delivery of Poorly Soluble Drugs : From Nanoformulation to Clinical Approval. *Adv. Drug Deliv. Rev.* **2020**, *156*, 80–118, doi:10.1016/j.addr.2020.09.009.

178. Vinod, N.; Hwang, D.; Azam, S.H.; Van Swearingen, A.E.D.; Wayne, E.; Fussell, S.C.; Sokolsky-Papkov, M.; Pecot, C. V; Kabanov, A. V High-Capacity Poly(2-Oxazoline) Formulation of TLR 7/8 Agonist Extends Survival in a Chemo-Insensitive, Metastatic Model of Lung Adenocarcinoma. *Sci. Adv.* **2020**, *6*, doi:10.1126/sciadv.aba5542.

179. Luxenhofer, R.; Schulz, A.; Roques, C.; Li, S.; Bronich, T.K.; Batrakova, E. V; Jordan, R.; Kabanov, A. V Biomaterials Doubly Amphiphilic Poly ( 2-Oxazoline ) s as High-Capacity Delivery Systems for Hydrophobic Drugs. *Biomaterials* **2010**, *31*, 4972–4979, doi:10.1016/j.biomaterials.2010.02.057.

180. Wan, X.; Beaudoin, J.J.; Vinod, N.; Min, Y.; Makita, N.; Bludau, H.; Jordan, R.; Wang, A.; Sokolsky, M.; Kabanov, A. V Biomaterials Co-Delivery of Paclitaxel and Cisplatin in Poly ( 2-Oxazoline ) Polymeric Micelles : Implications for Drug Loading , Release , Pharmacokinetics and Outcome of Ovarian and Breast Cancer Treatments. *Biomaterials* **2019**, *192*, 1–14, doi:10.1016/j.biomaterials.2018.10.032.

181. He, Z.; Schulz, A.; Wan, X.; Seitz, J.; Bludau, H.; Alakhova, D.Y.; Darr, D.B.; Perou, C.M.; Jordan, R.; Ojima, I.; et al. Poly(2-Oxazoline) Based Micelles with High Capacity for 3rd Generation Taxoids: Preparation, in Vitro and in Vivo Evaluation. *J. Control. Release* **2015**, *208*, 67–75, doi:10.1016/j.jconrel.2015.02.024.

182. Laschewsky, A.; Rosenhahn, A. Molecular Design of Zwitterionic Polymer Interfaces: Searching for the Difference. *Langmuir* **2019**, *35*, 1056–1071, doi:10.1021/acs.langmuir.8b01789.

183. Wang, W.; Yang, J.; Zhang, E.; Lu, Y.; Cao, Z. L-Carnitine Derived Zwitterionic Betaine Materials. *J. Mater. Chem. B* **2017**, *5*, 8676–8680, doi:10.1039/c7tb02431b.

184. Chien, H.W.; Cheng, P.H.; Chen, S.Y.; Yu, J.; Tsai, W.B. Low-Fouling and Functional Poly(Carboxybetaine) Coating via a Photo-Crosslinking Process. *Biomater. Sci.* **2017**, *5*, 523–531, doi:10.1039/c6bm00637j.

185. Lima Giacobbo, B.; Doorduin, J.; Klein, H.C.; Dierckx, R.A.J.O.; Bromberg, E.; de Vries,

E.F.J. Brain-Derived Neurotrophic Factor in Brain Disorders: Focus on Neuroinflammation. *Mol. Neurobiol.* **2019**, *56*, 3295–3312, doi:10.1007/s12035-018-1283-6.

186. Pan, W.; Banks, W.A.; Fasold, M.B.; Bluth, J.; Kastin, A.J. Transport of Brain-Derived Neurotrophic Factor across the Blood-Brain Barrier. *Neuropharmacology* **1998**, *37*, 1553–1561, doi:10.1016/S0028-3908(98)00141-5.

187. Squinto, S.P.; Stitt, T.N.; Aldrich, T.H.; Davis, S.; Bianco, S.M.; Radziejewski, C.; Glass, D.J.; Masiakowski, P.; Furth, M.E.; Valenzuela, D.M. TrkB Encodes a Functional Receptor for Brain-Derived Neurotrophic Factor and Neurotrophin-3 but Not Nerve Growth Factor. *Cell* **1991**, *65*, 885–893, doi:10.1016/0092-8674(91)90395-F.

188. Soppet, D.; Escandon, E.; Maragos, J.; Middlemas, D.S.; Raid, S.W.; Blair, J.; Burton, L.E.; Stanton, B.R.; Kaplan, D.R.; Hunter, T. The Neurotrophic Factors Brain-Derived Neurotrophic Factor and Neurotrophin-3 Are Ligands for the TrkB Tyrosine Kinase Receptor. *Cell* **1991**, *65*, 895–903, doi:10.1093/glycob/cwn084.

189. Minichiello, L. TrkB Signalling Pathways in LTP and Learning. *Nat. Rev. Neurosci.* **2009**, *10*, 850–860, doi:10.1038/nrn2738.

190. Lu, B.; Pang, P.T.; Woo, N.H. The Yin and Yang of Neurotrophin Action. *Nat. Rev. Neurosci.* **2005**, *6*, 603–614, doi:10.1038/nrn1726.

191. Kline, D.D.; Ogier, M.; Kunze, D.L.; Katz, D.M. Exogenous Brain Derived Neurotrophic Factor Rescues Synaptic Dysfunction in Mecp2 Null Mice. *J. Neurosci.* **2010**, *30*, 5303–5310, doi:10.1523/JNEUROSCI.5503-09.2010.

192. Chang, Q.; Khare, G.; Dani, V.; Nelson, S.; Jaenisch, R. The Disease Progression of Mecp2 Mutant Mice Is Affected by the Level of BDNF Expression. *Neuron* **2006**, *49*, 341–348, doi:10.1016/j.neuron.2005.12.027.

193. Apfel, S.C.; Kessler, J. a; Adornato, B.T.; Litchy, W.J.; Sanders, C.; Rask, C. a Recombinant Human Nerve Growth Factor in the Treatment of Diabetic Polyneuropathy. *Neurology* **1998**, *51*, 695–702, doi:10.1212/WNL.51.3.695.

194. Afarid, M.; Torabi-Nami, M.; Zare, B. Neuroprotective and Restorative Effects of the Brain-Derived Neurotrophic Factor in Retinal Diseases. *J. Neurol. Sci.* **2016**, *363*, 43–50, doi:10.1016/j.jns.2016.02.024.

195. Kasarskis, E.J.; Shefner, J.M.; Miller, R. A Controlled Trial of Recombinant Methionyl Human BDNF in ALS: The BDNF Study Group (Phase III). *Neurology* **1999**, *52*, 1427–1433, doi:10.1212/WNL.52.7.1427.

196. Nagahara, A.H.; Merrill, D.A.; Coppola, G.; Tsukada, S.; Schroeder, B.E.; Shaked, G.M.; Wang, L.; Blesch, A.; Kim, A.; Conner, J.M.; et al. Neuroprotective Effects of Brain-Derived Neurotrophic Factor in Rodent and Primate Models of Alzheimer's Disease. *Nat. Med.* **2009**, *15*, 331–337, doi:10.1038/nm.1912.

197. Ma, X.; Liu, P.; Zhang, X.; Jiang, W.; Jia, M.; Wang, C.; Dong, Y.; Dang, Y.; Gao, C. Intranasal Delivery of Recombinant AAV Containing BDNF Fused with HA2TAT: A Potential Promising Therapy Strategy for Major Depressive Disorder. *Sci. Rep.* **2016**, *6*, 22404, doi:10.1038/srep22404.

198. Nagahara, A.H.; Tuszynski, M.H. Potential Therapeutic Uses of BDNF in Neurological and Psychiatric Disorders. *Nat Rev Drug Discov* **2011**, *10*, 209–219,

doi:10.1038/nrd3366.

199. Ploughman, M.; Windle, V.; MacLellan, C.L.; White, N.; Doré, J.J.; Corbett, D. Brain-Derived Neurotrophic Factor Contributes to Recovery of Skilled Reaching after Focal Ischemia in Rats. *Stroke* **2009**, *40*, 1490–1495, doi:10.1161/STROKEAHA.108.531806.

200. Kanato, Y.; Kitajima, K.; Sato, C. Direct Binding of Polysialic Acid to a Brain-Derived Neurotrophic Factor Depends on the Degree of Polymerization. *Glycobiology* **2008**, *18*, 1044–1053, doi:10.1093/glycob/cwn084.

201. Kanato, Y.; Ono, S.; Kitajima, K.; Sato, C. Complex Formation of a Brain-Derived Neurotrophic Factor and Glycosaminoglycans. *Biosci. Biotechnol. Biochem.* **2009**, *73*, 2735–2741, doi:10.1271/bbb.90637.

202. Zhao, H.; Alam, A.; San, C.-Y.; Eguchi, S.; Chen, Q.; Lian, Q.; Ma, D. Molecular Mechanisms of Brain-Derived Neurotrophic Factor in Neuro- Protection: Recent Developments. *Brain Res.* **2017**, *1665*, 1–21, doi:10.1016/j.brainres.2017.03.029.

203. Yi, X.; Manickam, D.S.; Brynskikh, A.; Kabanov, A. V. Agile Delivery of Protein Therapeutics to CNS. *J. Control. Release* **2014**, *190*, 637–663, doi:10.1016/j.jconrel.2014.06.017.

204. Lochhead, J.J.; Thorne, R.G. Intranasal Delivery of Biologics to the Central Nervous System. *Adv. Drug Deliv. Rev.* **2012**, *64*, 614–628, doi:10.1016/j.addr.2011.11.002.

205. Lochhead, J.J.; Wolak, D.J.; Pizzo, M.E.; Thorne, R.G. Rapid Transport within Cerebral Perivascular Spaces Underlies Widespread Tracer Distribution in the Brain after Intranasal Administration. *J. Cereb. Blood Flow Metab.* **2015**, *35*, 371–381, doi:10.1038/jcbfm.2014.215.

206. Ali, N.; Mattsson, K.; Rissler, J.; Karlsson, H.M.; Svensson, C.R.; Gudmundsson, A.; Lindh, C.H.; Jönsson, B.A.G.; Cedervall, T.; Kåredal, M. Analysis of Nanoparticle-Protein Coronas Formed in Vitro between Nanosized Welding Particles and Nasal Lavage Proteins. *Nanotoxicology* **2016**, *10*, 226–234, doi:10.3109/17435390.2015.1048324.

207. Soderquist, R.G.; Milligan, E.D.; Sloane, E.M.; Harrison, J.A.; Douvas, K.K.; Potter, J.M.; Hughes, T.S.; Chavez, R.A.; Johnson, K.; Watkins, L.R.; et al. PEGylation of Brain-Derived Neurotrophic Factor for Preserved Biological Activity and Enhanced Spinal Cord Distribution. *J. Biomed. Mater. Res. - Part A* **2009**, *91*, 719–729, doi:10.1002/jbm.a.32254.

208. Natarajan, G.; Perriotte-Olson, C.; Bhinderwala, F.; Powers, R.; Desouza, C. V.; Talmon, G.A.; Yuhang, J.; Zimmerman, M.C.; Kabanov, A. V.; Saraswathi, V. Nanoformulated Copper/Zinc Superoxide Dismutase Exerts Differential Effects on Glucose vs Lipid Homeostasis Depending on the Diet Composition Possibly via Altered AMPK Signaling. *Transl. Res.* **2017**, *188*, 10–26, doi:10.1016/j.trsl.2017.08.002.

209. Ma, Y.; Wang, J.; Gao, J.; Yang, H.; Wang, Y.; Manithody, C.; Li, J.; Rezaie, A.R. Antithrombin Up-Regulates AMP-Activated Protein Kinase Signalling during Myocardial Ischaemia/Reperfusion Injury. *Thromb. Haemost.* **2015**, *113*, 338–349, doi:10.1160/TH14-04-0360.

210. Nagahara, A.H.; Merrill, D. a; Coppola, G.; Tsukada, S.; Schroeder, B.E.; Shaked, G.M.; Wang, L.; Blesch, A.; Kim, A.; Conner, J.M.; et al. Neuroprotective Effects of Brain-Derived Neurotrophic Factor in Rodent and Primate Models of Alzheimer's Disease. *Nat. Med.* **2009**, *15*, 331–337, doi:10.1038/nm.1912.

211. Peterson, A.; Bansal, A.; Hofman, F.; Chen, T.C.; Zada, G. A Systematic Review of Inhaled Intranasal Therapy for Central Nervous System Neoplasms: An Emerging Therapeutic Option. *J. Neurooncol.* **2014**, *116*, 437–446, doi:10.1007/s11060-013-1346-5.

212. M. Bentivoglio, F. E. Bloom, A. Björklund, S. B. Dunnett, T. Hökfelt, L. Kaczmarek, M. J. Kuhar, O. P. Ottersen, C. Owman, R. Quirion, H. A. Robertson, H. W. M. Steinbusch, J. Storm-Mathisen, L. W. Swanson, M. Tohyama, J. D. Vente, S.R.V. *Handbook of Chemical Neuroanatomy*. *Vol. 2*; 1983; ISBN 978-0-444-90330-3.

213. Mu, Q.; Hu, T.; Yu, J. Molecular Insight into the Steric Shielding Effect of PEG on the Conjugated Staphylokinase: Biochemical Characterization and Molecular Dynamics Simulation. *PLoS One* **2013**, *8*, 1–10, doi:10.1371/journal.pone.0068559.

214. McDonald, I.K.; Thornton, J.M. Satisfying Hydrogen Bonding Potential in Proteins. *J. Mol. Biol.* **1994**, *238*, 777–793, doi:10.1006/jmbi.1994.1334.

215. Baker, E.N.; Hubbard, R.E. Hydrogen Bonding in Globular Proteins. *Prog. Biophys. Mol. Biol.* **1984**, *44*, 97–179, doi:10.1016/0079-6107(84)90007-5.

216. Burns, M.L.; Malott, T.M.; Metcalf, K.J.; Hackel, B.J.; Chan, J.R.; Shusta, E. V. Directed Evolution of Brain-Derived Neurotrophic Factor for Improved Folding and Expression in Saccharomyces Cerevisiae. *Appl. Environ. Microbiol.* **2014**, *80*, 5732–5742, doi:10.1128/AEM.01466-14.

217. Zezin, A.B.; Kabanov, V.A. A New Class of Complex Water-Soluble Polyelectrolytes A New Class of Complex Water-Soluble Polyelectrolytes. *Russ. Chem. Rev.* **1982**, *51*, 833–855.

218. Bradford, M.M. A Rapid and Sensitive Method for the Quantitation of Microgram Quantities of Protein Utilizing the Principle of Protein-Dye Binding. *Anal. Biochem.* **1976**, *72*, 248–254, doi:10.1016/0003-2697(76)90527-3.

219. Holappa, S.; Kantonen, L.; Andersson, T.; Winnik, F.; Tenhu, H. Overcharging of Polyelectrolyte Complexes by the Guest Polyelectrolyte Studied by Fluorescence Spectroscopy. *Langmuir* **2005**, *21*, 11431–11438, doi:10.1021/la051866r.

220. Zintchenko, A.; Rother, G.; Dautzenberg, H. Transition Highly Aggregated Complexes - Soluble Complexes via Polyelectrolyte Exchange Reactions: Kinetics, Structural Changes, and Mechanism. *Langmuir* **2003**, *19*, 2507–2513, doi:10.1021/la0265427.

221. Dautzenberg, H. Polyelectrolyte Complex Formation in Highly Aggregating Systems. 1. Effect of Salt: Polyelectrolyte Complex Formation in the Presence of NaCl. *Macromolecules* **1997**, *30*, 7810–7815, doi:10.1021/ma970803f.

222. Zhang, H.; Saiani, A.; Guenet, J.M.; Curtis, R. Effect of Stereoregular Polyelectrolyte on Protein Thermal Stability. *Macromol. Symp.* **2007**, *251*, 25–32, doi:10.1002/masy.200750504.

223. Cousin, F.; Gummel, J.; Ung, D.; Boué, F. Polyelectrolyte–Protein Complexes: Structure and Conformation of Each Specie Revealed by SANS. *Langmuir* **2005**, *21*, 9675–9688, doi:10.1021/la0510174.

224. Stogov, S. V.; Muronetz, V.I.; Izumrudov, V.A. Short Synthetic Polyelectrolytes Destabilize Proteins Most Efficiently. *Dokl. Biochem. Biophys.* **2009**, *427*, 187–190, doi:10.1134/S160767290904005X.

225. Callahan, W.J.; Narhi, L.O.; Kosky, A.A.; Treuheit, M.J. Sodium Chloride Enhances the

Storage and Conformational Stability of BDNF and PEG-BDNF. *Pharm. Res.* **2001**, *18*, 261–266, doi:10.1023/A:1011034425896.

226. Fryer, R.H.; Kaplan, D.R.; Kromer, L.F. Truncated TrkB Receptors on Nonneuronal Cells Inhibit BDNF-Induced Neurite Outgrowth in Vitro. *Exp. Neurol.* **1997**, *148*, 616–627, doi:10.1006/exnr.1997.6699.

227. Nakamura, T.; Sanokawa, R.; Sasaki, Y.; Ayusawa, D.; Oishi, M.; Mori, N. N-Shc: A Neural-Specific Adapter Molecule That Mediates Signaling from Neurotrophin/Trk to Ras/MAPK Pathway. *Oncogene* **1996**, *13*, 1111–1121.

228. Hunter, R.L.; Cheng, B.; Choi, D.Y.; Liu, M.; Liu, S.; Cass, W.A.; Bing, G. Intrastriatal Lipopolysaccharide Injection Induces Parkinsonism in C57/B6 Mice. *J. Neurosci. Res.* **2009**, *87*, 1913–1921, doi:10.1002/jnr.22012.

229. Bertram, J.P.; Rauch, M.F.; Chang, K.; Lavik, E.B. Using Polymer Chemistry to Modulate the Delivery of Neurotrophic Factors from Degradable Microspheres: Delivery of BDNF. *Pharm. Res.* **2010**, *27*, 82–91, doi:10.1007/s11095-009-0009-x.

230. Tan, J.; Wang, Y.; Yip, X.; Glynn, F.; Shepherd, R.K.; Caruso, F. Nanoporous Peptide Particles for Encapsulating and Releasing Neurotrophic Factors in an Animal Model of Neurodegeneration. *Adv. Mater.* **2012**, *24*, 3362–3366, doi:10.1002/adma.201200634.

231. Mehrotra, S.; Lynam, D.; Maloney, R.; Pawelec, K.M.; Tuszynski, M.H.; Lee, I.; Chan, C.; Sakamoto, J. Time Controlled Protein Release from Layer-by-Layer Assembled Multilayer Functionalized Agarose Hydrogels. *Adv. Funct. Mater.* **2010**, *20*, 247–258, doi:10.1002/adfm.200901172.

232. Craft, S.; Baker, L.D.; Montine, T.J.; Minoshima, S.; Watson, G.S.; Claxton, A.; Arbuckle, M.; Callaghan, M.; Tsai, E.; Plymate, S.R.; et al. Intranasal Insulin Therapy for Alzheimer Disease and Amnestic Mild Cognitive Impairment. *Arch Neurol.* **2012**, *69*, 29–38, doi:10.1001/archneurol.2011.233.Intranasal.

233. Vaka, S.R.K.; Murthy, S.N.; Balaji, A.; Repka, M.A. Delivery of Brain-Derived Neurotrophic Factor via Nose-to-Brain Pathway. *Pharm. Res.* **2012**, *29*, 441–447, doi:10.1007/s11095-011-0572-9.

234. Chen, H.; Yang, G.Z.X.; Getachew, H.; Acosta, C.; Sierra Sánchez, C.; Konofagou, E.E. Focused Ultrasound-Enhanced Intranasal Brain Delivery of Brain-Derived Neurotrophic Factor. *Sci. Rep.* **2016**, *6*, 1–8, doi:10.1038/srep28599.

235. Casado, B.; Pannell, L.K.; Iadarola, P.; Baraniuk, J.N. Identification of Human Nasal Mucous Proteins Using Proteomics. *Proteomics* **2005**, *5*, 2949–2959, doi:10.1002/pmic.200401172.

236. Iliff, J.J.; Wang, M.; Liao, Y.; Plogg, B.A.; Peng, W.; Gundersen, G.A.; Benveniste, H.; Vates, G.E.; Deane, R.; Goldman, S.A.; et al. A Paravascular Pathway Facilitates CSF Flow Through the Brain Parenchyma and the Clearance of Interstitial Solutes, Including Amyloid β. *Sci. Transl. Med.* **2012**, *4*, 147ra111, doi:10.1126/scitranslmed.3003748.

237. Ruigrok, M.J.R.; de Lange, E.C.M. Emerging Insights for Translational Pharmacokinetic and Pharmacokinetic-Pharmacodynamic Studies: Towards Prediction of Nose-to-Brain Transport in Humans. *AAPS J.* **2015**, *17*, 493–505, doi:10.1208/s12248-015-9724-x.

238. Gref, R.; Minamitake, Y.; Peracchia, M.T.; Torchilin, V.; Langer, R.; Peracchia, T.; Trubetskoy, V.; Torchilin, V.; Langerllf, R. Biodegradable Long-Circulating Polymeric

Nanospheres. *Science* **1994**, *263*, 1600–1603.

239. Somiya, M.; Mine, S.; Yasukawa, K.; Ikeda, S. Sex Differences in the Incidence of Anaphylaxis to LNP-MRNA COVID-19 Vaccines. *Vaccine* 2021, *39*, 3313–3314.

240. Tsukahara, T.M.D.; Takeda, M.M..; Shimohama, S.M..; Ohara, O.P..; Hashimoto, N.M.. Effects of Brain-Derived Neurotrophic Factor on 1-Methyl-4-Phenyl-1,2,3,6-Tetrahydropyridine-Induced Parkinsonism in Monkeys. *Neurosurgery* **1995**, *37*, 733–741, doi:10.1227/00006123-199510000-00018.

241. Veronese, F.M.; Mero, A.; Pasut, G. Protein PEGylation, Basic Science and Biological Applications. In *PEGylated Protein Drugs: Basic Science and Clinical Applications*; Veronese, F.M., Ed.; Birkhäuser Basel: Basel, 2009; pp. 11–31 ISBN 978-3-7643-8679-5.

242. He, Z.; Miao, L.; Jordan, R.; S-Manickam, D.; Luxenhofer, R.; Kabanov, A. V. A Low Protein Binding Cationic Poly(2-Oxazoline) as Non-Viral Vector. *Macromol. Biosci.* **2015**, *15*, 1004–1020, doi:10.1002/mabi.201500021.

243. Miyata, K.; Nishiyama, N.; Kataoka, K. Rational Design of Smart Supramolecular Assemblies for Gene Delivery: Chemical Challenges in the Creation of Artificial Viruses. *Chem. Soc. Rev.* **2012**, *41*, 2562–2574, doi:10.1039/C1CS15258K.

244. He, Z.; Wan, X.; Schulz, A.; Bludau, H.; Dobrovolskaia, M.A.; Stern, S.T.; Montgomery, S.A.; Yuan, H.; Li, Z.; Alakhova, D.; et al. Biomaterials A High Capacity Polymeric Micelle of Paclitaxel : Implication of High Dose Drug Therapy to Safety and in Vivo Anti-Cancer Activity. *Biomaterials* **2016**, *101*, 296–309, doi:10.1016/j.biomaterials.2016.06.002.

245. Tong, J.; Yi, X.; Luxenhofer, R.; Banks, W.A.; Jordan, R.; Zimmerman, M.C.; Kabanov, A. V. Conjugates of Superoxide Dismutase 1 with Amphiphilic Poly(2-Oxazoline) Block Copolymers for Enhanced Brain Delivery: Synthesis, Characterization and Evaluation in Vitro and in Vivo. *Mol. Pharm.* **2013**, *10*, 360–377, doi:10.1021/mp300496x.

246. Cheung, D.L.; Lau, K.H.A. Atomistic Study of Zwitterionic Peptoid Antifouling Brushes. *Langmuir* **2019**, *35*, 1483–1494, doi:10.1021/acs.langmuir.8b01939.

247. Luxenhofer, R.; Schulz, A.; Roques, C.; Li, S.; Bronich, T.K.; Batrakova, E. V; Jordan, R.; Kabanov, A. V Doubly-Amphiphilic Poly(2-Oxazoline)s as High Capacity Delivery Systems for Hydrophobic Drugs. *Biomaterials* **2011**, *31*, 4972–4979, doi:10.1016/j.biomaterials.2010.02.057.Doubly-Amphiphilic.

248. Lu, M.; Ozcelik, A.; Grigsby, C.L.; Zhao, Y.; Guo, F.; Leong, K.W.; Huang, T.J. Microfluidic Hydrodynamic Focusing for Synthesis of Nanomaterials. *Nano Today* **2016**, *11*, doi:http://dx.doi.org/10.1016/j.nantod.2016.10.006.

249. Guimaraes Sa Correia, M.; Briuglia, M.L.; Niosi, F.; Lamprou, D.A. Microfluidic Manufacturing of Phospholipid Nanoparticles: Stability, Encapsulation Efficacy, and Drug Release. *Int. J. Pharm.* **2017**, *516*, 91–99, doi:10.1016/j.ijpharm.2016.11.025.

250. Borukhov, I.; Andelman, D.; Borrega, R.; Cloitre, M.; Leibler, L.; Orland, H. Polyelectrolyte Titration: Theory and Experiment. *J. Phys. Chem. B* **2000**, *104*, 11027–11034, doi:10.1021/jp001892s.

251. Bodnarchuk, M.S.; Doncom, K.E.B.; Wright, D.B.; Heyes, D.M.; Dini, D.; O'Reilly, R.K. Polyelectrolyte PKa from Experiment and Molecular Dynamics Simulation. *RSC Adv.* **2017**, *7*, 20007–20014, doi:10.1039/c6ra27785c.

252. *ITC Data Analysis in Origin*; 7th ed.; MicroCal LLC: Northhampton, MA, 2004;

253. Ulbricht, J.; Jordan, R.; Luxenhofer, R. On the Biodegradability of Polyethylene Glycol, Polypeptoids and Poly(2-Oxazoline)S. *Biomaterials* **2014**, *35*, 4848–4861, doi:10.1016/j.biomaterials.2014.02.029.

254. Koshkina, O.; Westmeier, D.; Lang, T.; Bantz, C.; Hahlbrock, A.; Würth, C.; Resch-Genger, U.; Braun, U.; Thiermann, R.; Weise, C.; et al. Tuning the Surface of Nanoparticles: Impact of Poly(2-Ethyl-2-Oxazoline) on Protein Adsorption in Serum and Cellular Uptake. *Macromol. Biosci.* **2016**, *16*, 1287–1300, doi:10.1002/mabi.201600074.

255. Kim, W.; Yamasaki, Y.; Jang, W.D.; Kataoka, K. Thermodynamics of DNA Condensation Induced by Poly(Ethylene Glycol)- Block -Polylysine through Polyion Complex Micelle Formation. *Biomacromolecules* **2010**, *11*, 1180–1186, doi:10.1021/bm901305p.

256. Kim, W.; Yamasaki, Y.; Kataoka, K. Development of a Fitting Model Suitable for the Isothermal Titration Calorimetric Curve of DNA with Cationic Ligands. *J. Phys. Chem. B* **2006**, *110*, 10919–10925, doi:10.1021/jp057554e.

257. Bronich, T.; Kabanov, A. V.; Marky, L.A. A Thermodynamic Characterization of the Interaction of a Cationic Copolymer with DNA. *J. Phys. Chem. B* **2001**, *105*, 6042–6050, doi:10.1021/jp004395k.

258. Friedman, N. Hydrogen Bonding and Heat of Solution. *J. Chem. Educ.* **1977**, *54*, 248, doi:10.1021/ed054p248.

259. Kabanov, A. V.; Bronich, T.K.; Kabanov, V.A.; Yu, K.; Eisenberg, A. Soluble Stoichiometric Complexes from Poly( N -Ethyl-4-Vinylpyridinium) Cations and Poly(Ethylene Oxide)- Block -Polymethacrylate Anions. *Macromolecules* **1996**, *29*, 6797–6802, doi:10.1021/ma960120k.